THE EFFECT OF BIAXIAL LOADING ON THE CRITICAL RESOLVED SHEAR STRESS OF ZINC SINGLE CRYSTALS

Thesis for the Degree of Ph. D.

MICHIGAN STATE UNIVERSITY

JERRY ALLEN BARENDREGHT

1971

This is to certify that the

thesis entitled

THE EFFECT OF BIAXIAL LOADING
ON THE CRITICAL RESOLVED SHEAR
STRESS OF ZINC SINGLE CRYSTALS

presented by

Jerry Allen Barendreght

has been accepted towards fulfillment
of the requirements for

Ph. D. degree in Mechanical Engineering

William N. Sharpe Jr.
Major professor

Date August 5, 1971

O-169

ABSTRACT

THE EFFECT OF BIAXIAL LOADING ON THE CRITICAL RESOLVED SHEAR STRESS OF ZINC SINGLE CRYSTALS

By

Jerry Allen Barendreght

The macroscopic deformation of $\{0001\}$ $<2\bar{1}\bar{1}0>$ type slip in hexagonal close-packed zinc single crystals is investigated by subjecting the crystals to a uniform biaxial state of stress. This was accomplished by loading flat tensile specimens in both the axial and transverse direction. The transverse load was applied with specially designed rubber grips. This allowed the effects of the crystal orientation and the resolved normal stresses on the active slip system to be uncoupled. In this study the crystal orientation was held constant and the resolved normal stresses at yield were varied by varying the biaxial stress ratio at yield.

The design of the loading configuration that resulted in the largest region of uniform biaxial stress was verified by extensive elasticity and photoelasticity investigations. The elasticity investigation established the geometrical limits for the flat tensile specimen by modelling the specimen as a finite rectangular beam loaded transversely along it's sides. Fourier analysis was utilized in solving for the stresses in the beam. The photoelasticity investigation with models tested at these limits verified the elasticity solution, established the geometry of the rubber grips and determined

the limit that was experimentally practical.

A series of uniaxial single crystal tests established the critical resolved shear stress to be 70 $\pm$ 2 grams/mm^2. The results of the biaxial shear stress experiments showed that the critical resolved shear stress of zinc single crystals decreases as the resolved normal stresses acting on the active slip system increases. These results were for $\{0001\}$ $\langle 2\bar{1}\bar{1}0 \rangle$ type slip when the angle between the slip plane and the tensile axis and the angle between the slip direction and the tensile axis are both 45 degrees.

THE EFFECT OF BIAXIAL LOADING ON THE CRITICAL RESOLVED SHEAR STRESS OF ZINC SINGLE CRYSTALS

By

Jerry Allen Barendreght

A THESIS

Submitted to
Michigan State University
in partial fulfillment of the requirements
for the degree of

DOCTOR OF PHILOSOPHY

Department of Mechanical Engineering

1971

671758

ACKNOWLEDGEMENTS

The author wishes to express his appreciation to Dr. W.N. Sharpe, Jr. for his guidance and support throughout the course of this study. He appreciates the guidance of the other members of his graduate committee, Dr. R.T. Hinkle, Dr. H.L. Womochel, and Dr. G.L. Cloud.

The expert assistance of Dr. K.N. Subramanian with respect to crystal growth and preparation is gratefully acknowledged. The assistance of Dr. G.L. Cloud in regards to suggestions for the photoelasticity setup is deeply appreciated. Also, the helpful discussions and assistance of Dr. R.W. Little with the elasticity solution and Dr. J.L. Lubkin's computer results used to verify the author's computer program are gratefully appreciated.

The author is thankful for the patient encouragement of his wife, Sharon.

Finally, special thanks to Mr. J.W. Hoffman and the Division of Engineering Research, College of Engineering for continuous support.

TABLE OF CONTENTS

LIST OF TABLES

LIST OF FIGURES

Figure		Page
11	Fractional fringe order determination	27
12	Loading frame for photoelasticity investigation	27
13	Load cell and load cell calibration curves	28
14	Photoelasticity specimen details	30
15	Bondability index of common elastomers	31
16	Rubber grip details	32
17	a. Rubber grip cutting jig	33
	b. Gluing jig for photoelastic specimens	33
18	Effect of rubber grip slits on the stress distribution in a finite rectangular beam. Slits cut to within 1/8 inch of bonded interface	34
19	Calibration curve for photoelasticity modelling material	37
20	Zinc specimen details	45
21	Crucible design	49
22	Specimen packed in crucible (schematic)	50
23	Crystal growing furnace (schematic)	51
24	Specimen holders a. Holder A b. Holder B	52
25	Wire saw	54
26	Gluing jig for zinc specimens	54
27	Aluminum grip details	55
28	Biaxial testing machine	57
29	Effects of improper alignment and no prestress on biaxial loading of specimen	59
30	Typical nominal stress-strain curve	61
31	Photomicrograph of slip in specimen's test section	62

I INTRODUCTION

The usual testing procedure in the investigation of the mechanical properties of single crystals is uniaxial tension or compression. It has been shown that, when a uniaxial stress is applied to a specimen and macroscopic yield occurs, the resolved shear stress acting on a slip system is constant and is independent of the crystal orientation with respect to the tensile axis of the specimen (1, 2). However, there have been cases where the critical resolved shear stress has been found to vary (3, 4, 5, 6). All of these experiments have been in uniaxial tension or compression, where a variation in the crystal orientation is accompanied by a variation in the resolved normal stresses on the slip plane.

The concept of critical resolved shear stress in single crystals is a well known concept first investigated by Schmid (1). Schmid showed that the yield stress of hexagonal metals (cadmium, zinc, and magnesium) varied greatly with orientation. Later, Schmid, Boas et al., (2) showed that when the tensile stress σ_t was converted to a resolved shear stress using,

$$\tau = \sigma_t \sin \chi \cos \Psi ,$$

the resulting shear stress at yield was constant for each metal. This constancy of yield stress is usually referred to as Schmid's law. Ψ is the angle between the uniaxial stress axis and the slip direction, and ϕ is the angle between the uniaxial stress axis and the slip plane normal. See Figure 1. τ is the shear stress on the slip plane and the shear stress at yield is referred to as the critical resolved shear stress (CRSS).

The CRSS of many metals was examined further by different investigators who found differences concerning the constancy of the CRSS (or τ_0) for all orientations of the standard stereographic triangle. Opinion on the orientation-dependence of τ_0 now is divided, partly because of difficulties inherent in the accurate measurement of τ_0. Often it is very difficult to determine when plastic flow commences; and τ_0 is quite structure-sensitive, being affected markedly by trace impurities or dislocations introduced in handling (7).

Rosi and Mathewson (8) investigated high-purity aluminum single crystals for the change in the CRSS with temperature and found that the Schmid law was obeyed. They used this uniformity of behavior as an indication that their method for producing and preparing tensile-test specimens resulted in structurally-uniform single crystals. Rose (9), studying plastic properties of copper crystals, found that the Schmid law was confirmed (with the possible exceptions of the [100] and [111] orientations). The investigation of Fenn, Hibbard and Leppers (10) on axial extension of alpha brass (70/30) single crystals show good agreement with the critical resolved shear stress law. More recently, Hassen (3) expressed the opinion that τ_0 at a given temperature is independent of orientation in nickel; although, some experimental scatter was observed in his experiments. On the other hand, Andrade and Aboau (4), and Diehl (5) found that, in

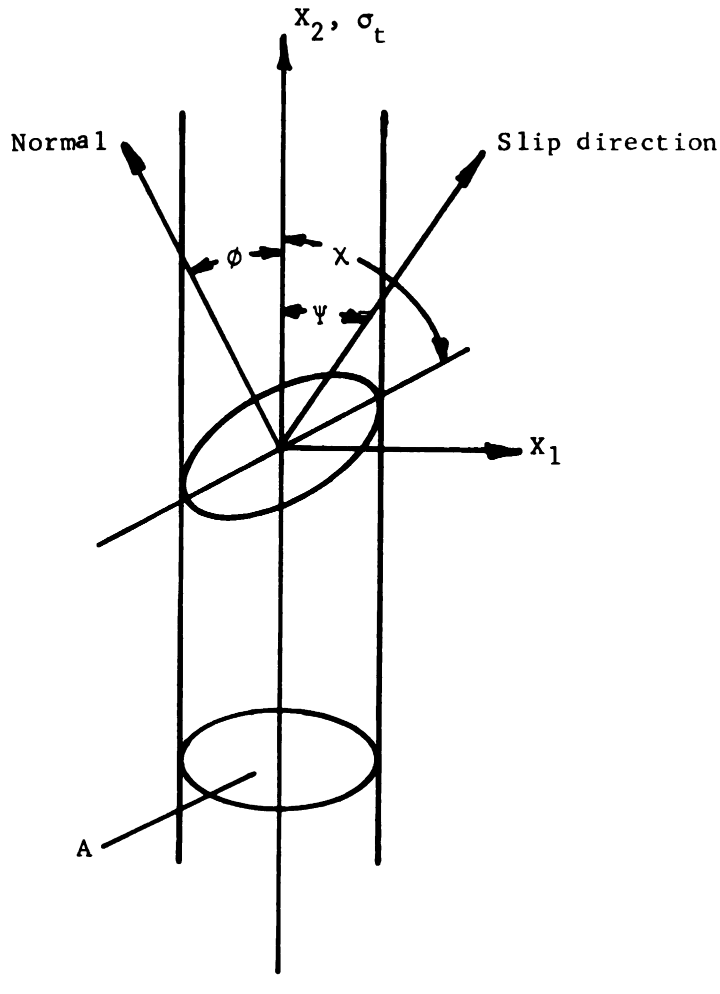

Figure 1. Coordinates for calculating resolved shear stresses.

copper, orientations near the center of the stereographic triangle gave nearly constant values of τ_0, but this result was no longer true for orientations approaching the boundaries of the triangle where the operation of other slip systems becomes more likely. Further evidence that FCC single crystals do not obey the Schmid law was demonstrated by Lücke and Lange (6) using 99.5 and 99.99 percent pure aluminum single crystals. In Maddin's and Chen's review of "Glide in Face Centered Cubic Metals," they stated that "Similar results (to Lücke and Lange) for high purity copper single crystals have been reported by Cupp and Chalmers" (11).

Barrett (12) reported that an increase of hydrostatic pressure increased the flow stress for nickel and aluminum during plastic deformation; earlier, he had stated that the normal stress from hydrostatic pressure up to 40 atm. had no effect on the CRSS (13).

Hull, Byron and Noble (14) reported that tantalum and silicon-iron single crystals having orientations between [110] and [111] along the edge of the unit triangle obey the Schmid law when deformed in tension. Tungsten single crystals, however, do not obey such a law in this region and exhibit a change in slip system which cannot be accounted for by geometrical considerations alone. Also, their results for compression tests cannot be explained in terms of a simple Schmid law.

HCP metals have agreed with the Schmid law more closely than have BCC and FCC metals. Jillson (15) found that zinc in uniaxial tension was highly consistent with the Schmid law for slip along the basal plane; similar results were obtained by Burke and Hibbard (16). This constancy of CRSS also has been demonstrated for cadmium and magnesium.

Since theories for predicting the stress-strain curve of a polycrystalline aggregate use τ_0 as a basis for predicting the yield stress, it is evident that the dependence of τ_0 upon complex stresses needs to be understood. Honeycombe (17) reviewed those theories which led generally to the determination of the mean orientation factor $\bar{m}$ for the relationship $\sigma = \bar{m}\tau$, between the tensile stress and the resolved shear stress. Sachs (18) and Taylor (19) found values for $\bar{m}$ of 2.238 and 3.06 respectively, and Bishop and Hill (20) confirmed that the approximate value for $\bar{m}$ is about 3.1. When these values for $\bar{m}$ were calculated, the Schmid law was always assumed valid. The validity of this law has been shown only for uniaxial tension in HCP single crystals but not for the complex state of stress actually occurring in crystals in the aggregate.

All of the investigators mentioned above have studied the mechanical properties of metals subjected to uniaxial stress fields. This type of testing leaves the normal stress and orientation effects coupled.

The purpose of this experimental investigation is to test the hypothesis that macroscopic yield in single crystals is determined only by the shear stress on the active slip system and is independent of the resolved normal stresses. This hypothesis is, of course, based on the assumption that all other variables such as dislocation density, impurities, oxide films, temperature and etc. can be held constant.

In order to test the hypothesis, one needs to separate the effect of the two above mentioned variables, namely, the crystal orientation and the resolved normal stresses. This separation of variables was accomplished by testing single crystals of zinc in a uniform biaxial state of stress. The uniform biaxial stress field was imposed on an ordinary flat tensile specimen by gluing rubber grips to the edges as shown in Figure 2.

The relation between stresses on the slip plane and a biaxial load may be understood from Figure 3. The crystals were oriented such that the slip plane normal, the slip direction, and the tensile axis were all in the same plane. For this special orientation, the $X_1'X_2'X_3'$ coordinate system is simply a rotation of θ degrees about the X_3 axis. X_1' is perpendicular to the slip plane and X_2' is colinear with the slip direction and $\Psi = \chi = 90 - \phi$. The stresses in the unprimed axis are transformed to the primed axis by

$$\sigma'_{ij} = \alpha_{ir}\,\alpha_{js}\,\sigma_{rs}\ . \qquad (2)$$

The first subscript indicates the direction of the normal to the plane on which the stress is considered; the second subscript denotes the direction of the stress itself. Noting that $\Psi = 90 - \phi$, the stress components on the slip system (primed coordinates) as a function of ϕ are:

$$\sigma'_{11} = \sigma_{11} \sin \phi + \sigma_{22} \cos \phi\ , \qquad (3)$$

$$\sigma'_{22} = \sigma_{11} \cos \phi + \sigma_{22} \sin \phi\ , \qquad (4)$$

$$\sigma'_{12} = (\sigma_{22} - \sigma_{11}) \sin \phi \cos \phi\ , \qquad (5)$$

for

$$\sigma_{12} = \sigma_{21} = \sigma_{31} = \sigma_{13} = \sigma_{33} = \sigma_{23} = \sigma_{32} = 0\ . \qquad (6)$$

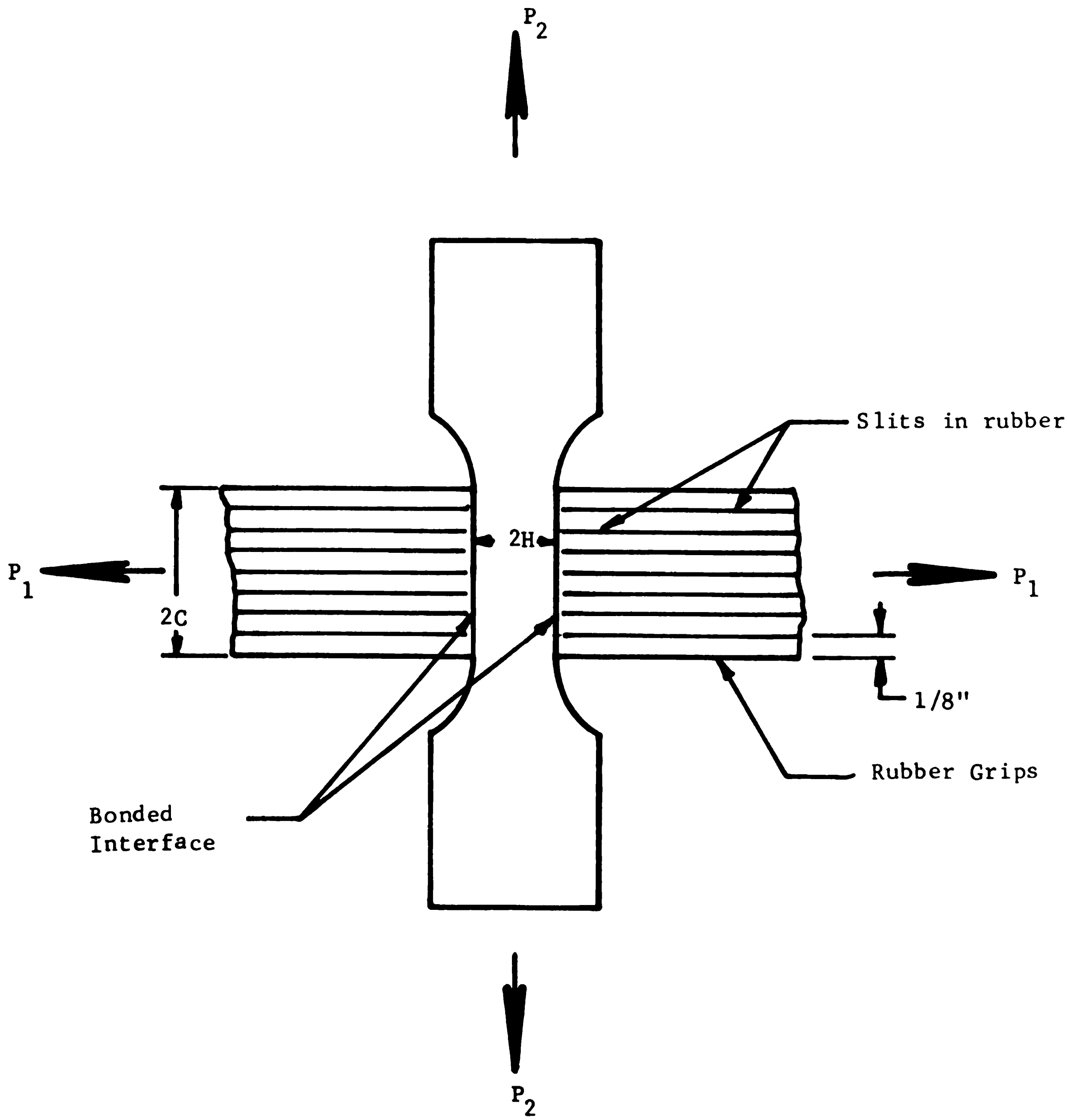

Figure 2. Biaxial loading of flat tensile specimen.

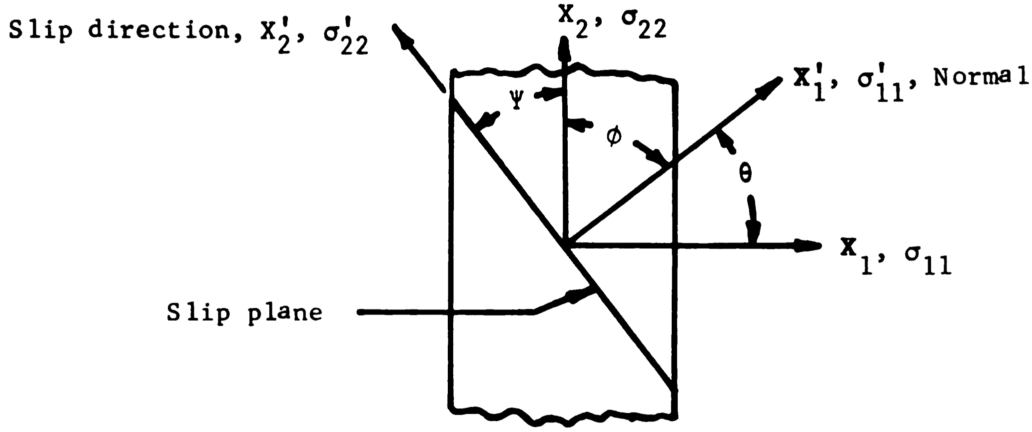

Figure 3. Coordinate transformation and stress definition.

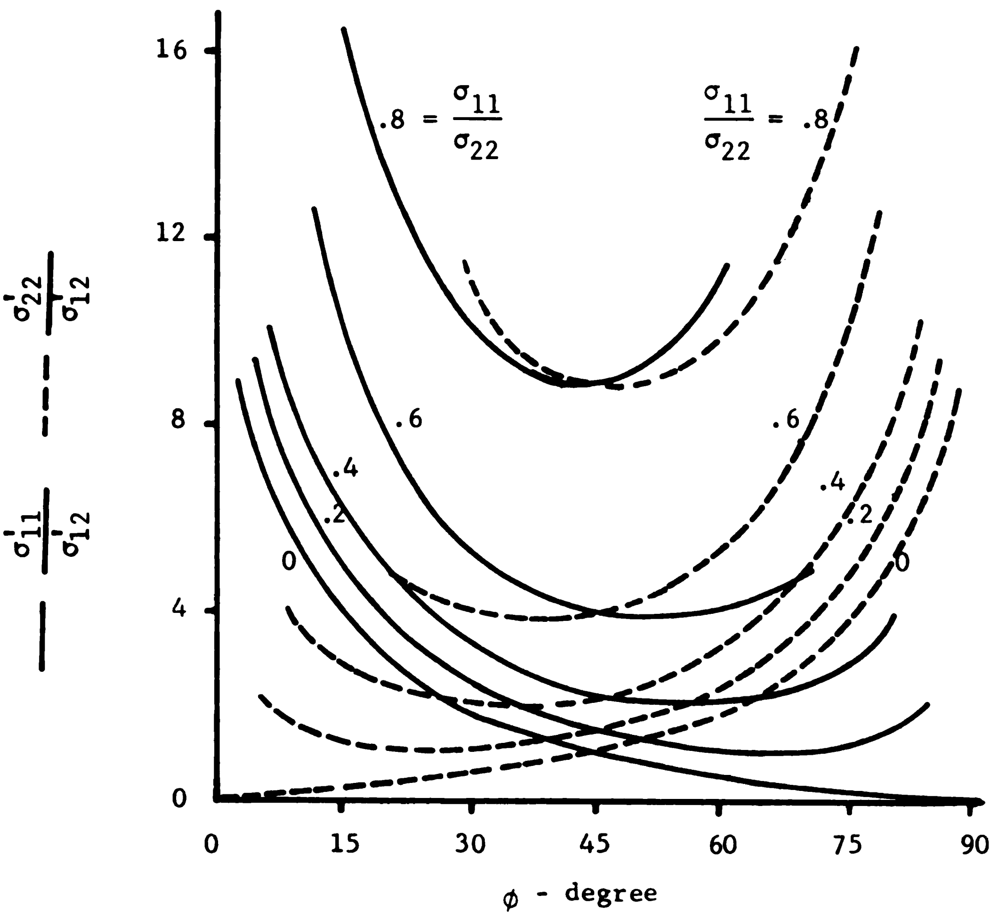

Figure 4. Resolved normal stress as a function of orientation (ϕ).

These formulae may be written in terms of the ratios of normal stresses on the slip plane to the shear stress on the slip plane as:

$$\sigma'_{11}/\sigma'_{12} = \frac{\sigma_{11}/\sigma_{22}}{1 - \sigma_{11}/\sigma_{22}} \tan \phi + \frac{1}{1 - \sigma_{11}/\sigma_{22}} \cot \phi \qquad (7)$$

$$\sigma'_{22}/\sigma'_{12} = \frac{\sigma_{11}/\sigma_{22}}{1 - \sigma_{11}/\sigma_{22}} \cot \phi + \frac{1}{1 - \sigma_{11}/\sigma_{22}} \tan \phi \; . \qquad (8)$$

These equations are plotted in Figure 4 with the stress ratio σ_{11}/σ_{22} as a parameter. The parameter σ_{11}/σ_{22} introduced by the biaxial load permits independent variation of the resolved normal stresses and the crystal orientation.

The effect of the resolved normal stress on the CRSS of single crystals can be investigated by holding ϕ constant while the resolved normal stress is varied by varying σ_{11}/σ_{22}. On the other hand, if one wants to study the effect of crystal orientation on the CRSS, σ'_{11} and σ'_{22} at yield can be made constant while the orientation is varied by adjusting the biaxial load. However, the specimen geometry does not permit complete variation of the normal stresses since only tensile forces are applied. The curves for $\sigma_{11}/\sigma_{22} = 0$ are thus lower boundaries on the stress ratios. In this research program, ϕ was held constant and σ'_{11} and σ'_{22} at yield were varied by varying σ_{11}/σ_{22}.

An elasticity solution coupled with a photoelasticity investigation established the design of the loading configuration. The elasticity solution fixed the limits on the width of specimen (2H) to length of loading (2C) ratio (H/C). These geometrical limits were such that 80 percent of the central portion (test section) of the specimen was subjected to a uniform biaxial stress field.

The photoelasticity investigation verified that the rubber grips generated a uniform normal surface traction at the bonded interface. These rubber grips were slit in order to reduce the Poisson effect of the rubber and minimize the shear stress at the bonded interface between the rubber grip and the specimen. If this shear stress is reduced to zero, the stress applied to the specimen boundary is effectively a pure normal stress.

The zinc single crystals used in the shear stress experiments were grown by the modified Bridgman (21) technique. There was no attempt to obtain the lowest value for the critical resolved shear stress, but the emphasis was on generating single crystal specimens that would yield consistently. The crystal orientation was such that $\phi = \Psi$ was equal to 45 degrees; therefore, σ'_{11} equals σ'_{22}.

The results obtained from a series of uniaxial tests showed reproducible yielding of the zinc single crystals. The results of the biaxial shear stress experiments indicated that when the orientation was held constant, and the normal stresses acting on the basal slip system at yield increased, the resolved shear stress at yield decreased. By varying σ_{11}/σ_{22} at yield from 0.0 to 0.62, σ'_{11}/τ_0 was varied from 1 to 3. This variation in the resolved normal stresses resulted in a decrease of σ'_{12}/τ_0 from 1.0 to 0.7 for σ'_{11}/τ_0 greater than 2.

II LOADING CONFIGURATION

The objective of this section is to describe the design of a loading and specimen configuration that will allow one to test anisotropic structures and materials under biaxial loading.

There are several ways one can obtain a biaxial state of stress. A thin walled cylinder, a large flat plate, a biaxially loaded square or a flat tensile specimen may be used. The following must be considered in determining the loading configuration; goal of research program, type and structure of material needed to obtain this goal, size of loads required, and how state of stress can be verified. In this research program, the goal required the variation of the normal stress at yield on the active slip system of zinc single crystals. Zinc single crystals have a low yield strength; therefore, the load requirement will be low. The use of a thin walled cylinder was eliminated, because the axes of anistropy are continuously varying with respect to the principal stress axis. A large flat plate was eliminated by the inability to grow a sufficiently large single crystal of preferred orientation. A preliminary photoelasticity investigation of a thin square loaded biaxially showed a region of uniform biaxial stress too small to be useful. The final choice was a flat tensile specimen loaded in the transverse as well as the axial direction. This was the most favorable choice for the following reasons: it could be grown in the existing crystal-growing furnace to the size required for the shear stress experiments, preliminary photoelasticity investigation indicated that it had a large region of uniform biaxial stress, and the state of stress at the interface of the grips and specimen could be verified by comparing an isotropic elasticity solution with a photoelasticity solution.

The design and geometry of the specimen and rubber grips required careful investigation to insure that a large region of uniform biaxial stress would be available for observation. Therefore, an elasticity and photoelasticity solution were undertaken to verify the state of stress. The specimen was modelled as a finite rectangular beam 2L long and 2H wide with its sides subjected to a uniform normal surface traction over a length 2C. The elasticity solution was in the form of a single Fourier series. The results of this solution established the limits of the geometry parameter, H/C, which would produce the largest region of uniform biaxial stress.

The flat tensile photoelastic specimens were made to fall within these limits. The grips used to apply the transverse load to the flat tensile specimen were designed such that they would generate a uniform normal stress at the bonded interface yet not reinforce the sides of the specimen appreciably. The details of the elasticity and photoelasticity investigations are discussed at length in section A and B below.

The results of the elasticity and photoelasticity investigation verified that the rubber grips could be used to generate a uniform normal stress at the bonded interface between the rubber grips and the specimen. The biaxial stress difference $(\sigma_{22} - \sigma_{11})$ for a region that covered approximately 80 percent of the test section was equal to 102$\pm$5 percent of the applied transverse stress σ_{11}^{I}. For this entire region, the photoelasticity and elasticity solutions were within $\pm$ 2 percent of each other. Therefore, rubber grips slit at 1/8 inch interval and to within 0.035 inch of the bonded interface can be used to generate the uniform normal surface traction needed to carry out the shear stress experiments.

A. Elasticity Solution

The purpose of the elasticity investigation was to determine the specimen geometry that would insure the largest region of uniform biaxial stress when loaded in both the axial and transverse direction.

1. Theory

The solution of the stress distribution in the specimen's test section was considered in two parts, and the results were superimposed. The first part was that of a simple tensile specimen subjected to and axial load. The solution to this part is $\sigma_{22} = \sigma_{22}^{I}$, where $\sigma_{22}^{I} = P_2/A_2$, $A_2 = 2Ht$ and t is the specimen thickness. For the second part, the specimen was modelled as a thin finite rectangular beam with a width (2H) to length (2L) ratio $(H/L) \ll 1$ which was subjected to a uniform normal stress, σ_{11}^{I}, in the X_1 direction as shown in Figure 5. Fourier analysis was utilized to determine the stress distribution in the finite rectangular beam (22).

The boundary conditions are:

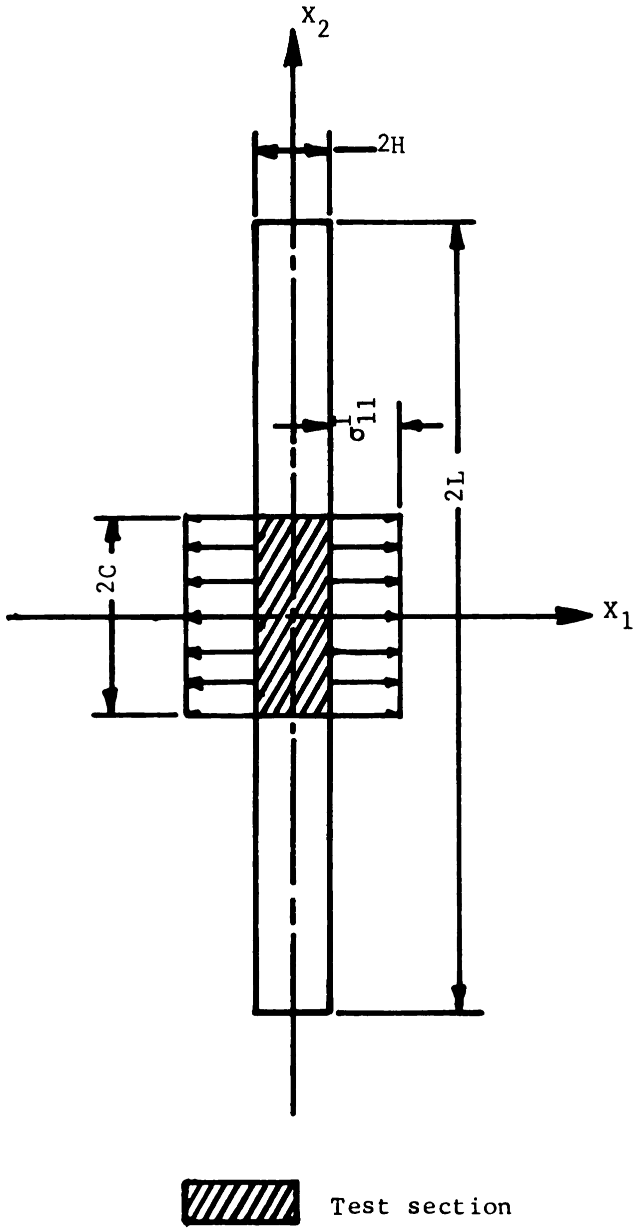

Figure 5. Finite rectangular beam for elasticity model.

$$X_1 = \pm H \qquad \sigma_{11} = \begin{cases} \sigma_{11}^{I} , & -C < X_2 < C \\ 0 , & -L < X_2 < -C \text{ and } C < X_2 < L, \end{cases}$$

$$\sigma_{12} = 0,$$

$$X_2 = \pm L, \ \sigma_{22} = 0, \ \sigma_{12} = 0 \ .$$

Since the body forces are zero, the following form of the Airy stress function was considered,

$$\Phi = \sum_{n=1}^{\infty} \text{Cos } \beta_n X_2 [A \text{ Cosh } \beta_n X_1 + D\beta_n X_1 \text{ Sinh } \beta_n X_1] + \frac{D_0 X_2^2}{2} \ . \tag{9}$$

Performing the necessary operations on equation (9), applying the boundary conditions to solve for the constants A and D, and selecting β_n equal to $n\pi/L$, one can arrive at the following solution for the stresses in the beam.

$$\sigma_{11} = \sum_{n=1}^{\infty} \left\{ \frac{2\sigma_{11}^{I}}{\beta_n L} \text{ Sin}\beta_n C \left[\frac{\text{Cosh}\beta_n X_1 (\beta_n H \text{ Cosh}\beta_n H + \text{Sinh}\beta_n H) - \beta_n X_1 \text{Sinh}\beta_n H \text{Sinh}\beta_n X_1}{\beta_n H + \text{Sinh } \beta_n H \text{ Cosh } \beta_n H} \right] \cdot (\text{Cos } \beta_n X_2) \right\} + \frac{\sigma_{11}^{I} C}{L} \tag{10}$$

$$\sigma_{22} = \sum_{n=1}^{\infty} \left\{ \frac{2\sigma_{11}^{I}}{\beta_n L} \text{ Sin}\beta_n C \left[\frac{(\beta_n X_1 \text{Sinh}\beta_n X_1 + 2\text{Cosh}\beta_n X_1)\text{Sinh}\beta_n H - \text{Cosh}\beta_n X_1 (\beta_n H \text{Cosh}\beta_n H + \text{Sinh}\beta_n H)}{\beta_n H + \text{Sinh } \beta_n H \text{ Cosh } \beta_n H} \right] \cdot (\text{Cos } \beta_n X_2) \right\} \tag{11}$$

$$\sigma_{12} = \sum_{n=1}^{\infty} \left\{ \frac{2\sigma_{11}^{I}}{\beta_n L} \text{ Sin}\beta_n C \left[\frac{(\beta_n X_1 \text{Cosh}\beta_n X_1 + \text{Sinh}\beta_n X_1)\text{Sinh}\beta_n H - \text{Sinh}\beta_n X_1 (\beta_n H \text{Cosh}\beta_n H + \text{Sinh}\beta_n H)}{\beta_n H + \text{Sinh } \beta_n H \text{ Cosh } \beta_n H} \right] \cdot (\text{Sin } \beta_n X_2) \right\} . \tag{12}$$

Equations (10), (11) and (12) were evaluated by summing the first 200 terms of the series to obtain the desired convergences of the solution (23). By dividing both sides of the equations (10), (11) and (12) by σ_{11}^{I}, the solution was obtained in dimensionless form.

To determine the effects of specimen geometry on the stress distribution, C was held constant, and H was varied such that the ratio of the width of the specimen to the length of loading (H/C) varied from 0.05 to 1.5.

2. Results

The results are plotted with the stress ratios on the ordinate and the geometric parameter (H/C) on the abscissa. Each family of curves, for each stress ratio, was plotted for a particular X_1/H distance along the X_1 axis with X_2/C as a parameter as shown in Figures 6 through 9. With the solution plotted in this form, the stress distribution can be determined for any H/C ratio for which $H/L \ll 1$. Figure 6a through 6d shows the following stress distribution in the specimen's test section for X_1/H equal to 0.0: a, $\sigma_{11}/\sigma_{11}^{I}$ vs. H/C; b, $\sigma_{22}/\sigma_{11}^{I}$ vs. H/C; c, $\sigma_{12}/\sigma_{11}^{I}$ vs. H/C; d, $(\sigma_{22} - \sigma_{11})/\sigma_{11}^{I}$ vs. H/C. Since the resolved shear stress is related to the stress difference $(\sigma_{22} - \sigma_{11})$, the specimen geometry that yields the largest region of uniform biaxial stress difference along with $\sigma_{12} = 0$ is the specimen geometry suited for the testing of the zinc single crystals. Therefore, only the stress difference and shear stress results are shown in Figures 7 through 9, for X_1/H equal to 0.5, 0.75 and 1.0, respectively. In examining the stress difference curves, it is observed that specimens with an H/C ratio equal to 0.25 have the largest region of uniform biaxial stress difference, i.e. $\sigma_{22} - \sigma_{11} = (1.02 \pm 0.02)\sigma_{11}^{I}$ over at least 80 percent of the specimen's test section. For H/C equal to 0.5, $\sigma_{22} - \sigma_{11}$ is equal to $(1.02 \pm 0.05)\sigma_{11}^{I}$ over 80 percent of the test section. As

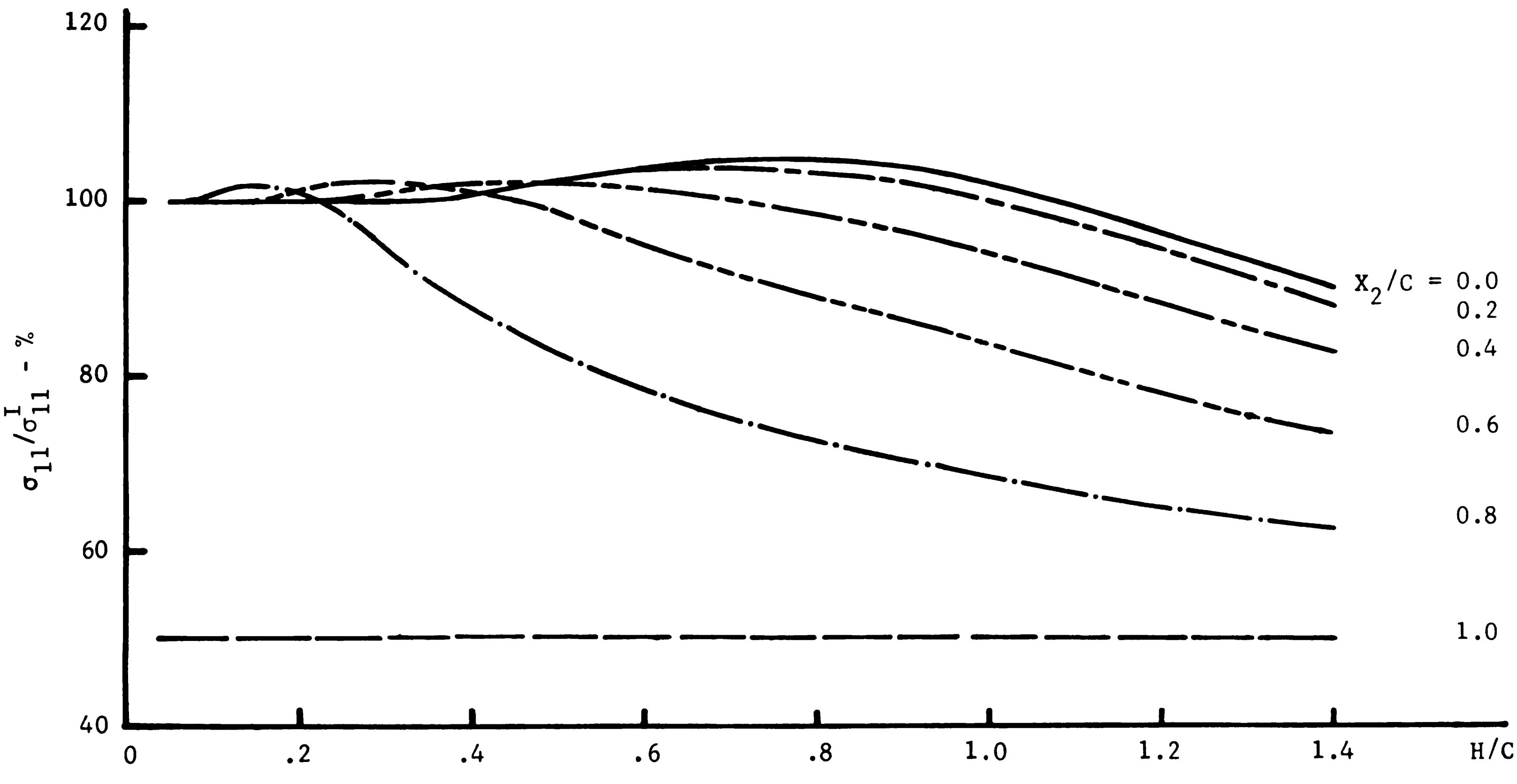

a. $\sigma_{11}/\sigma^{I}_{11}$ vs. H/C

Figure 6. Stress distribution in the test section of a finite rectangular beam for $X_1/H = 0.0$ and $H/L \ll 1$.

b. $\sigma_{12}/\sigma^I_{11}$ vs. H/C

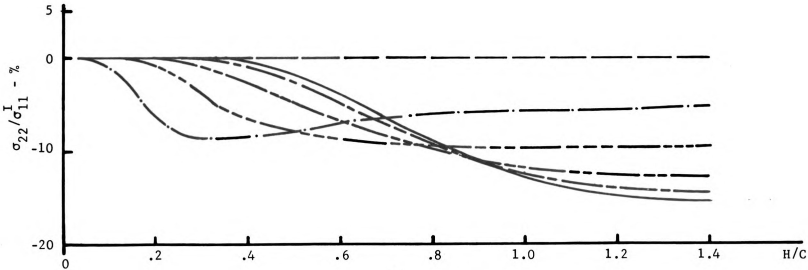

c. $\sigma_{22}/\sigma^I_{11}$ vs. H/C

Figure 6 (cont'd.)

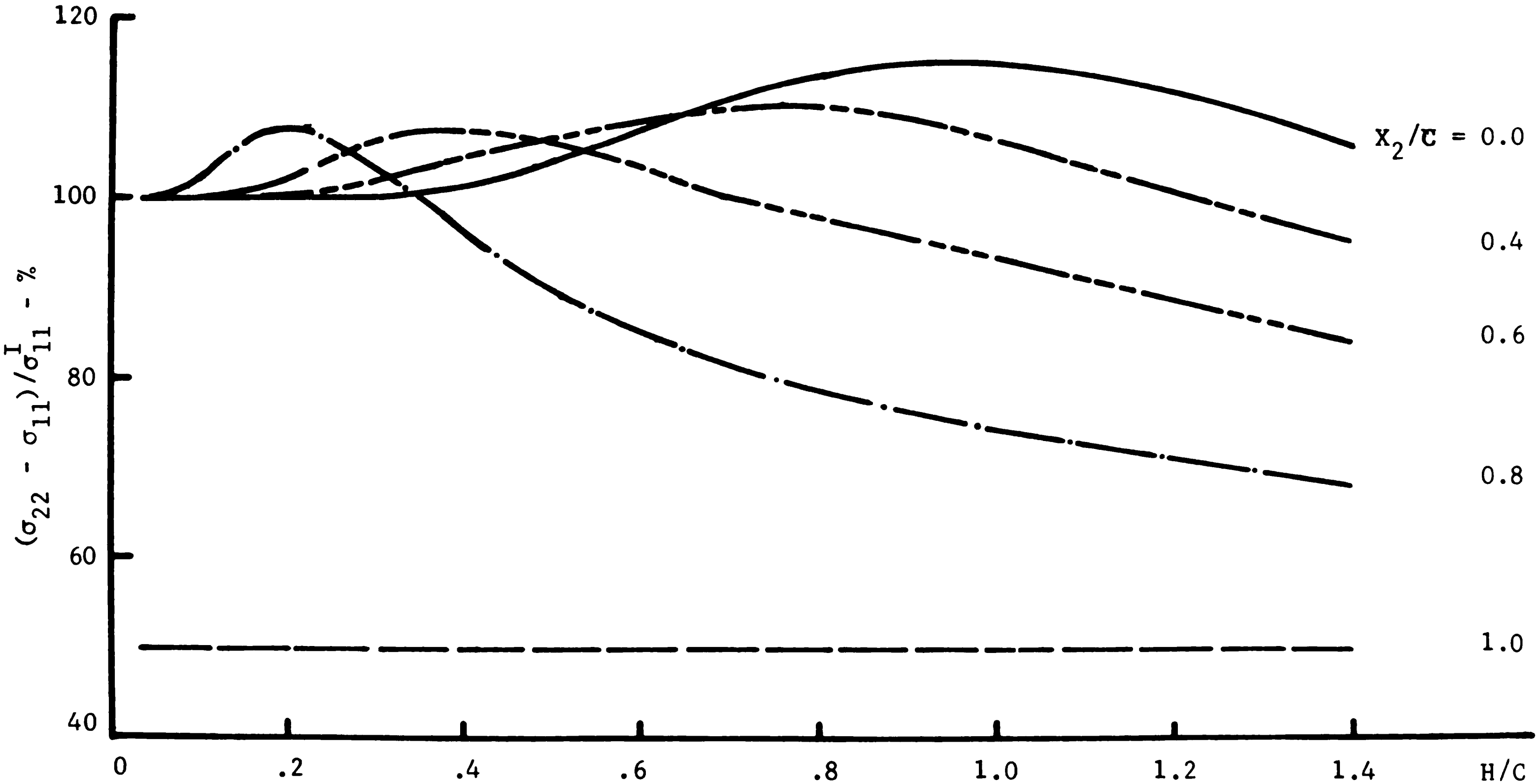

d. $(\sigma_{22} - \sigma_{11})/\sigma_{11}^{I}$ vs. H/C

Figure 6 (cont'd.)

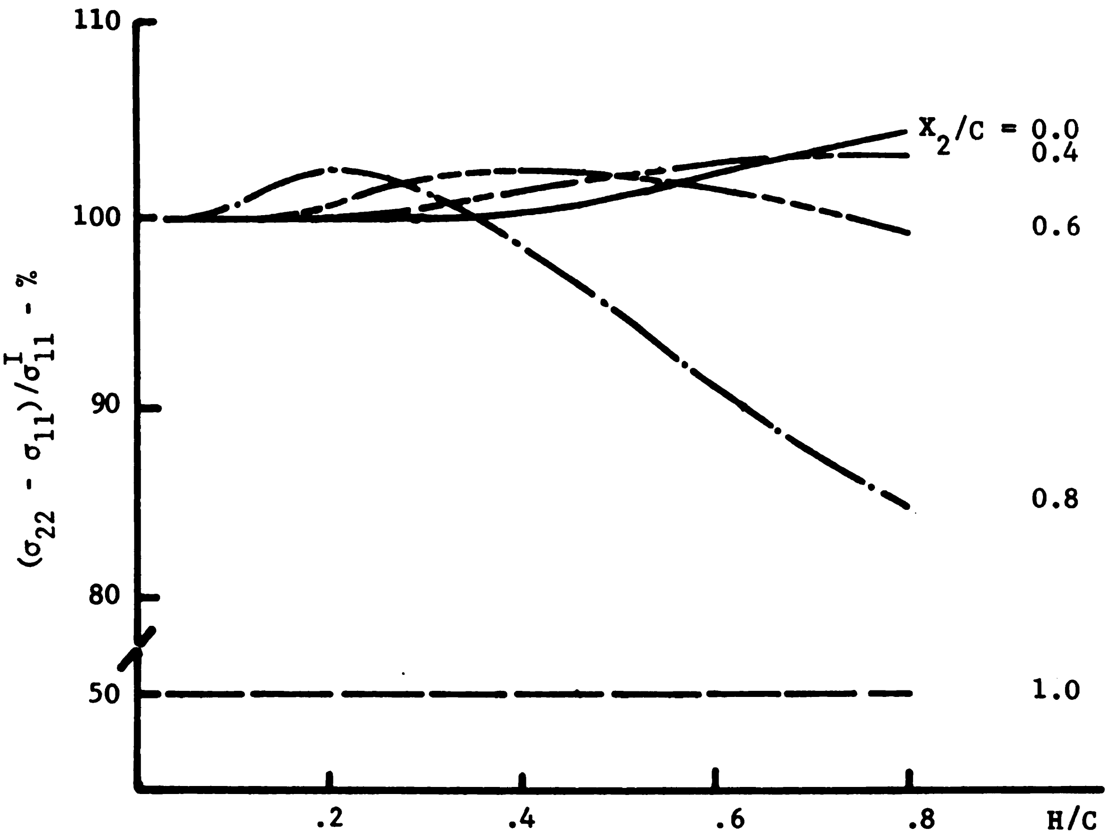

a. $(\sigma_{22} - \sigma_{11})/\sigma_{11}^{I}$ vs. H/C

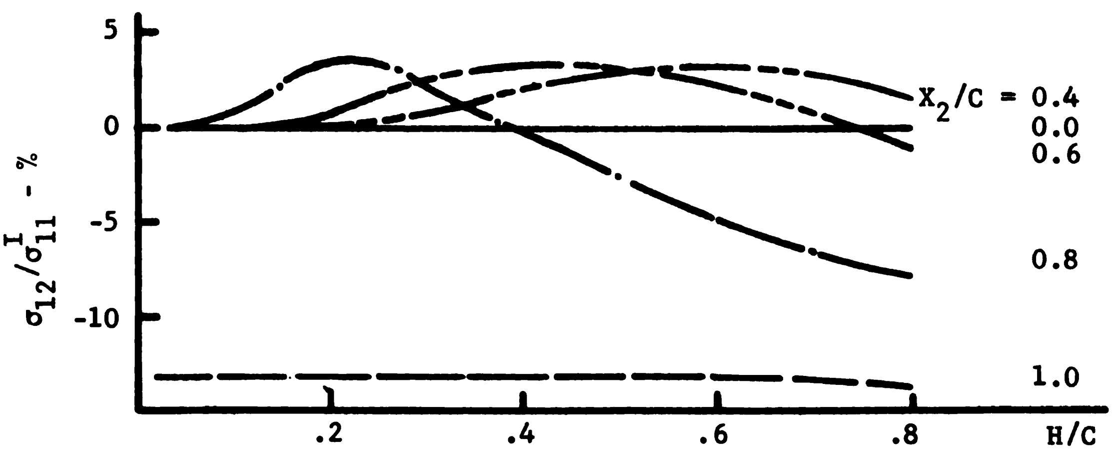

b. $\sigma_{12}/\sigma_{11}^{I}$ vs. H/C

Figure 7. Stress distribution in the test section of a finite rectangular beam for $X_1/H = 0.5$ and $H/L \ll 1$.

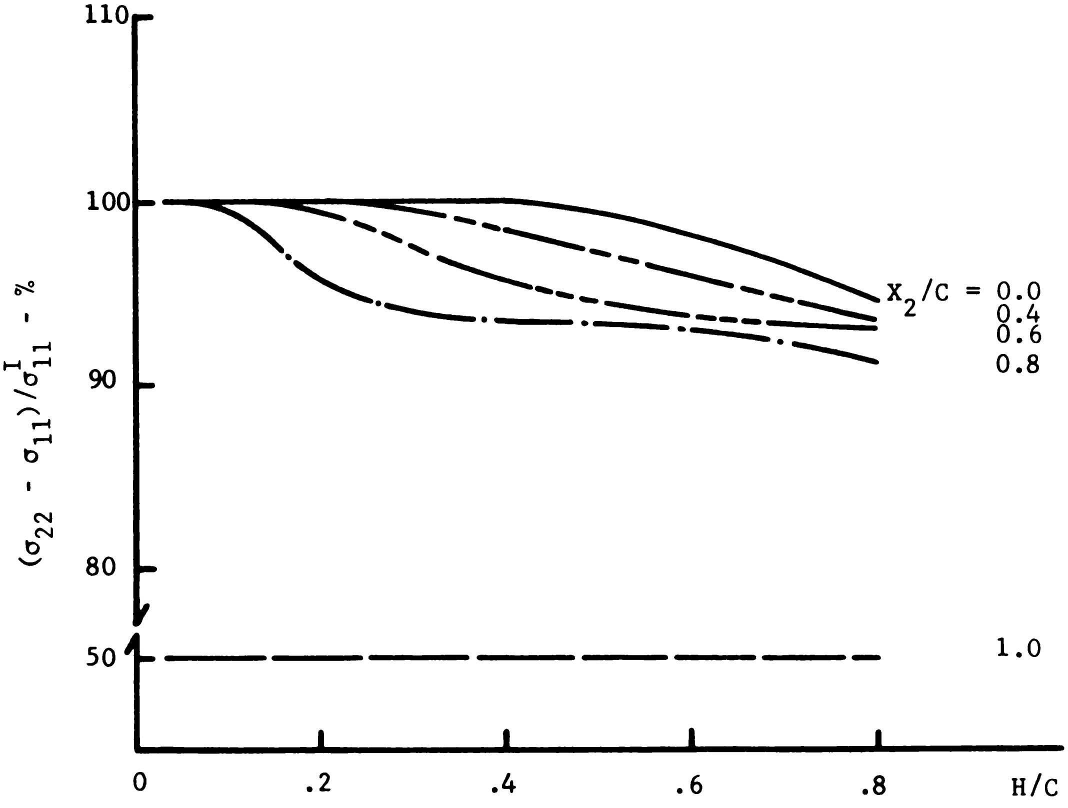

a. $(\sigma_{22} - \sigma_{11})/\sigma_{11}^I$ vs. H/C

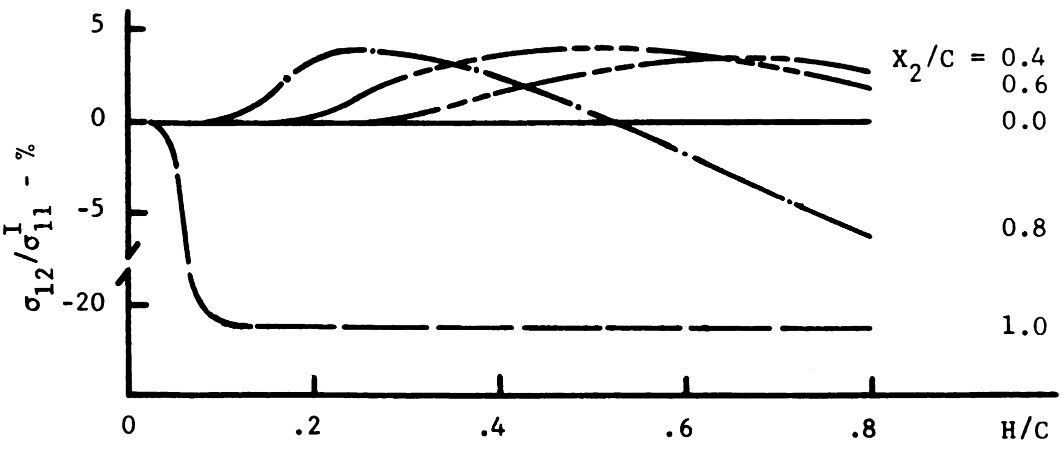

b. $\sigma_{12}/\sigma_{11}^I$ vs. H/C

Figure 8. Stress distribution in test section of a finite rectangular beam for $X_1/H = 0.75$ and $H/L \ll 1$.

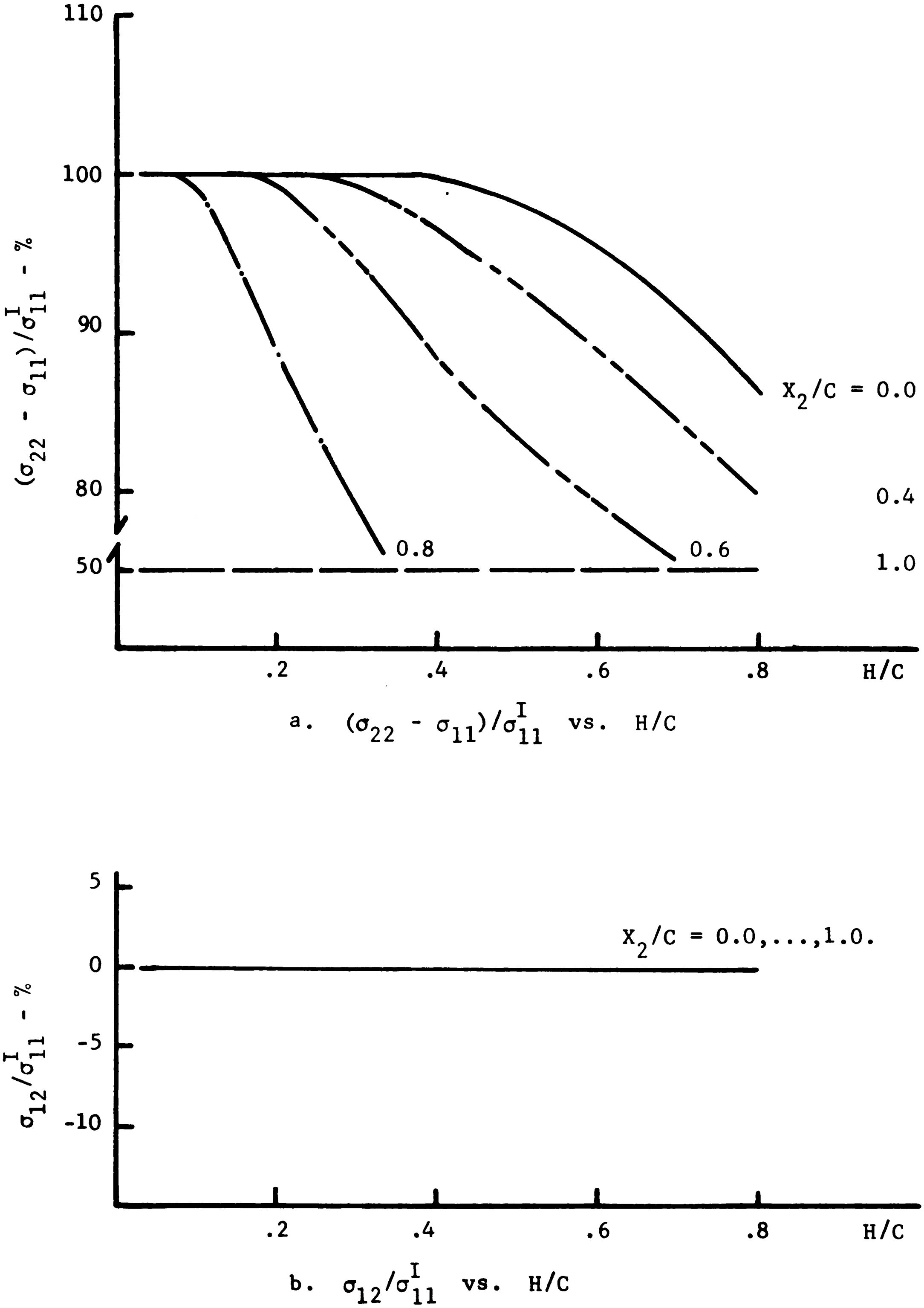

Figure 9. Stress distribution in the test section of a finite rectangular beam for $X_1/H = 1.0$ and $H/L \ll 1$.

H/C is increased above 0.5, the size of the uniform stress difference region steadily decreases. Therefore, for $\sigma_{22} - \sigma_{11}$ equal to $(1.02 \pm 0.05)\sigma_{11}^{I}$ over 80 percent of the central portion of the test section; the extreme limits of H/C were established to fall between 0.25 and 0.50. These limits allow one to subject a specimen to the largest region of uniform biaxial stress. Based on these results, the photoelastic specimens were made such that the stress distribution could be verified at the upper and lower limits of H/C.

B. Photoelasticity Investigation

The purpose of the photoelasticity investigation was to design rubber grips such that they would generate a uniform transverse normal stress at the bonded interface and to verify the specimen geometry suggested by the elasticity solution. Also, the lower experimental limit of H/C was to be established. The above were verified by demonstrating that the size and shape of the uniform biaxial stress region was the same as the elasticity solution for flat tensile specimens subjected to both transverse and biaxial loads.

Normal incidence was used to determine the principal stress difference $(\sigma_{II} - \sigma_{I})$ for all the tests. An oblique incidence study was attempted; but due to the large stress difference and the small value of σ_{I}, it was impossible to separate the stresses. This impossibility was verified by a calculation which showed that, for a one percent change in the oblique incidence fringe value, the principal stresses would have to change as much as 33 percent. Also, the elasticity solution showed a maximum change in the stress levels along principal axis of rotation of not more than 6 percent which would require the detection of less than 0.2 degrees rotation of the analyzer. This was less than the error band of the Tardy compensation method used to measure the fractional fringe orders.

Uniaxial tests with and without rubber grips were run to calibrate the modelling material and show that the rubber grips didn't reinforce the specimens, and photoelastic specimens were subjected to transverse and biaxial loads to design the rubber grips and to verify the elasticity solution.

The following equipment was used to test the models: a circular polariscope; a photodiode which was mounted on a X-Y scanner to sense the intensity of the light transmitted through the model; and a simple testing machine consisting of an 8 to 1 lever system to apply the longitudinal load, and a pulley system to apply the transverse load. The circular polariscope shown schematically in Figure 10 was equipped with a mercury light source. The camera shown to the right of the analyzer was used to project the image of the specimen onto the plane of the photodiode. The X-Y scanner allowed point by point determination of the fringe values for the entire test section. The output signal from the photodiode was observed on an oscilloscope. Then the fringe value was determined by rotating the analyzer to obtain the angle γ_m for which the intensity I was a minimum. The fringe value (N) was calculated by using the relationship, $N = n + \gamma_m/180$, where n is the value of the dark-field isochromatic fringe that is moved to the point of interest by a clockwise rotation of the analyzer. The error in determining the fringe value (24) was reduced to a minimum by reading the value of γ both before and after the minimum intensity, where the noise level was the

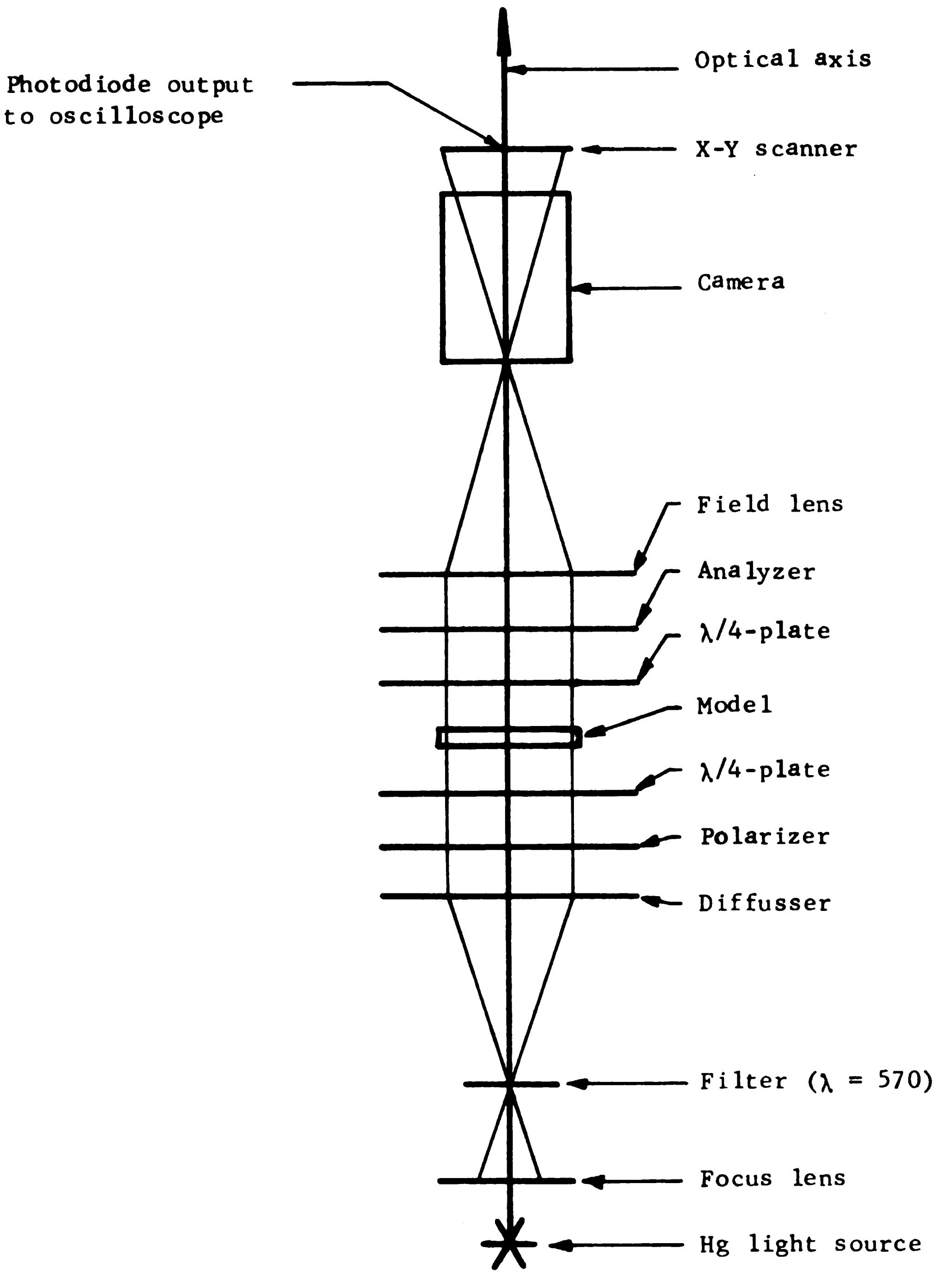

Figure 10. Circular polariscope (schematic).

lowest, see Figure 11. Then the following equation was used to determine γ_m, $\gamma_m = (\gamma_a + \gamma_b)/2$ where γ_a and γ_b are the angular values of γ before and after the minimum intensity, respectively, required to produce the same intensity I_0. Even though the time required to record all the data was considerable, the value of the first point determined at the start of the test didn't vary by more than $\pm$ 3 percent when checked at the end of the test. When the datum points had been taken, the principal stress difference was determined by $\sigma_{II} - \sigma_I = KN$, where K is the calibration constant for the material.

The lever arm friction of the testing machine, see Figure 12, was such that when a 3 gram load was applied, a shift in the fringe value could be detected. The load cell and its calibration curve are shown in Figure 13. The load cell was used to measure P_2 for the uniaxial tests and P_1 for the transverse and biaxial tests. P_2 for the biaxial tests was calculated by a static moment equation derived for the lever arm system. The load cell was capable of detecting 10 gram change in the load. Hence, the error in determining the values of the input loads was less than $\pm$ 0.5 percent.

The comparison of the unaxial results indicated that the rubber grips didn't reinforce the specimen. The transverse and biaxial test results were compared with the elasticity solution and found to agree to within $\pm$ 2 percent.

1. Specimen Details

The specimens were milled out of 1/8 inch thick sheets of photoelastic material, PSM-1, purchased from Photolastic Corporation.

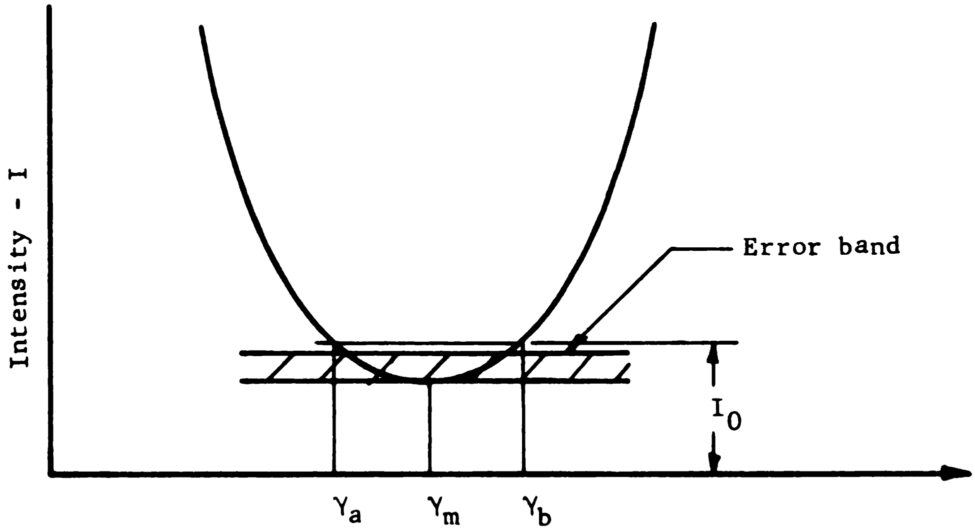

$$\gamma_m = (\gamma_a + \gamma_b)/2 \quad , \quad N = n + \gamma_m/180 \ .$$

Figure 11. Fractional fringe order determination.

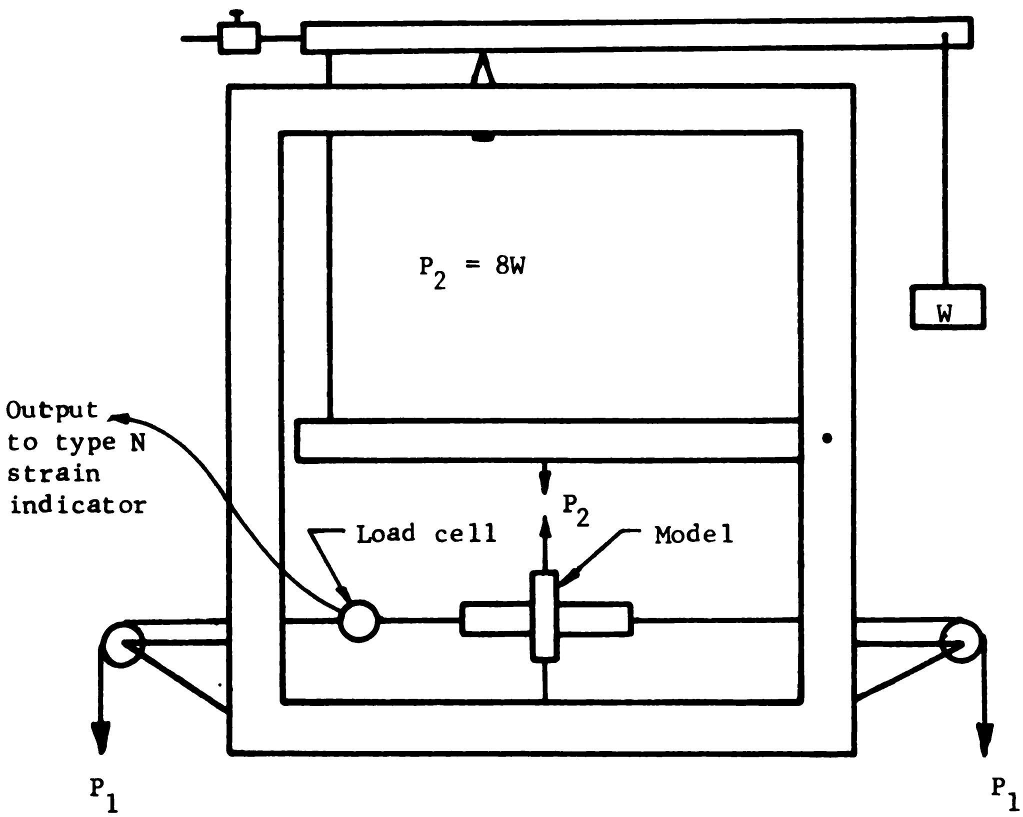

Figure 12. Loading frame for photoelasticity investigation.

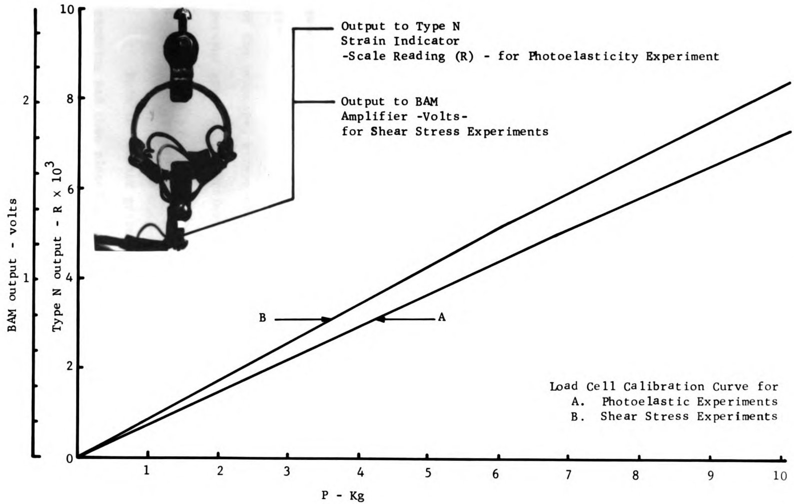

Figure 13. Load Cell and Load Cell Calibration Curves

The photoelastic models were made to specifications that would allow investigation of the upper and lower limits of H/C. These specimen dimensions are shown in Figure 14. Specimen A is for the lower limit of H/C, and specimen B is for the upper limit.

The selection of rubber for the rubber grips was based on: elastomer bonding index shown in Figure 15 (25, 26, 27), strength, and availability. The rubber selected on these basis was neoprene. The rubber grips were cut to the geometry shown in Figure 16 with the aid of the cutting jig shown in Figure 17a. The slits were cut at 1/8 inch intervals. This was the narrowest that the strips could be cut and still maintain a uniform cross section the full length of the strip. The slits were cut to within 0.035 inch of the grip end that was bonded to the specimen. Cutting the slits this close to the end effectively reduced the shear stresses at the bonded interface to zero. The results of not cutting the slits close enough to the bonded interface are shown in Figure 18. The rubber grips used to obtain these results were slit to within 1/8 inch from the bonded interface. This resulted in the uniform biaxial stress region and the maximum value of the principal stress differences being 50 percent less and 25 percent greater, respectively, than that of the elasticity solution.

2. Specimen Preparation

Both the rubber grips and the specimen were given a thorough cleaning and then placed in a furnace to remove any moisture from the surfaces to be bonded. Next, the bond surfaces were cleaned abrasively to roughen the surfaces and then wiped clean with acetone. The cleaning of the bond surfaces with acetone just prior to the application

Dimensions (inches)

Specimen	2C	D	E	2H	2L	R	T	H/C
A	1	1 1/2	3/4	1/4	4	1/2	1/8	0.25
B	1	1 1/2	3/4	1/2	4	1/2	1/8	0.50

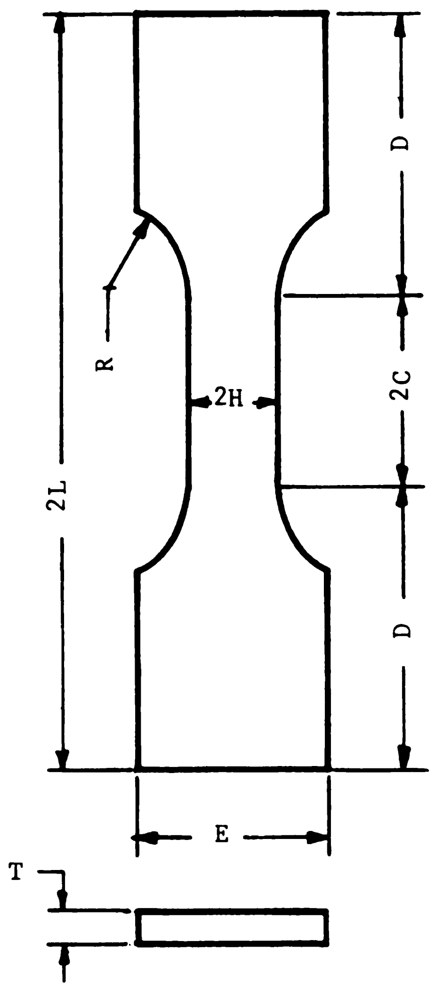

Figure 14. Photoelasticity specimen details

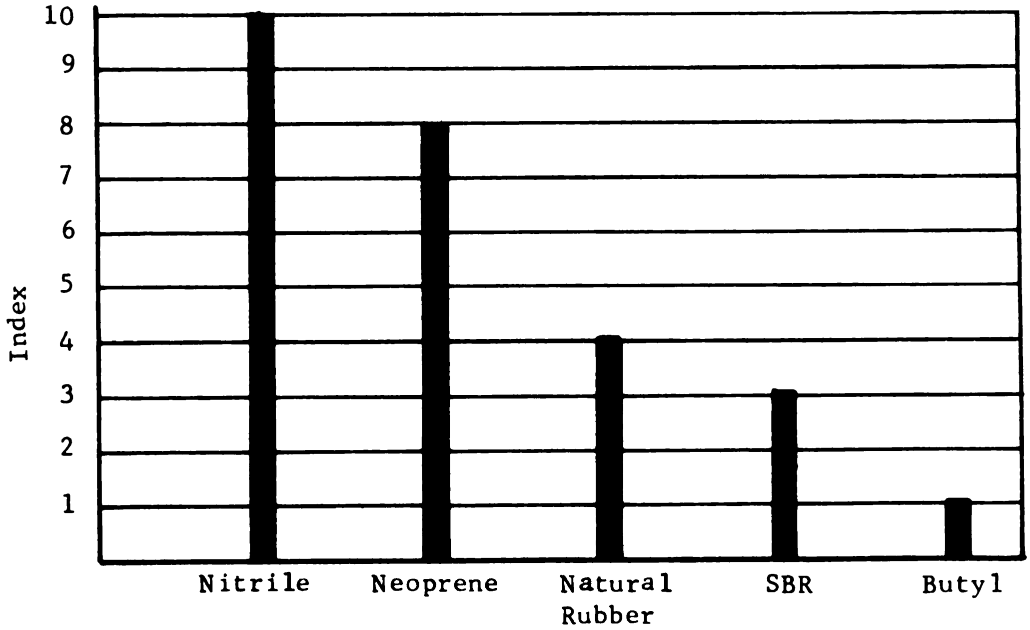

Figure 15. Bondability index of common elastomers (25).

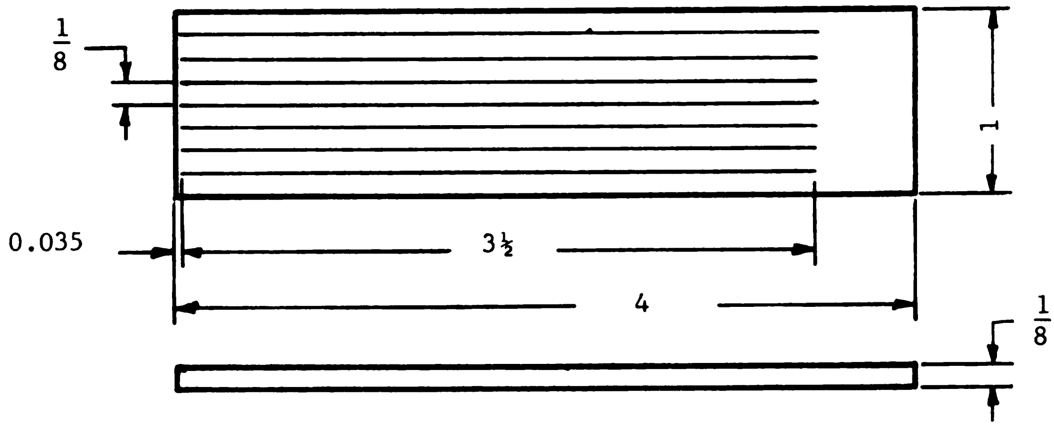

Rubber grip details

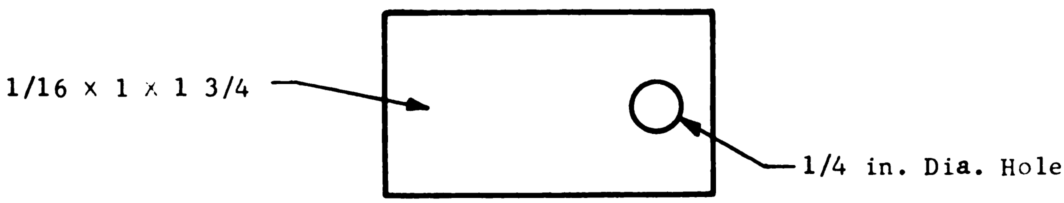

Aluminum end for rubber grip details

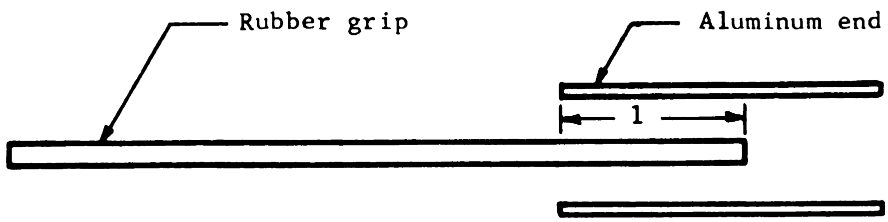

Rubber grip assemble

Figure 16. Rubber grip details

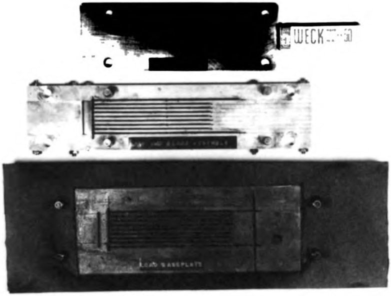

Figure 17a. Rubber grip cutting jig.

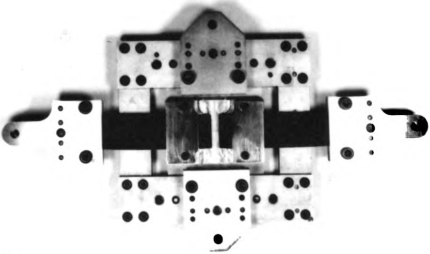

Figure 17b. Gluing jig for photoelastic specimen.

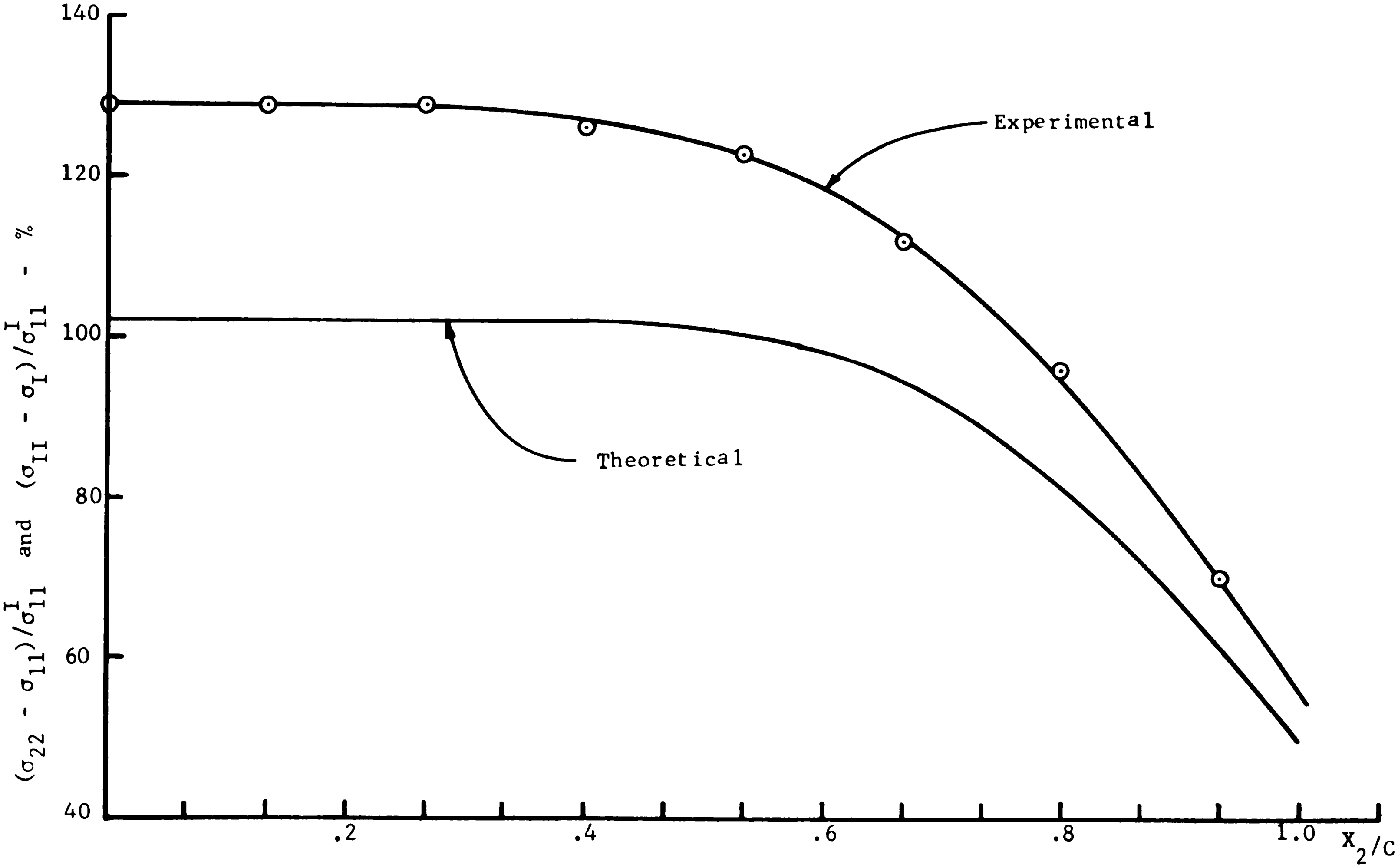

Figure 18. Effect of rubber grip slits on the stress distribution in a finite rectangular beam. Slits cut to within 1/8 inch of bonded interface.

of the adhesive was necessary to remove the abraded particles and to soften the surface of the photoelastic material. This softening of the photoelastic material insured a strong rubber to plastic bond. Next, the bond surfaces were sparingly coated with Chemlok 305 two part epoxy based adhesive (28) and aligned with the aid of the gluing jig shown in Figure 17b. Then the entire assembly was placed in a furnace at 120°F to cure. The full strength of the bond was developed after about 24 hours curing time. The final step in the specimen preparation was to apply a fine opaque cross to mark the center of the test section. When this cross was moved over the photodiode, the intensity of the transmitted light dropped approximately 20 percent. This made it possible to accurately locate the center of the model and still determine the fringe value at that point.

3. Testing Procedure

The prepared specimen was positioned in the testing machine and preloaded. After the specimen temperature distribution due to handling had equilibrated, the specimen alignment was checked with a laser and mirror system to be certain that the specimen was perpendicular to the optical axis of the circular polariscope. The optical elements in the circular polariscope were arranged such that the quarter-wave plates were crossed, and the polarizer and analyzer were crossed; i.e., a dark field arrangement. The quarter-wave plates were removed, and the principal stress directions were checked. Then, with the quarter-wave plates in position, the specimen was visually checked for bending.

The data was taken in the form of a matrix which covered one quadrant of the test section. The first row was taken parallel to the X_2 axis with X_1/H equal to zero. There were 9 equally spaced points taken along this line. The remainder of the matrix was made up of rows of data taken for X_1/H equal to 0.25, 0.5, 0.75 and 0.875. This made it possible to compare the size and shape of the photoelasticity solution with the elasticity solution.

4. Experimental Results

The results of the uniaxial tests are shown in Figure 19 in the form of a calibration curve for the photoelastic material. Both with and without rubber grips, the models yielded the same results. Therefore, the rubber grips didn't reinforce the specimen test section. The results of the transverse and biaxial tests are tabulated in Tables 1 through 3. Table 4 shows the theoretical shear stress distribution for H/C equal to 0.5. These tables represent one quadrant of the test section. The rows of the matrix are for X_1/H equal to 0.0, 0.25, 0.50, 0.75 and 0.875. The columns are at the positions X_2/C designated in the tables. The tabulated values represent $(\sigma_{II} - \sigma_I)\sigma_{11}^I$ for the photoelasticity solution and $(\sigma_{22} - \sigma_{11})/\sigma_{11}^I$ for the elasticity solution. Each row is made up of two rows of values. The values above the line are for the experimental results, and those values below the line are for the elasticity solution. This made it easy to compare the two solutions. When comparing the solution, one must remember that $(\sigma_{II} - \sigma_I) = (\sigma_{22} - \sigma_{11})$ is only true when σ_{12} is zero, and σ_{22} and σ_{11} can be considered principal stresses.

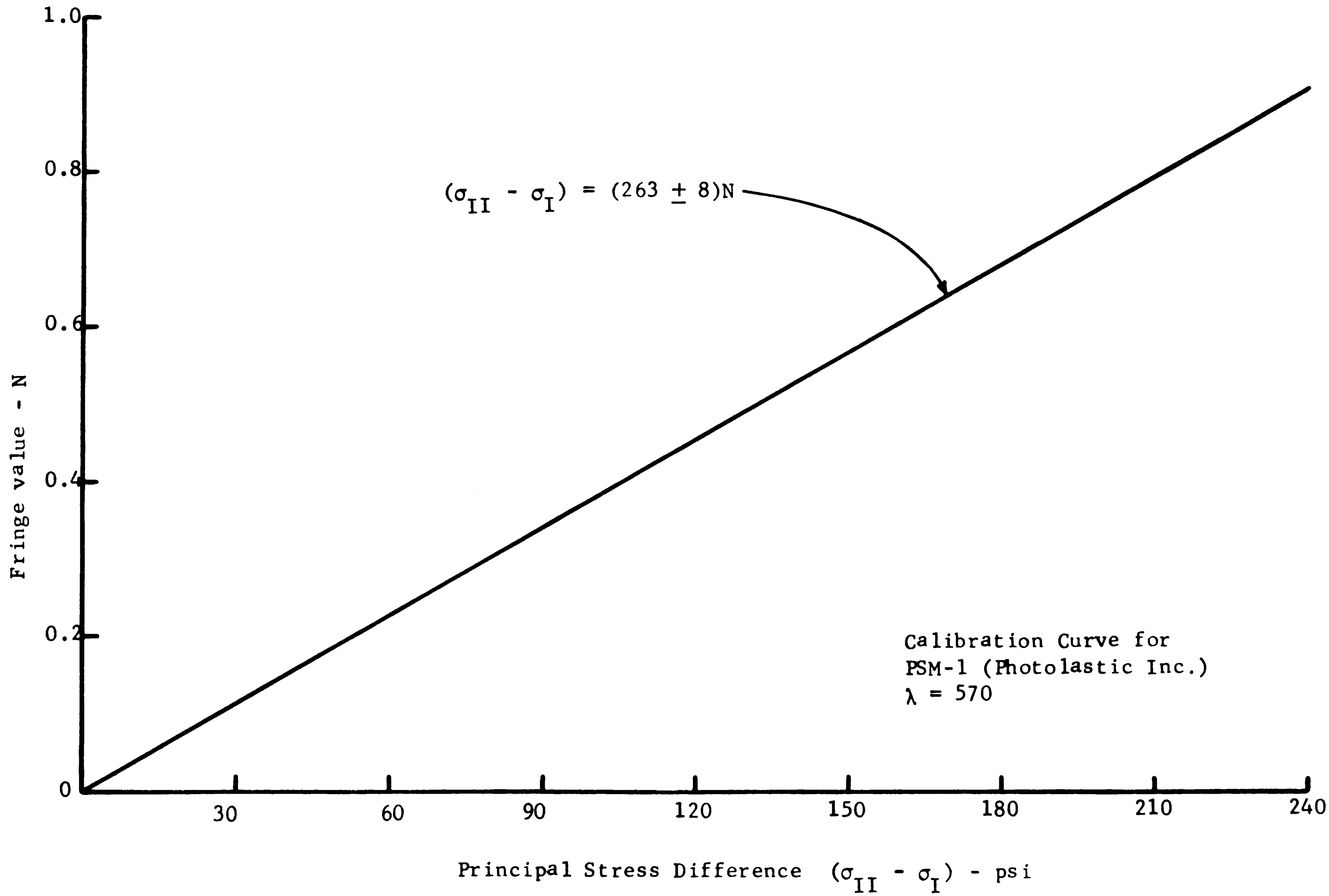

Figure 19. Calibration curve for photoelastic modelling material.

The results of loading specimen A in the transverse direction are tabulated in Table 1. The solutions agree along the center line of the specimen. But the experimental solution away from the centerline of the specimen fluctuates above and below the theoretical results, because the specimens test section is too narrow for the 1/8 inch thickness of the specimen. Therefore, this specimen geometry is experimentally impractical for use in the shear stress experiments.

The results of loading specimen B in the transverse direction are tabulated in Table 2, and the results of loading specimen B biaxially are tabulated in Table 3. Here the solutions agree throughout the entire test section. Table 4 is the elasticity solution of $\sigma_{12}/\sigma_{11}^{I}$ for sepcimen B loaded transversely. This indicates that the shear stress throughout the entire central portion of the test section is less than $\pm$ 5 percent of σ_{11}^{I}. Since the solutions agreed where the shear stress was zero, one can safely say that the elasticity and photoelasticity solutions agree to within $\pm$ 2 percent for the size and shape of the uniform biaxial stress field, and that the rubber grips did generate a uniform normal surface traction at the bonded interface for H/C equal to 0.5. Also, by comparing the transverse and the biaxial results of specimen B, it is observed that even when the rubber grips are subjected to a load the specimen test section isn't reinforced.

C. Discussion of Results

The loading configuration design was established to be a flat tensile specimen subjected to both axial and transverse loads. The transverse loads were applied by adhering slitted rubber grips to

Table 1. Results of Loading Photoelastic Specimen A in Transverse Direction

x_1/H										
0.875		1.08	1.02	0.88	1.11	1.18	1.12	1.10	1.17	0.70
0.750		1.15	1.08	1.06	1.08	1.15	1.05	1.02	0.95	
		1.00	1.00	1.00	1.00	1.00	0.98	0.95	0.86	
0.500		1.05	0.98	1.02	1.02	1.04	1.00	1.04	0.86	0.60
		1.00	1.00	1.00	1.00	1.01	1.02	1.02	0.86	0.50
0.250		1.03	1.09	1.09	1.02	1.02	1.06	0.99	0.64	0.49
		1.00	1.00	1.00	1.00	1.02	1.04	1.05	0.82	0.50
0	(Expr.)	1.02	0.97	1.02	1.04	1.04	1.05	1.05	0.81	0.55
	(Theo.)	1.00	1.00	1.00	1.01	1.02	1.05	1.05	0.80	0.50

x_2/C: 0, 0.2, 0.4, 0.6, 0.8, 1.0

Table 2. Results of Loading Photoelastic Specimen B in Transverse Direction

X_1/H									
0.875	1.11	1.04	1.11	1.02	1.07	1.06	0.89	0.97	0.80
0.750	1.03	0.98	1.01	1.01	1.04	1.03	0.92	0.79	0.67
	1.01	0.99	0.97	1.00	0.94	0.94	0.98	0.80	0.50
0.500	1.02	1.01	1.02	1.05	1.07	1.03	0.92	0.70	0.58
	1.02	1.01	1.02	1.03	1.02	1.01	0.95	0.75	0.50
0.250	1.06	1.05	1.06	1.08	1.08	1.02	0.89	0.66	0.54
	1.03	1.03	1.05	1.06	1.06	1.02	0.92	0.69	0.50
0	1.05	1.05	1.06	1.07	1.07	1.01 (Expr.)	0.88	0.64	0.55
	1.04	1.04	1.05	1.07	1.07	1.02 (Theo.)	0.90	0.68	0.50

0 0.2 0.4 0.6 0.8 1.0

X_2/C

Table 3. Results of Loading Photoelastic Specimen B Biaxially

x_1/H									
0.875	1.06	1.09	1.14	1.00	1.18	1.19	1.27	1.10	0.61
0.750	1.03	1.03	1.03	1.03	1.04	1.03	0.98	0.86	0.61
	1.01	0.99	0.97	1.00	0.94	0.94	0.98	0.80	0.50
0.500	1.03	1.04	1.03	1.02	1.01	1.01	0.88	0.73	0.60
	1.02	1.01	1.02	1.03	1.02	1.01	0.95	0.75	0.50
0.250	1.03	1.03	1.04	1.03	1.03	1.01	0.91	0.63	0.56
	1.03	1.03	1.05	1.06	1.06	1.02	0.92	0.69	0.50
0	1.05	1.04	1.05	1.05	1.05	1.00 (Expr.)	0.87	0.63	0.54
	1.04	1.04	1.05	1.07	1.07	1.02 (Theo.)	0.90	0.68	0.50

0 0.2 0.4 0.6 0.8 1.0

x_2/C

Table 4. Theoretical Shear Stress Distribution for Transverse Loading - H/C = 0.5

x_1/H									
1.00	0.0	0.0	0.0	0.0	0.0	0.0	0.0	0.0	0.0
0.75	0.0	0.0	0.03	0.03	0.04	0.05	0.0	-0.12	-0.17
0.50	0.0	0.01	0.02	0.03	0.03	0.02	-0.03	-0.10	-0.13
0.25	0.0	0.01	0.01	0.02	0.02	0.01	-0.02	-0.05	-0.06
0	0.0	0.0	0.0	0.0	0.0	0.0	0.0	0.0	0.0

0 0.2 0.4 0.6 0.8 1.0

x_2/C

the edge of the specimen's test section.

An elasticity solution coupled with a photoelasticity investigation verified this loading configuration. The elasticity solution suggested that the geometrical limit (H/C) of the specimen should fall between 0.25 and 0.50 for a uniform biaxial stress region that covered approximately 80 percent of the specimen's test section. The biaxial stress difference in this uniform biaxial stress region was equal to 102 $\pm$ 5 percent of the input stress σ_{11}^{I}, i.e. $(\sigma_{22} - \sigma_{11}) = (1.02 \pm 0.05)\sigma_{11}^{I}$. The photoelasticity investigation established the geometry of the rubber grips to be 1/8 x 1 x 4 inches with slits at 1/8 inch intervals which were slit to within 0.035 inch of the bonded interface. Photoelastic models were made to specifications that would yield models for testing at the upper and lower limits of H/C. When the results of the photoelastic models subjected to transverse and biaxial loads with the rubber grips were compared with the elasticity solution, it was observed that the solutions at the upper limit of H/C agreed to within $\pm$ 2 percent throughout the entire region of uniform biaxial stress, but the lower limit proved to be experimentally impractical. Therefore, the dimensions of the zinc specimen were made to the same specification as the photoelastic models with H/C equal to 0.5 except for minor changes which enable the zinc single crystals to be grown. The details of these changes are covered in section A of Chapter III. Also, since the uniform biaxial stress region symmetrically covered 80 percent of the specimen's test section, the clip gage length for the clip gage to be used in the shear stress experiments was established at 0.8 inch and located symmetrically about the X_1 axis along the centerline of the specimen.

III SHEAR STRESS EXPERIMENTS

The elasticity solution and the photoelasticity investigation suggest that the zinc specimen for the shear stress experiments should have a geometric parameter, H/C, of 0.5 to obtain the largest region of uniform biaxial stress. The flat tensile specimen shown in Figure 20 meets these geometric requirements and still falls within the specimen size limit (maximum width of 3/4 inch) of the crystal growing furnace to be discussed in section A below.

The purpose of the shear stress experiments was to subject zinc single crystals to a uniform biaxial state of stress in order to determine the effect of the resolved normal stress on the critical resolved shear stress. This was accomplished by loading the single crystals with rubber grips in the manner described in the previous chapter. Since the crystals of an aggregate are subjected to a very complex stress field, the response of the crystals to biaxial loading may lead to a better understanding of the behavior of aggregates.

The specimen orientation was such that ϕ and Ψ were both 45 degrees. This choice of orientation was based on the following four reasons: (1) Jillson had the closest agreement with theory for this orientation, i.e. for a Schmid Factor ($\cos \phi \cos \Psi$) equal to 0.5; (2) One can easily determine the yield point for this orientation, because the easy-glide region of the stress-strain curve is nearly flat; (3) The yield strength is the lowest possible, therefore, one can vary σ_{11}/σ_{22} at yield over a larger range of values

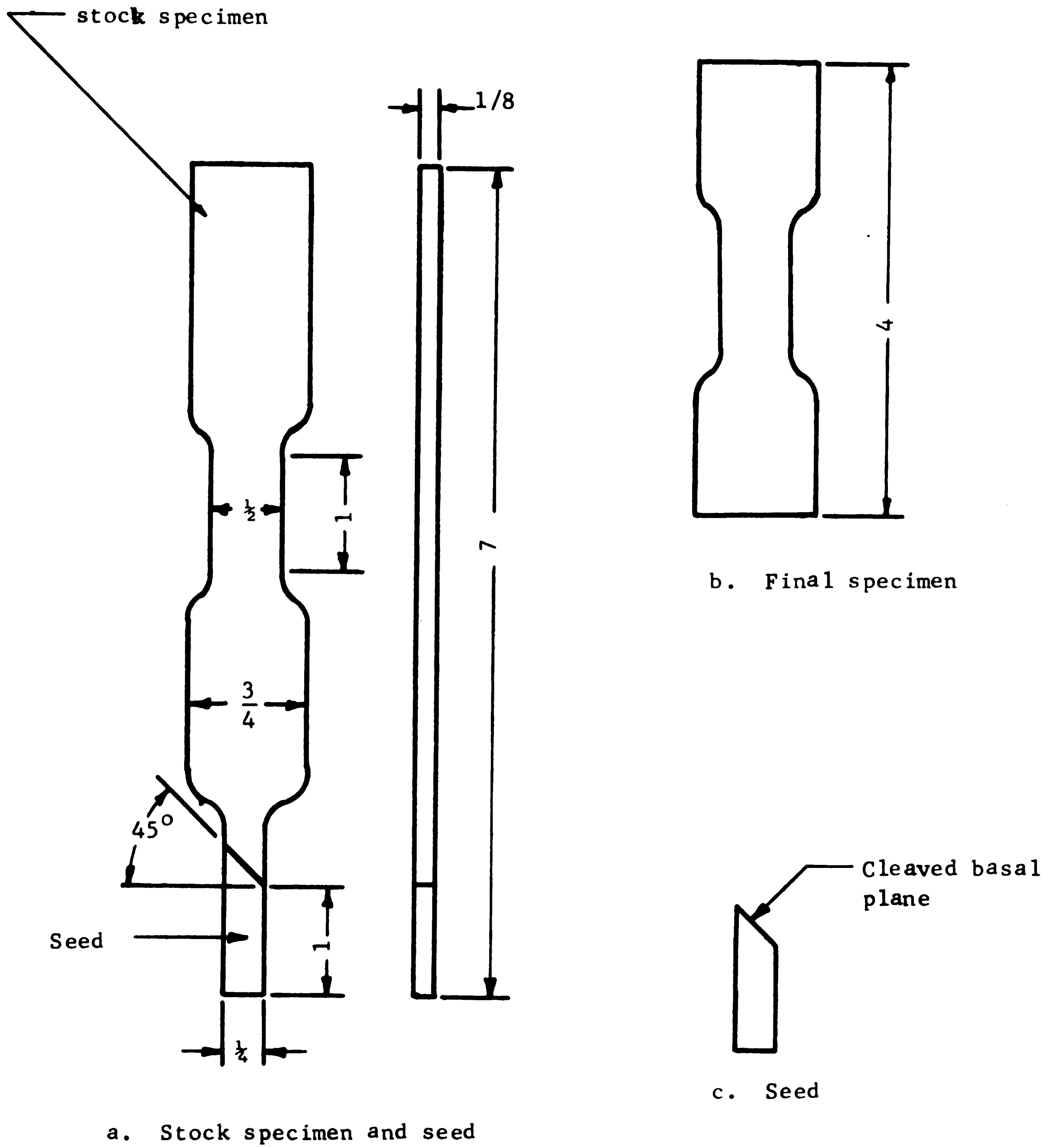

Figure 20. Zinc specimen details

than would be possible for a higher yield strength; and (4) Twinning won't occur for this orientation (29, 30, 31).

The approach in the crystal growth was to produce single crystals as nearly identical as possible, but not necessarily with a minimum τ_0. This was sucessfully accomplished and the details of crystal growth and handling procedure are given in section A and B below.

The shear stress experiments were carried out in uniaxial and biaxial tension. The uniaxial tension tests established the consistency of the CRSS, the negligible effect on the slip mechanism of gluing the rubber grips to the sides of the crystals, and the uniformity of the surface traction generated by the rubber grips. Specimens with and without rubber grips were tested with the load applied parallel to the tensile axis. To test the uniformity of the surface traction at the bonded interface, additional specimens were loaded in tension in the transverse direction and polished and etched to determine the uniformity of the slip throughout the test section. The result of the etching verified the existence of uniform slip. The biaxial tension tests required simultaneous application of P_1 and P_2. This was accomplished by a balance and pulley system coupled with an Instron. The details of the testing procedures are discussed in full in section C of the present chapter.

The results of the shear stress experiments show that for the uniaxial test τ_0 varied between 68 and 72 grams/mm^2. The results of the biaxial loading are plotted in Figure 53 where the resolved shear stress ratio at yield $(\sigma'_{12}|_y/\tau_0)$ is plotted as a function of the resolved normal stress to critical resolved shear stress ratio

$(\sigma'_{11}|_y/\tau_0)$ at yield. One can see that the experimental results fall well below the theoretical curve for $\sigma'_{11}|_y/\tau_0$ greater than 2. In conclusion, one could safely say that the resolved normal stress on the basal slip system does effect the CRSS of zinc single crystals. For a more detailed account of the results, see section D of the present chapter.

A. Crystal Growth

The specimen stock was machined from 1/4 inch thick strips sawed out of hexagonal ingots of high purity zinc (99.99+) purchased from Mattiessen and Hegeler Zinc Company. The specimen stock in Figure 20a was made long enough to yield the desired specimen size shown in Figure 20b. It was necessary to round all corners to prevent the nucleation of crystals of different orientation at these corners. The lower end (stem) of the specimen stock was machined at a 45 degree angle with respect to the tensile axis. Also, the seed was cleaved on the basal plane by chilling it in liquid nitrogen (31) which made it possible to obtain the exact orientation of the seed. The cleaved surface of the seed was then welded to the 45 degree surface of the stem with an acetylene torch using ammonium chloride as a flux. Both the specimen stock and seed were cleaned in dilute hydrochloric acid before and after welding. Next, the orientation of the seed with respect to the stock was checked by Laue' back-reflection. The stem was bent when necessary to obtain the correct orientation. Then the seed and seed end of the specimen were polished for 5 minutes in polishing solutions developed by Vreeland et al. (32) to remove dislocations introduced during handling and by sharp corners at the weld joint.

The seed end of the specimen was then placed in the slot of the lower thermal block (T_L) shown in Figure 21. The slot of the upper thermal block (T_U) was placed over the top of the specimen, and the alumina powder mixture was packed around the specimen through the openings in T_U. The thermocouples used to record the axial temperature gradient were positioned inside the crucible at the upper and lower thermal blocks as shown in Figure 22. This made it possible to control the solidus-liquidus interface at 3/8 $\pm$ 1/8 inch from the bottom of the seed. The packed crucible was then suspended by alumel wire such that the lower end of the seed was 2 inches below the top of the lower furnace as shown in Figure 23.

The furnace was preheated to the temperature necessary to melt the entire specimen except for the lower 3/8 inch of the seed. Then the soak period was set of 3 1/2 hours. This soak was required to obtain a uniform temperature distribution throughout the entire specimen. At the end of the soak period, the furnace was program cooled such that the crystal growth rate was 1 mm/min.; and at the same time, a constant axial temperature gradient was maintained. A typical axial temperature gradient, as recorded by the thermocouples in the crucible during soak, is as follows:

Upper thermocouple......490°C,

Lower thermocouple.....412°C.

B. Crystal Preparation

During all the specimen preparation, the specimens were transported by means of the holders shown in Figure 24. Holder A was

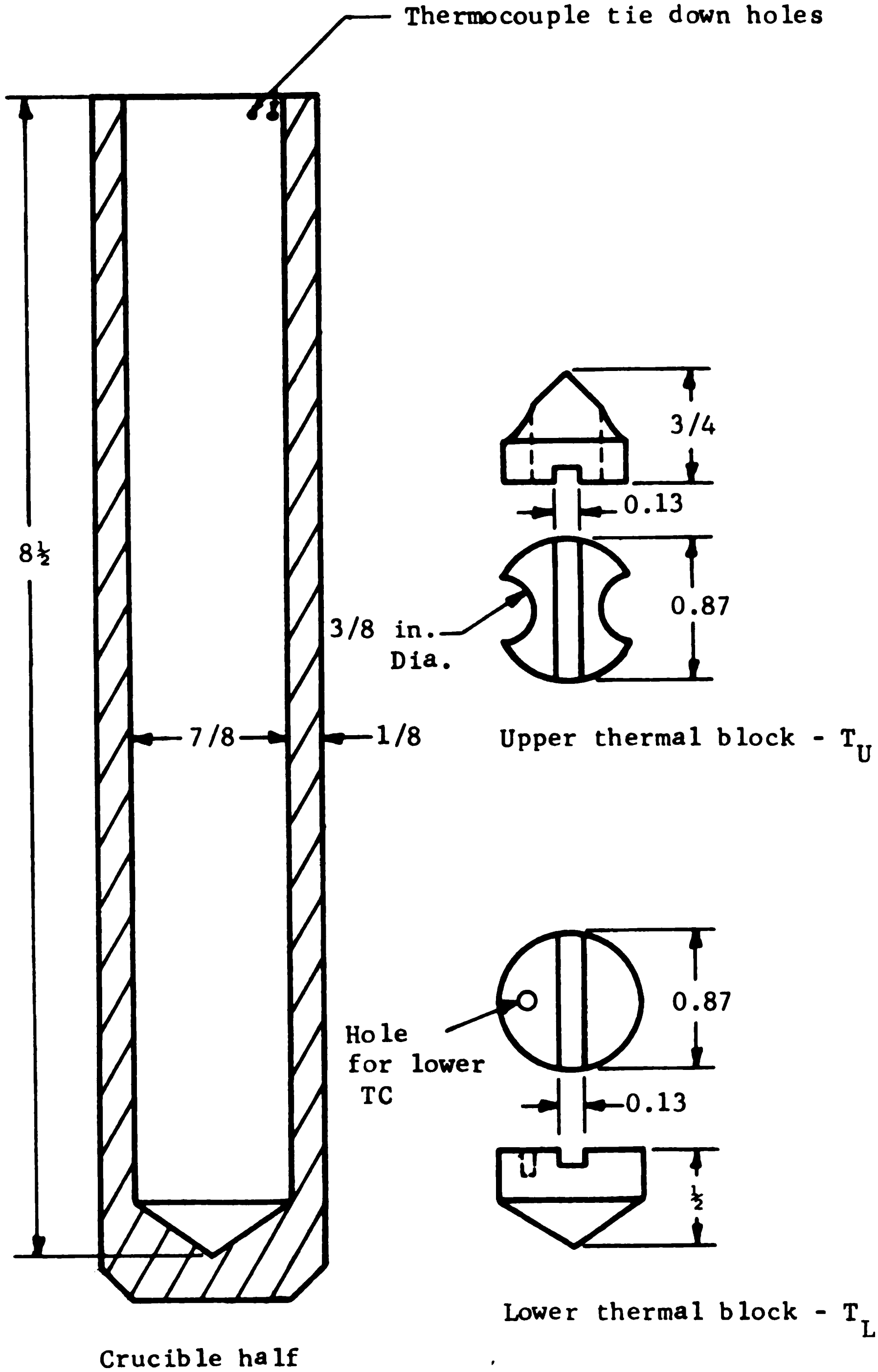

Figure 21. Crucible design

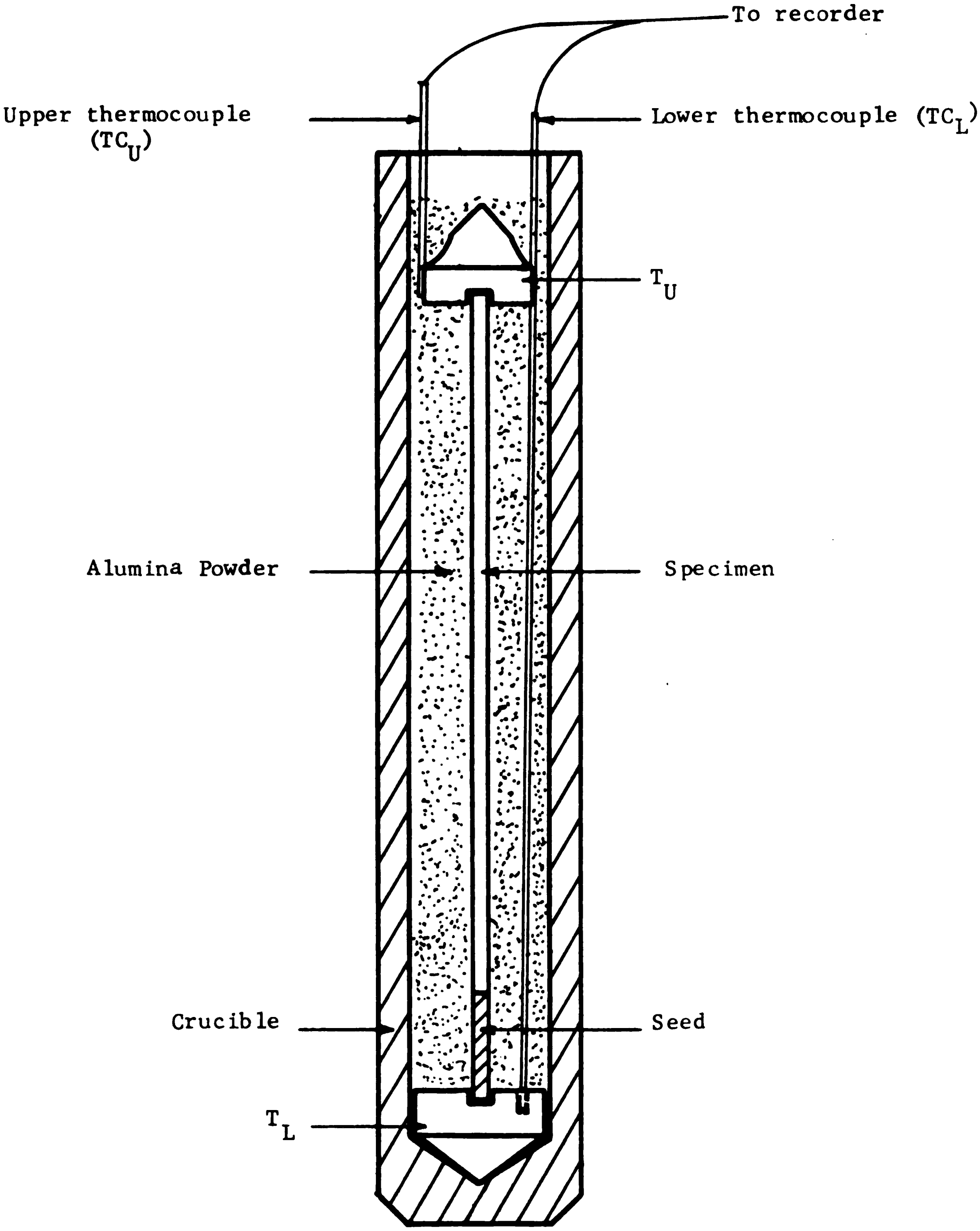

Figure 22. Specimen packed in crucible (schematic)

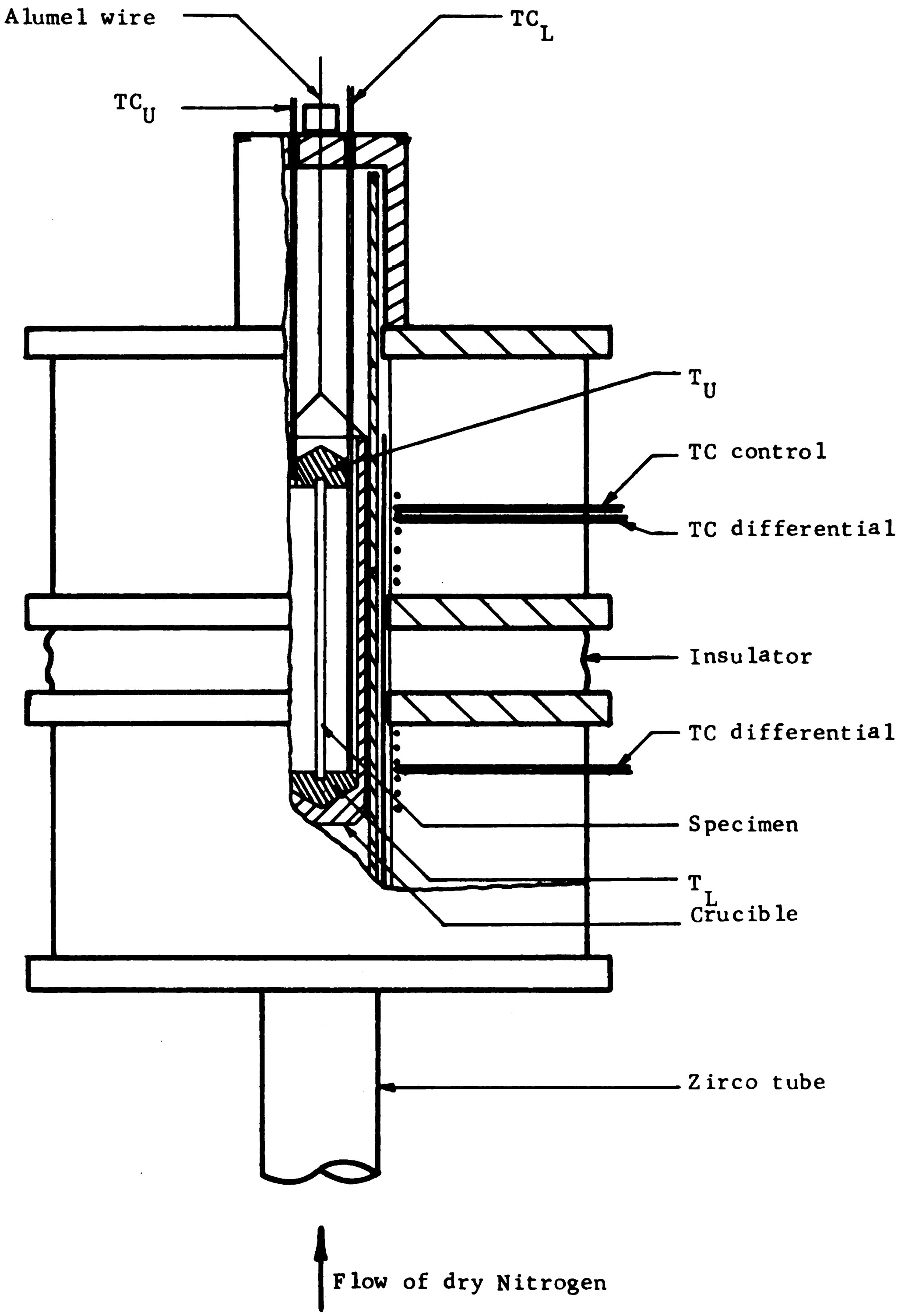

Figure 23. Crystal growing furnace (schematic)

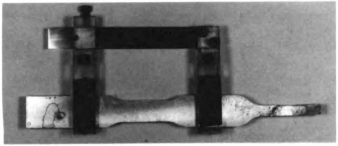

b. Holder A

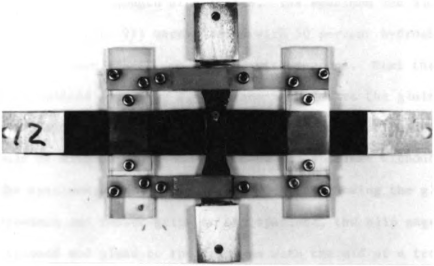

a. Holder B

Figure 24. Specimen holders

designed to hold the specimen during the X-ray of the specimen and the cutting of the specimen to length. Holder B was designed such that the remaining specimen preparation could be completed without the specimen ever being removed from the holder or handled directly. Both holders were made of plexiglas, and the specimens were held firmly in position with neoprene rubber pads. This handling precaution was taken to keep the specimen's dislocation density from increasing. Also, the holders protected the test section from accidental damage.

The crystal specimen was cleaned in concentrated hydrochloric acid and visually examined. Next the crystal was placed in holder A and x-rayed to insure that the crystal was a single crystal and of the correct orientation. The crystal and holder A were then positioned on the wire saw table as shown in Figure 25, and the specimen was cut to an overall length of 4 inches. The specimen and aluminum grips (shown in Figure 27) were cleaned with 50 percent hydrochloric acid, and the rubber grips were cleaned with acetone. Next the specimen was placed in holder B, and then fastened to the gluing jig as shown in Figure 26. The gluing jig was designed such that all the grips could be aligned and then adhered to the specimen without removing the specimen or holder B from the jig. Following the gluing of the aluminum and rubber grips to the specimen, the clip gage tabs were positioned and glued to the specimen with the aid of a traveling microscope. After the tabs had been cured in the furnace, the entire specimen was chemically polished for two minutes with solutions suggested by Vreeland et al. Then, the specimen was thoroughly dried with a hot air dryer, and the specimen dimensions were measured.

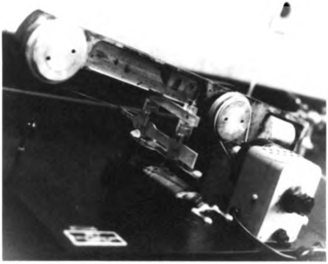

Figure 25. Wire saw

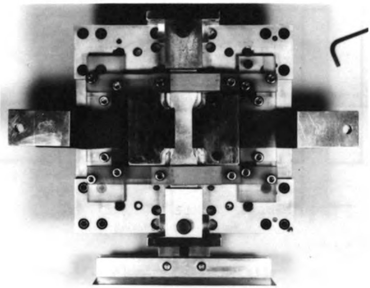

Figure 26. Gluing jig for zinc specimens

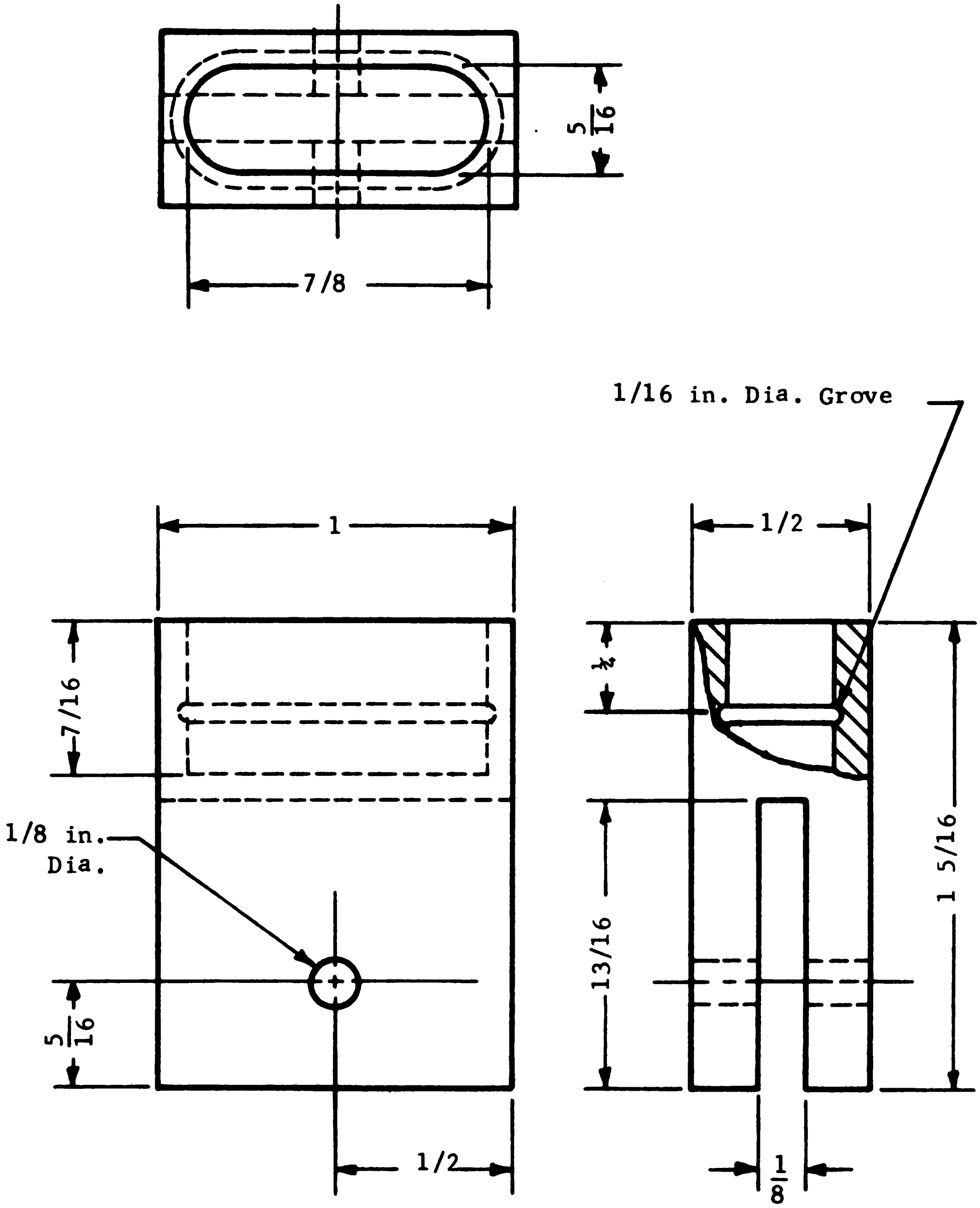

Figure 27. Aluminum grip details

Chemlok 305 two part epoxy based adhesive was used for adhering all the grips and clip gage tabs to the specimen. In all cases, the bonded joints were cured in a furnace for 8 hours at $120^{\circ}F$ to obtain the maximum bonding strength. The clip gage tabs were 1/16 Diameter X 3/32 eyelets purchased from United Shoe Division Machinery.

It is believed that the consistent growth procedures, the careful handling of the specimen, and the careful specimen preparation as described above were the reasons for the consistent results obtained in the shear stress experiments.

C. Testing Procedure

The prepared specimen and holder B were loaded into the testing machine, and all the grips were pinned to their appropriate loading links before the holder was removed. Then the clip gage was attached, and the specimen was preloaded with 200 grams. The sensitivity of the clip gage was such that one could sense a 5×10^{-5} in/in change in the gage length. Immediately following the preload, the subsequent loading was started with as little delay as possible. The strain rate in the specimen test section was 27×10^{-4} percent per second. In all the tests P_2 was applied with the Instron and P_1 with the pulley system shown in Figure 28. This pulley system was actuated by filling a 20 gallon bucket with water at a constant rate. P_1 was measured with the load cell shown in Figure 13, and the continuous P_1 vs. time curve was recorded on an X-Y recorder. The test equipment was calibrated just prior to running each test.

For the uniaxial tests, the load P_2 was applied with a constant crosshead speed of 0.02 cm/min. The specimens with the

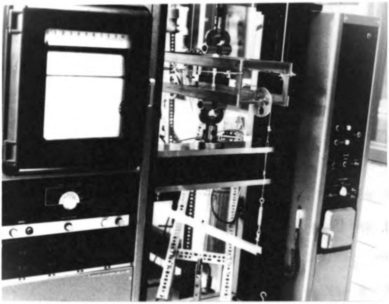

Front view

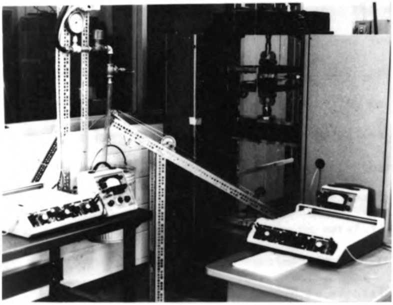

Back view

Figure 28. Biaxial testing machine

rubber grips glued to the edge of the test section were preloaded in the P_1 direction with 180 grams, before the axial load was applied. This kept the rubber grips aligned with the specimen so that there wasn't any bending stress applied to the test section. The P_2 vs. time curve was recorded on the Instron chart recorder, and P_2 vs. percent strain curve was continuously recorded on a X-Y recorder. The uniaxial transverse load was applied in the P_1 direction with the pulley system such that the strain rate in the test section was the same as the axial loading. The P_1 vs. time curve was recorded on an X-Y recorder, and the P_1 vs. percent strain curve was recorded on a second X-Y recorder.

The biaxial loading of the specimens required careful alignment of the Instron heads and the pulley system. It also required both axial and transverse preloading of the specimen. The effects of improper alignment and no preload on the simultaneous loading of the specimen are shown in Figure 29. A polycrystalline specimen was subjected to a biaxial load. Curve A shows a typical P_2 vs. time curve for proper prestress and alignment as recorded on the Instron chart recorder. Curve B is for improper alignment with correct prestress. Curve C is for no prestress with proper alignment. As can be seen from the above results, it is necessary to carefully align the equipment and properly prestress the specimen to insure the simultaneous loading of the specimen. It should be emphasized that the preloads were well below the load required for yielding.

Careful control of the loading was required to prevent negative straining (i.e. a negative elastic response caused by applying P_1 to fast.) and to prevent premature plastic deformation in

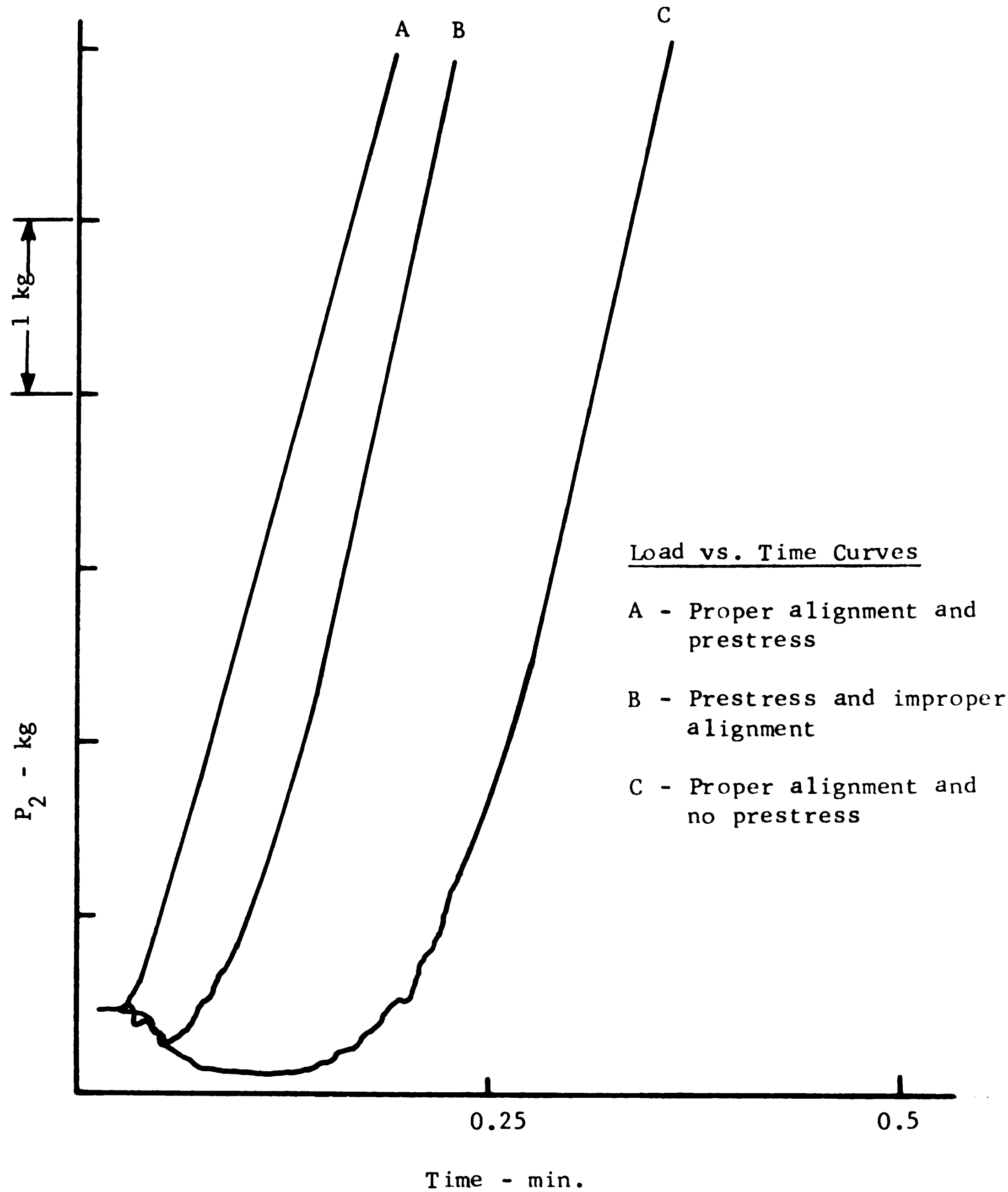

Figure 29. Effects of improper alignment and no prestress on biaxial loading of specimen.

the test section before P_1 was fully applied. If P_1 was applied too fast, the resulting negative strain has to be recovered before a positive resolved shear stress would result. Also, for large values of P_1, creep might occur. If P_1 was applied too slow, the test section would be plastically deformed by the axial load before P_1 was fully applied. But when the loads are applied simultaneously such that $\sigma_{11} < \sigma_{22}$ as shown in Figure 30, the creep doesn't occur, there is no negative strain to recover.

The single crystals were chemically polished and etched with Vreeland's solutions after they had been tested. Then they were examined on a Bausch and Lomb Research Metallograph. The etch pits revealed that the specimens yielded uniformly on the basal slip system throughout the entire uniform biaxial stress region of the test section. Figure 31 is a typical photomicrograph of uniform basal slip observed in the test section.

D. Shear Stress Results

All the single crystals with $\phi = \Psi = 45$ degrees were deformed under uniaxial and biaxial tension by $\{0001\}$ $\langle 2\bar{1}\bar{1}0 \rangle$ type slip. The deformation was stopped at one percent or less to save the specimens. The results of all the tests were plotted with the stress on the ordinate, and the strain on the abscissa.

The nominal stress-strain curve for the four uniaxial tests are plotted in Figures 32 through 34, and the resolved shear stress-strain curves are plotted in Figures 35 to 38. Test Numbers 2, 3, and 6 were run primarily for the purpose of testing the equipment. The crystals used were not good crystals; that is, the orientation

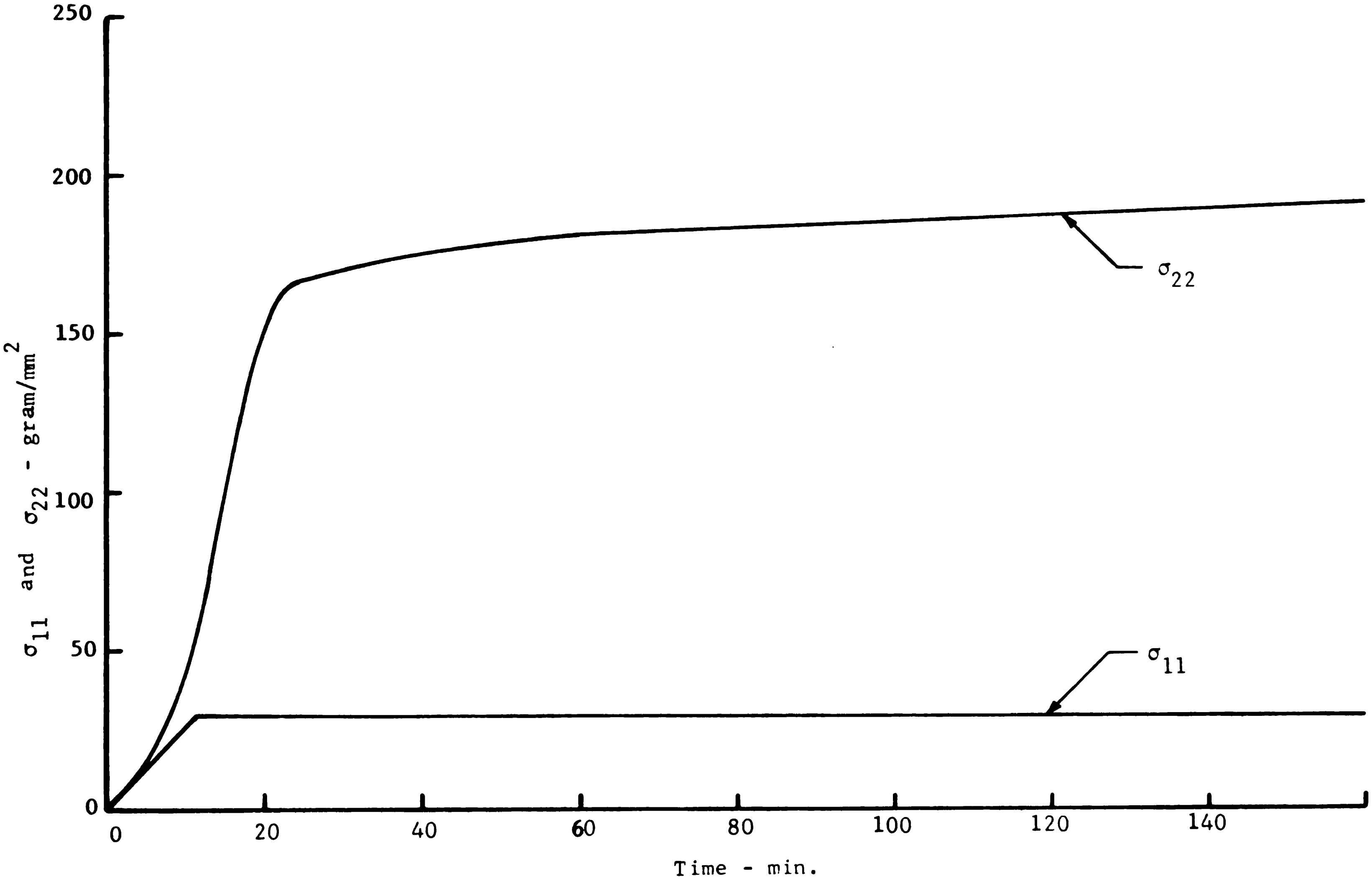

Figure 30. Typical nominal stress-time curve for biaxial loading of specimen.

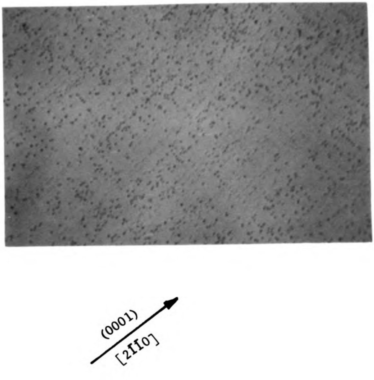

Figure 31. Photomicrograph of uniform slip in specimen test section.

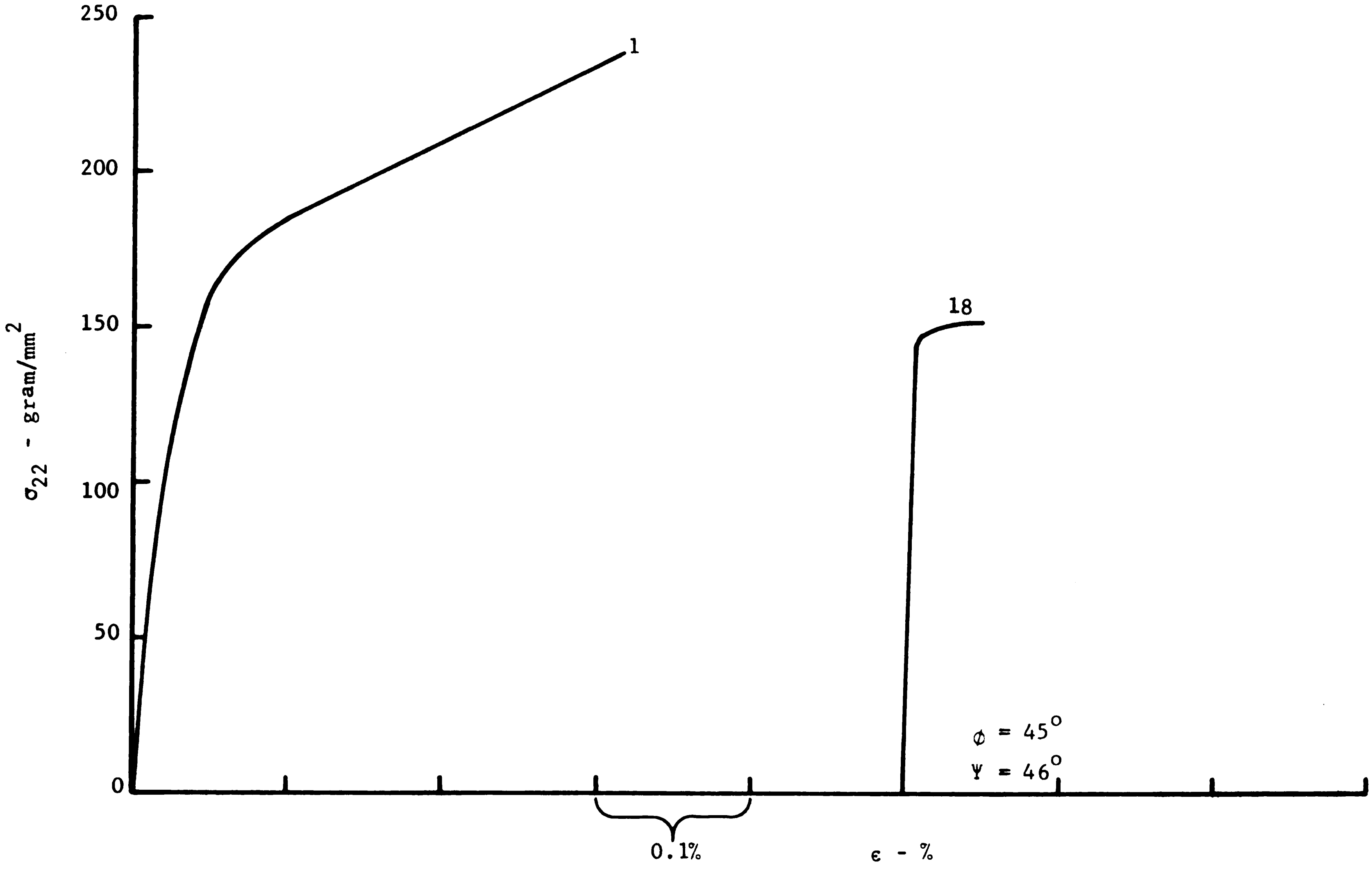

Figure 32. Nominal stress-strain curves Test No. 1 and 18.

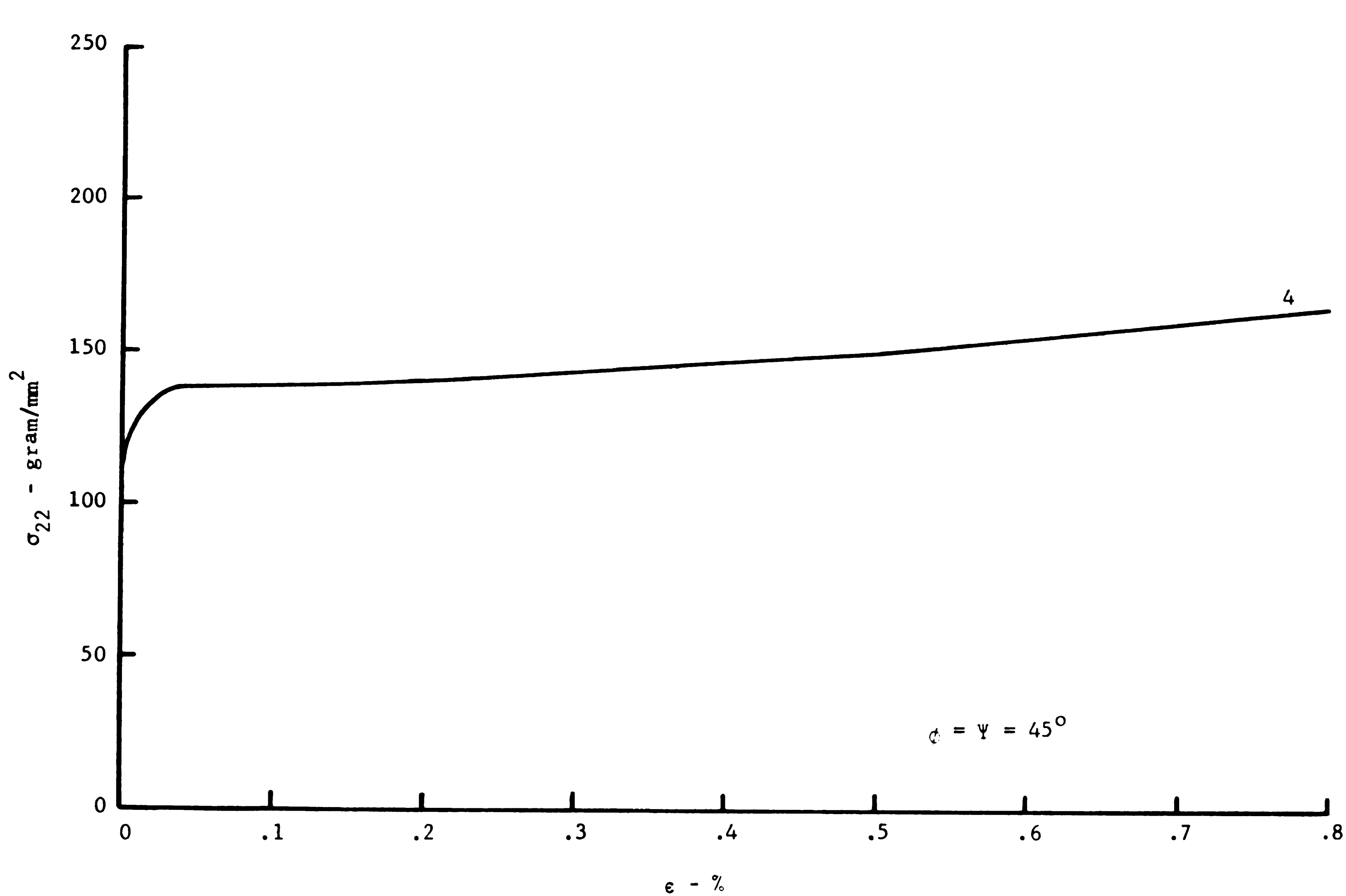

Figure 33. Nominal stress-strain curve Test No. 4

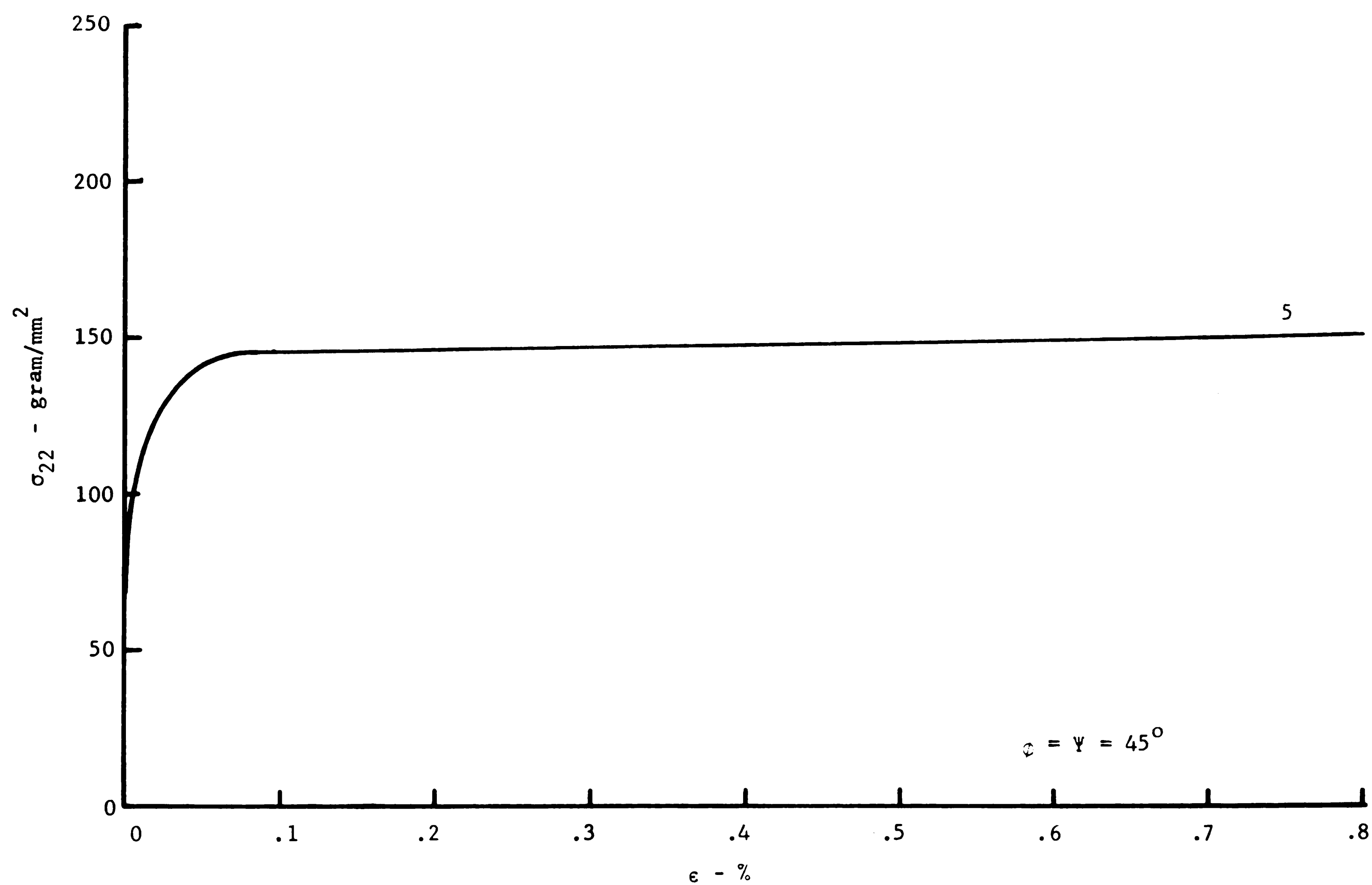

Figure 34. Nominal stress-strain curve Test No. 5

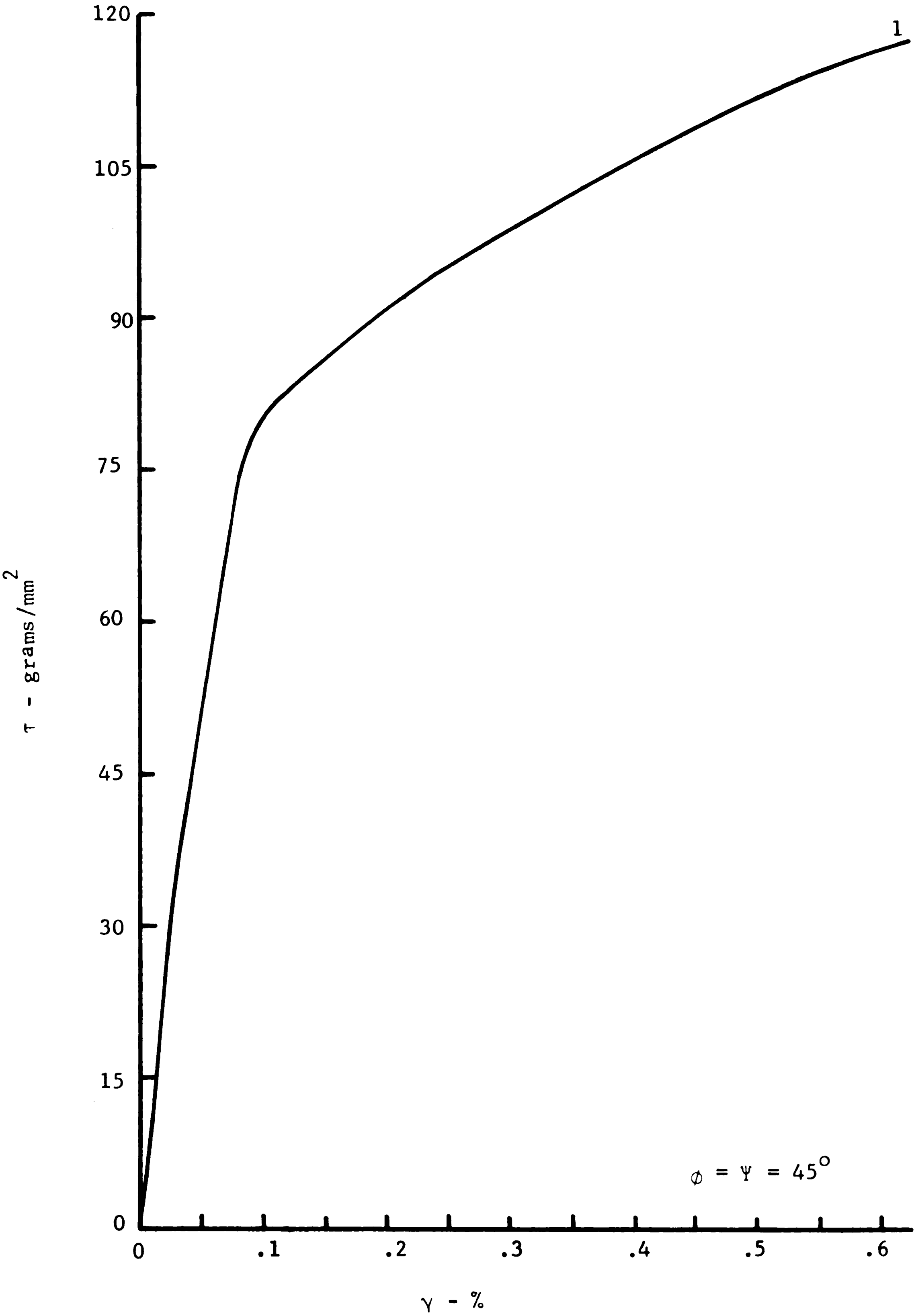

Figure 35. Resolved shear stress-strain curve Test No. 1

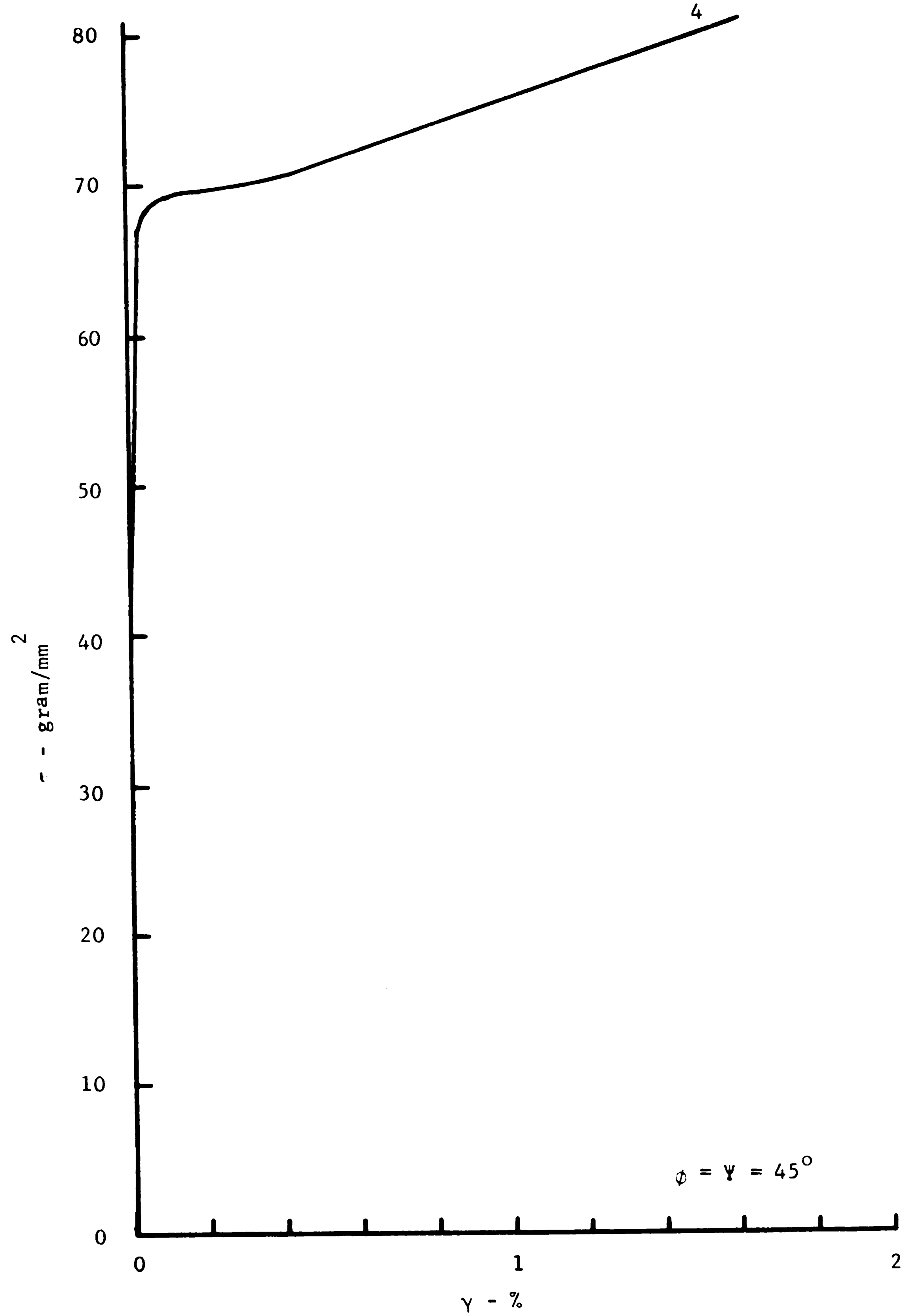

Figure 36. Resolved shear stress-strain curve Test No. 4

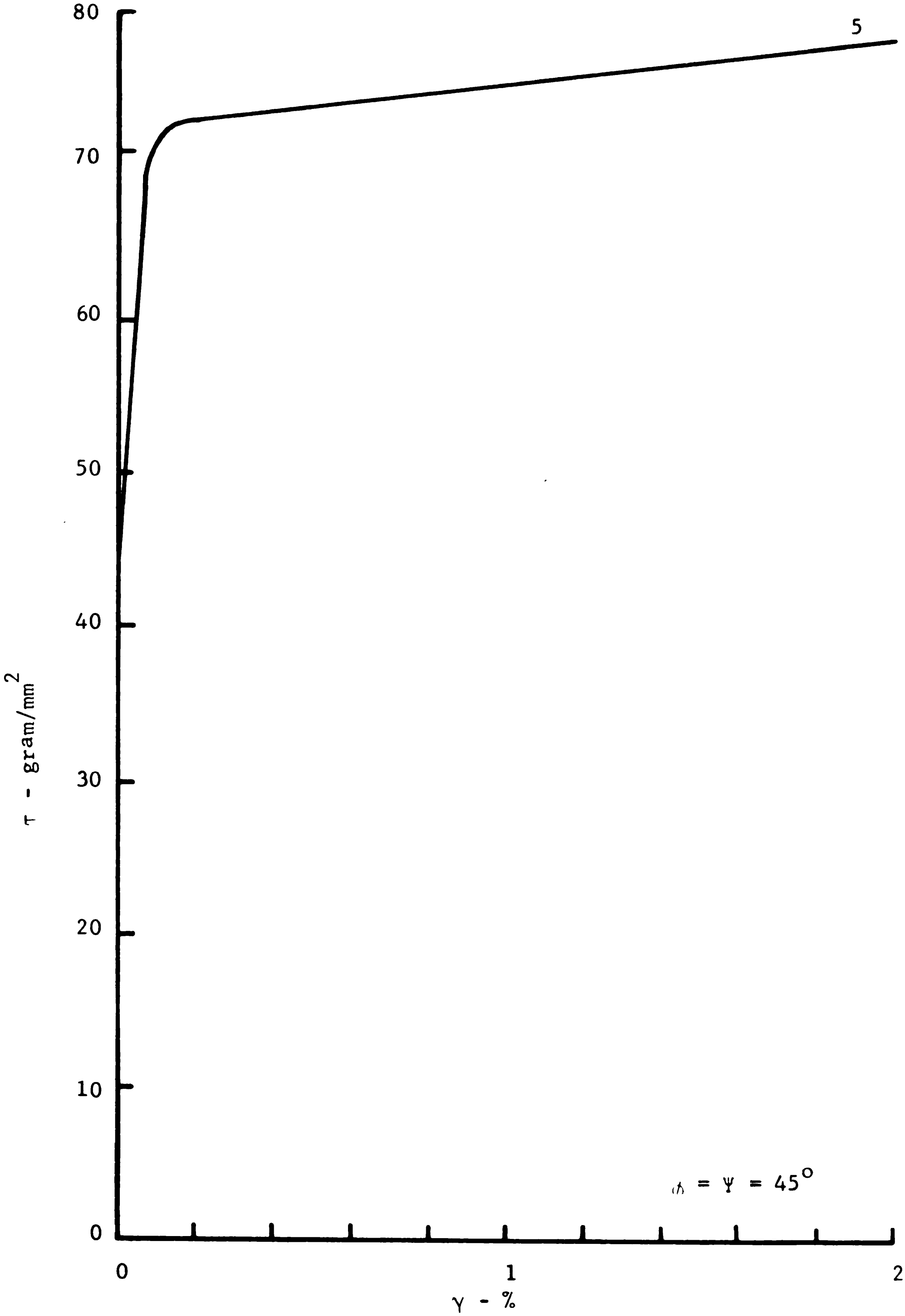

Figure 37. Resolved shear stress-strain curve Test No. 5

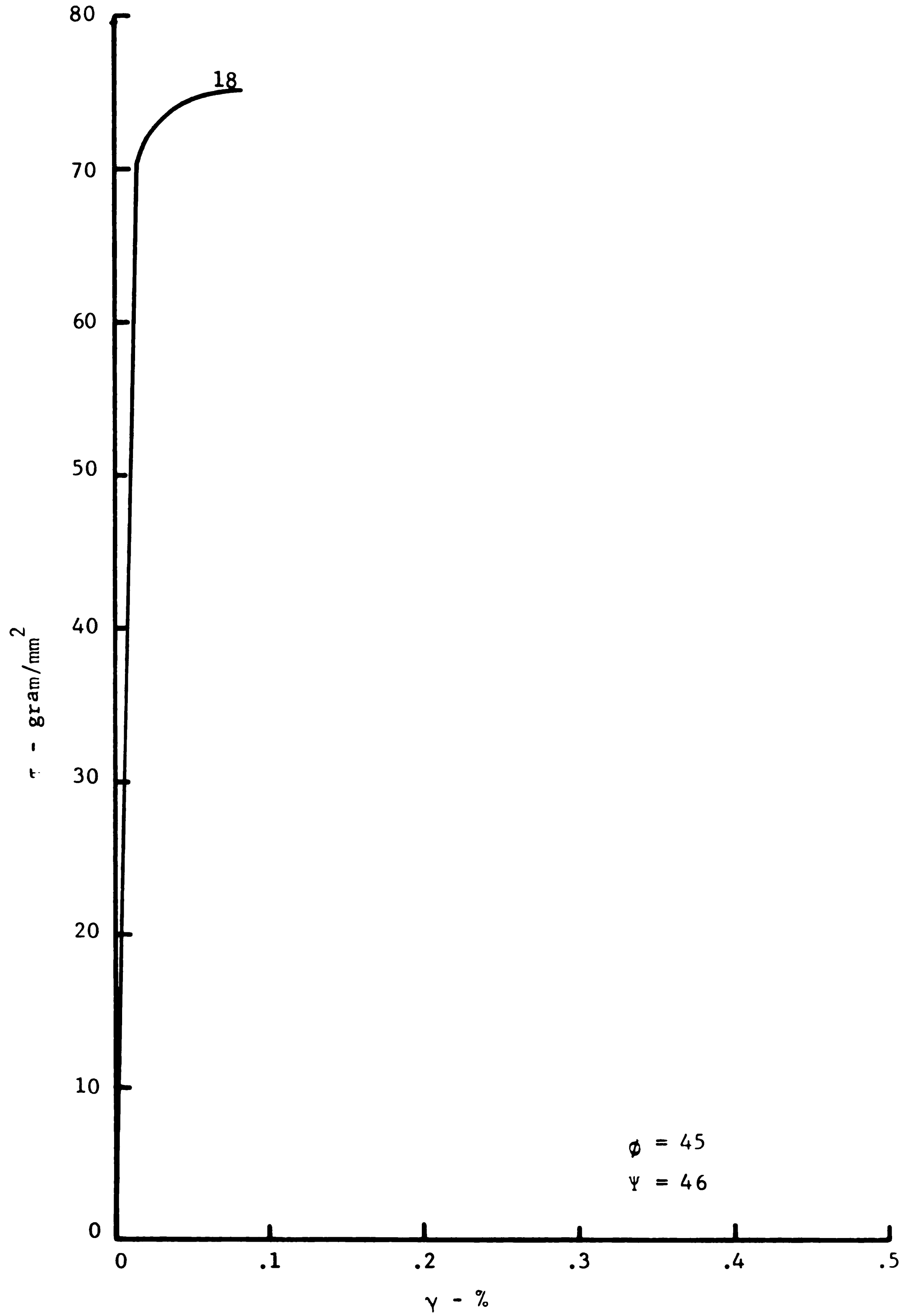

Figure 38. Resolved shear stress-strain curve Test No. 18

wasn't correct or the dislocation density wasn't the same as the other crystals. Therefore, the results of these tests were not included. Test No. 1 and 4 were specimens having rubber grips adhered to the test section. The load was applied in the P_2 direction after the specimen was preloaded in the P_1 direction. Test No. 5 was loaded in the axial direction without rubber grips glued to the test section. Test No. 18 was loaded transversely by applying the load with the pulley system. This test was run last because of the possibility of damaging the testing equipment. The test was ended abruptly, when it started to yield, to prevent catastrophic yielding due to the high energy stored in the extended rubber grips. The uniaxial results tabulated in Table 5 indicate reproducible yielding; i.e., τ_0 equal to 70 $\pm$ 2 gram/mm^2. The results also indicate that the rubber grips didn't effect the yielding of the crystals. These results verify that all the single crystals had approximately the same dislocation density and oxide film coating before running the tests. Therefore, since the specimens for the biaxial shear stress experiments were grown and prepared the same as the uniaxial specimens; the variation in the resolved shear stress at yield would primarily be due to the normal stresses.

The nominal stress-strain curves and the resolved shear stress-strain curves for the biaxial tests are plotted in Figures 39 to 43 and Figures 44 to 52, respectively. The yield point for all the curves was determined by the three methods described below. These methods were used to establish the error due to the interpretation of the results. The lowest possible value for yield was taken as the point where the resolved shear stress-strain curve showed

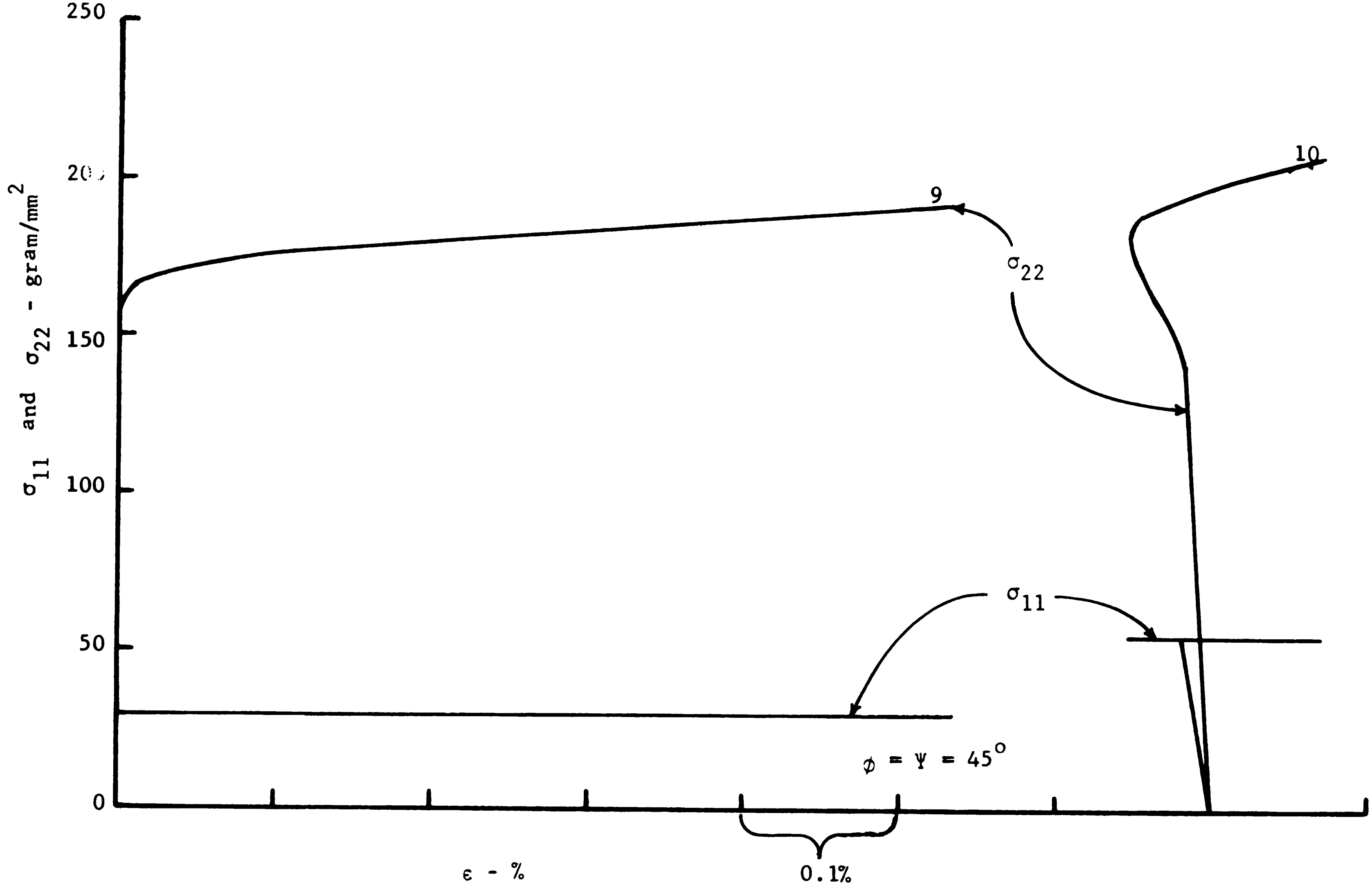

Figure 39. Nominal stress-strain curves Test No. 9 and 10

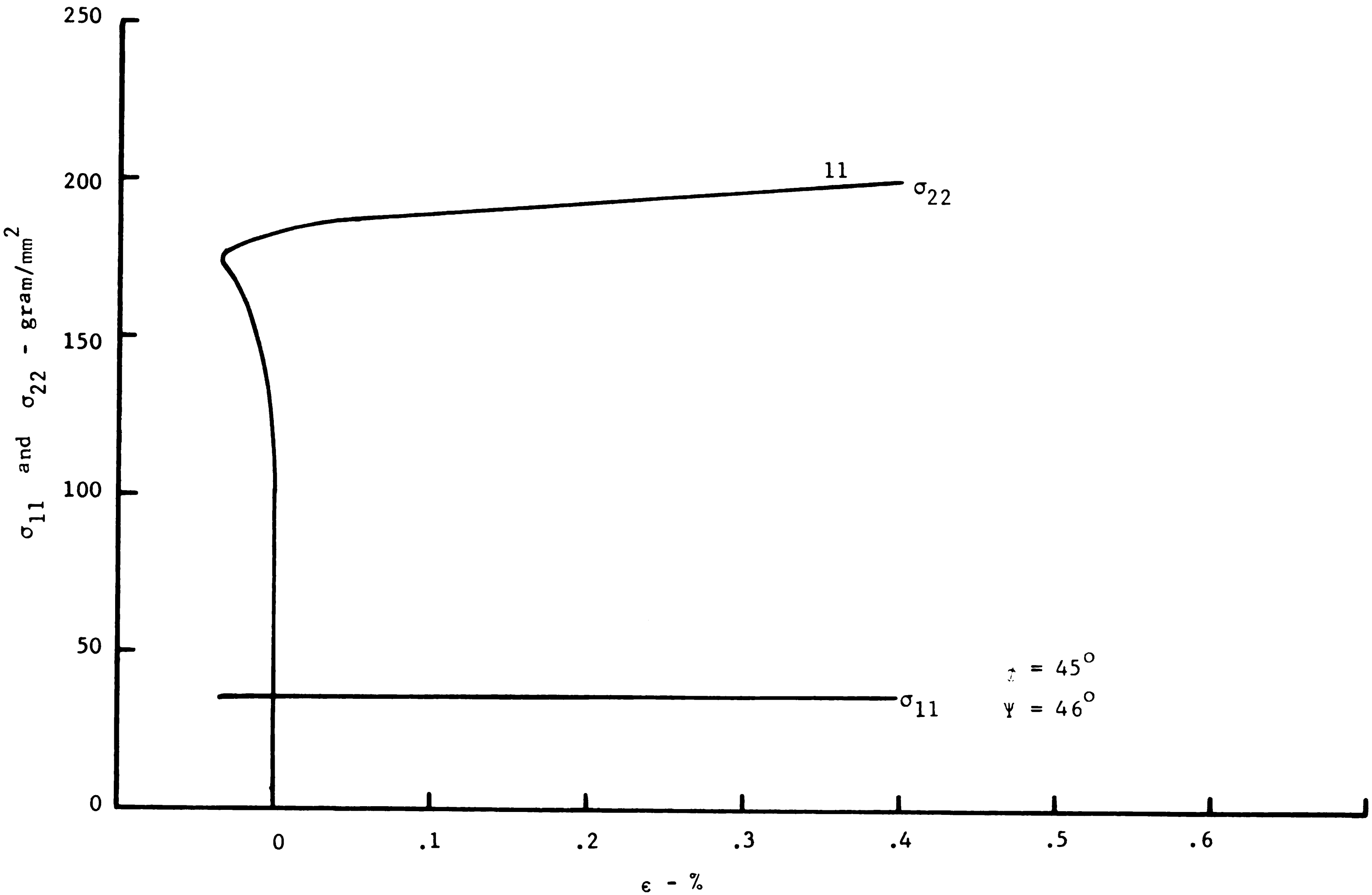

Figure 40. Nominal stress-strain curve Test No. 11

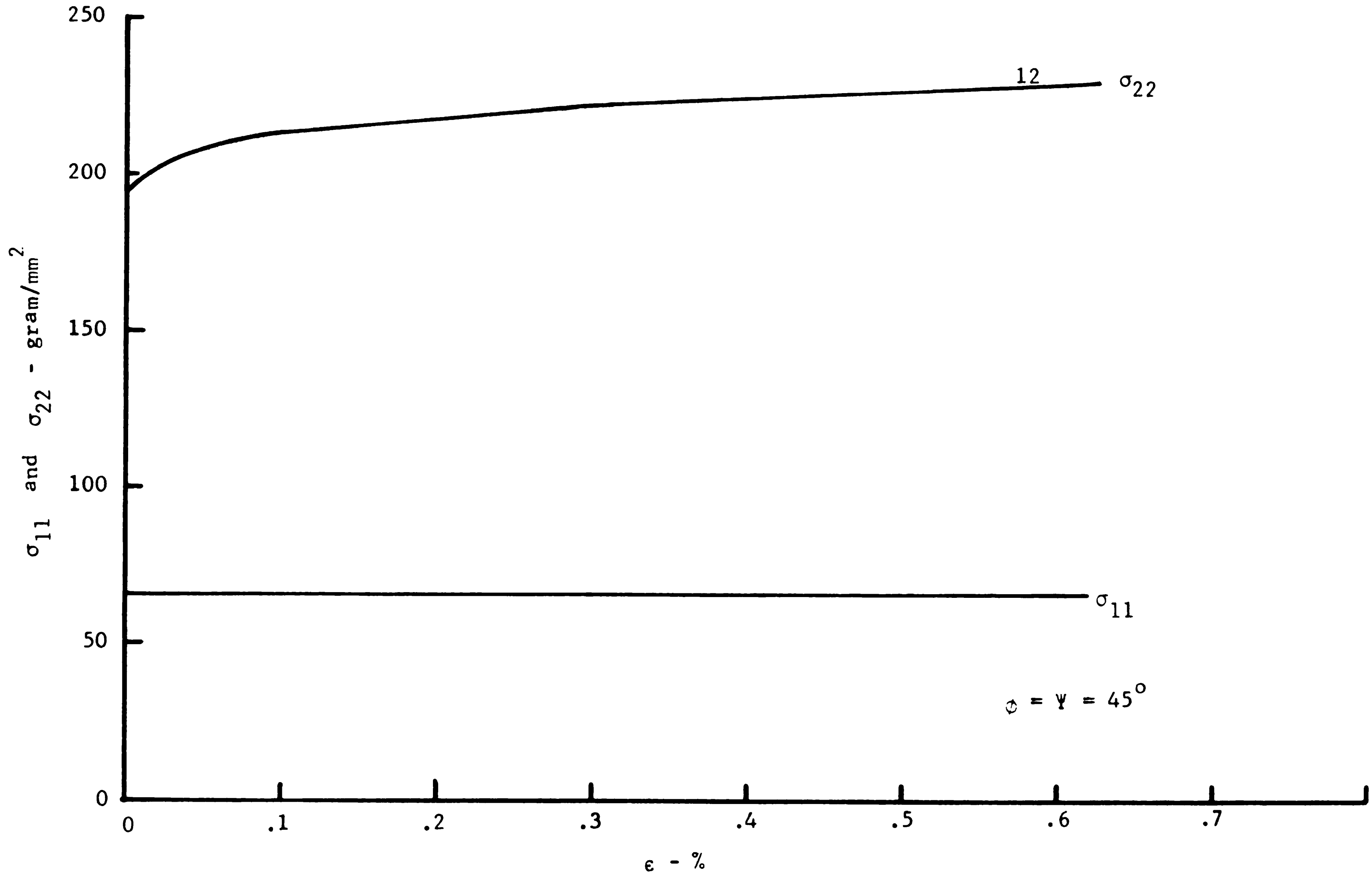

Figure 41. Nominal stress-strain curve Test No. 12

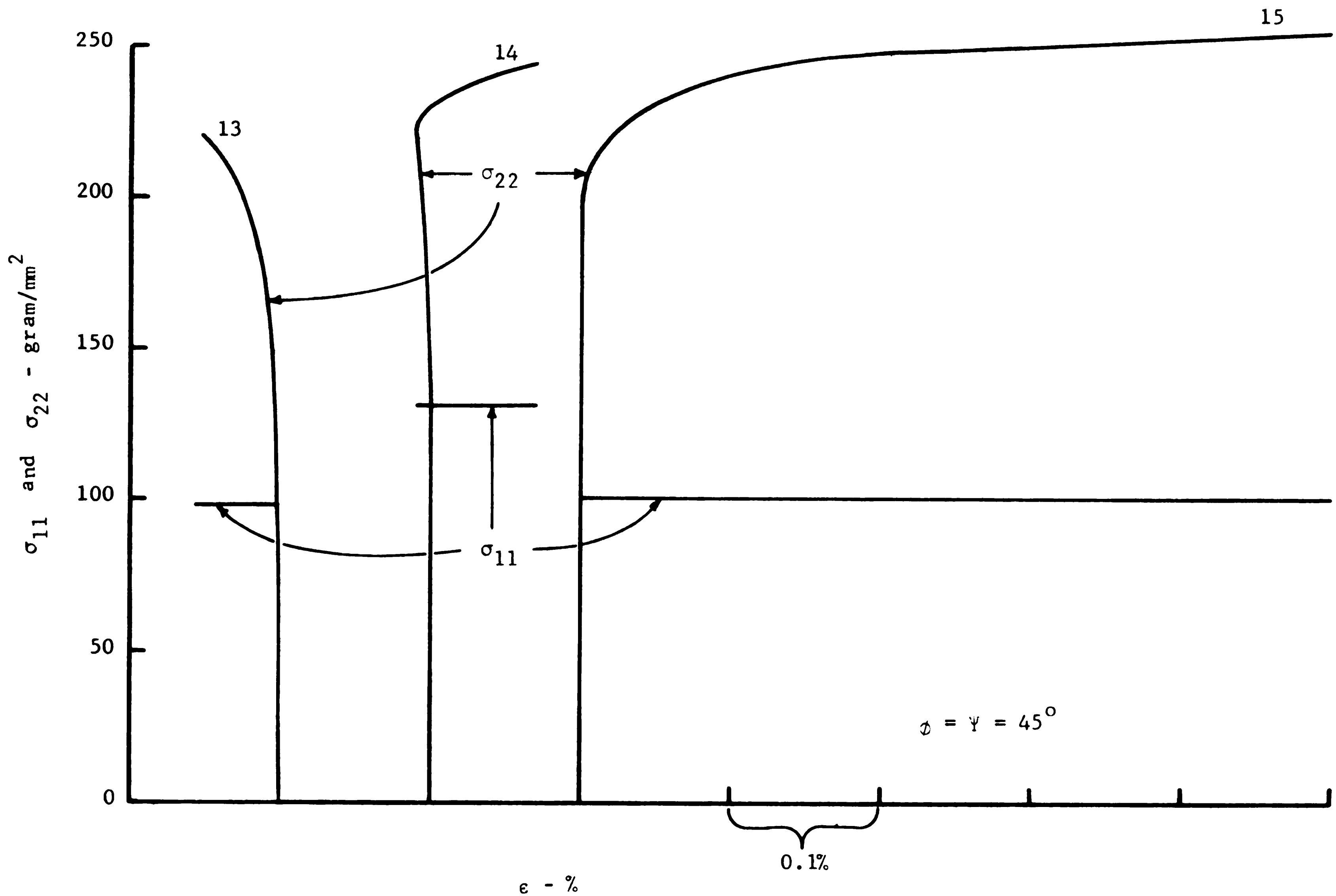

Figure 42. Nominal stress-strain curves Test 13, 14 and 15

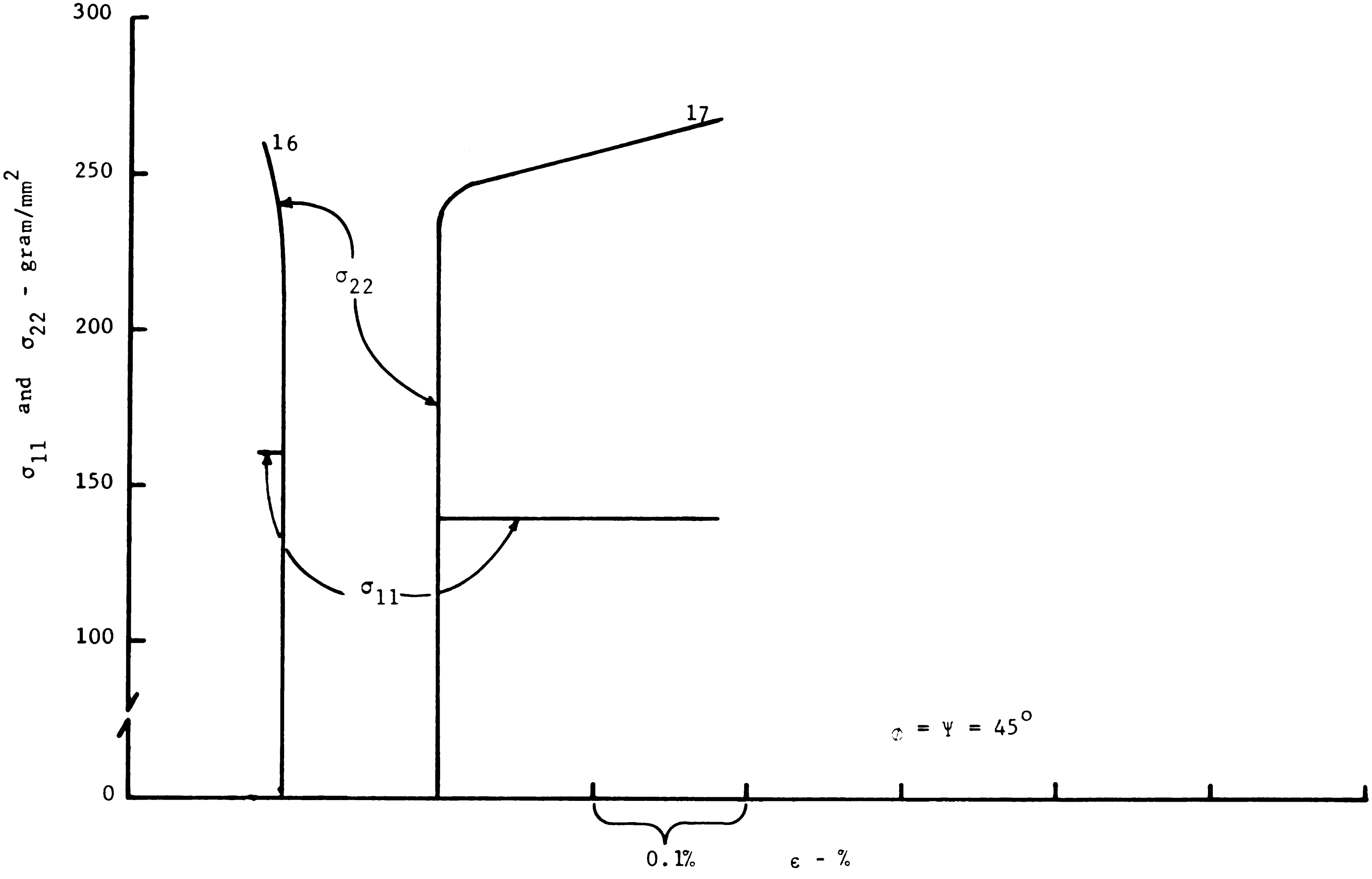

Figure 43. Nominal stress-strain curves Test No. 16 and 17

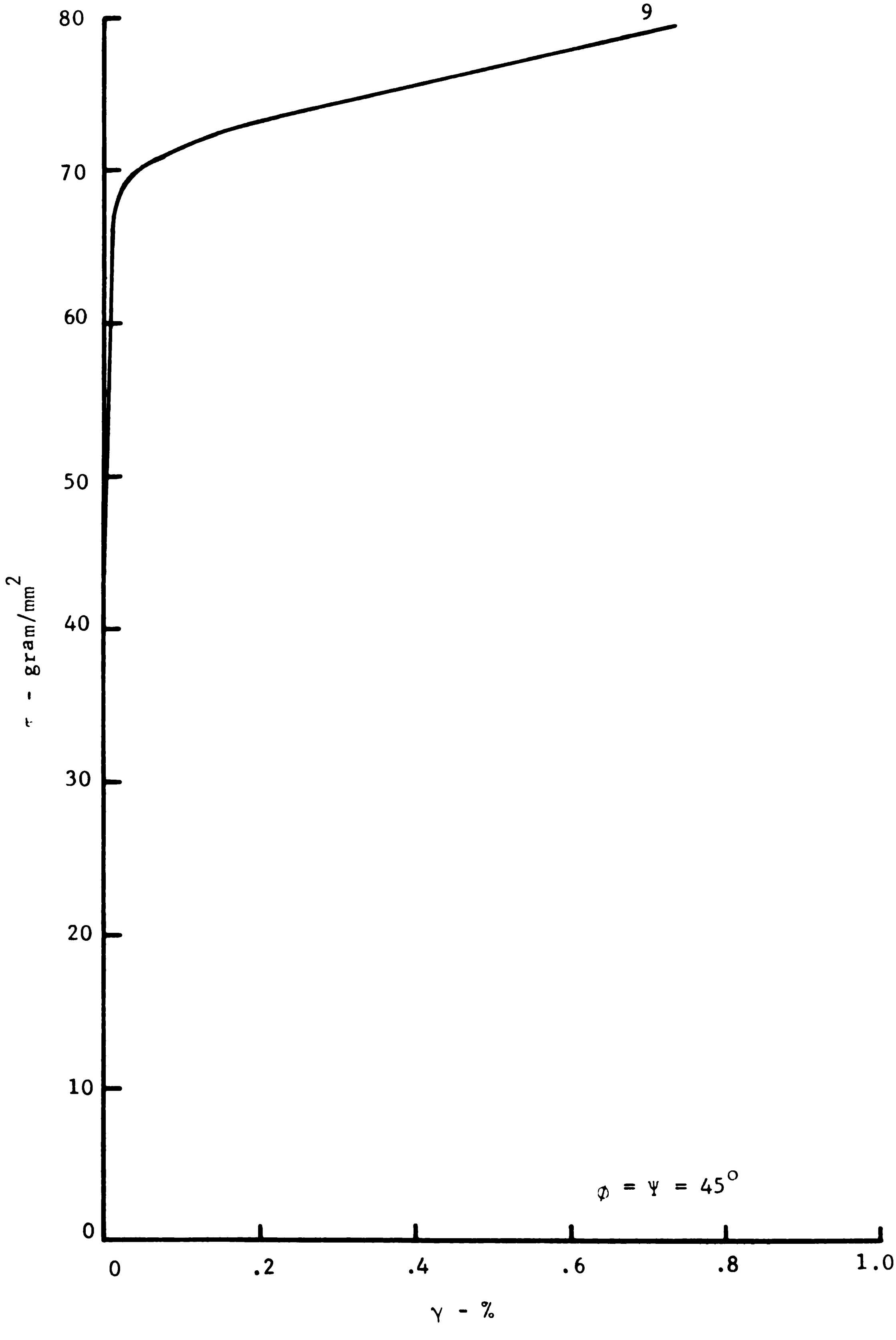

Figure 44. Resolved shear stress-strain curve Test No. 9

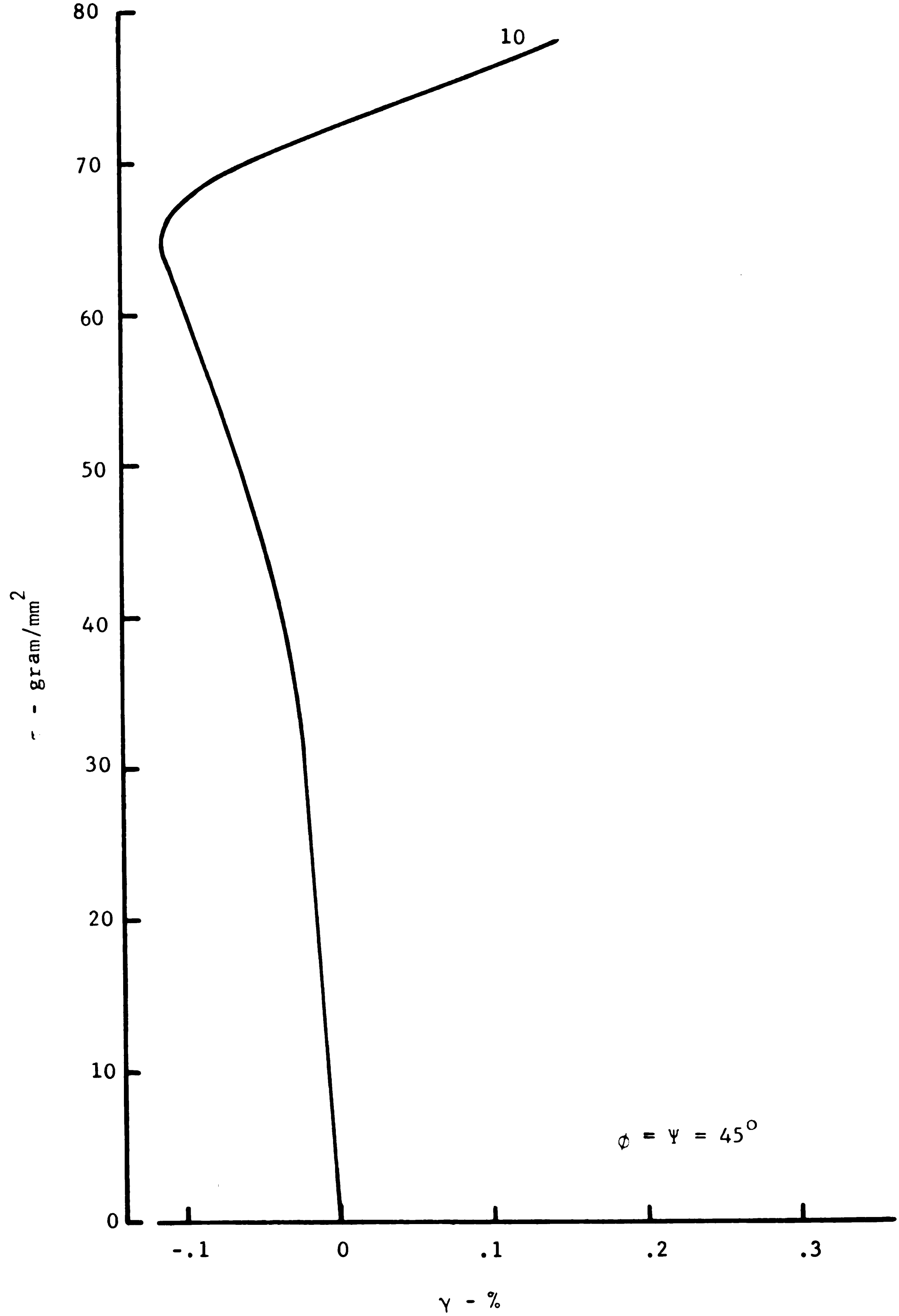

Figure 45. Resolved shear stress-strain curve Test No. 10

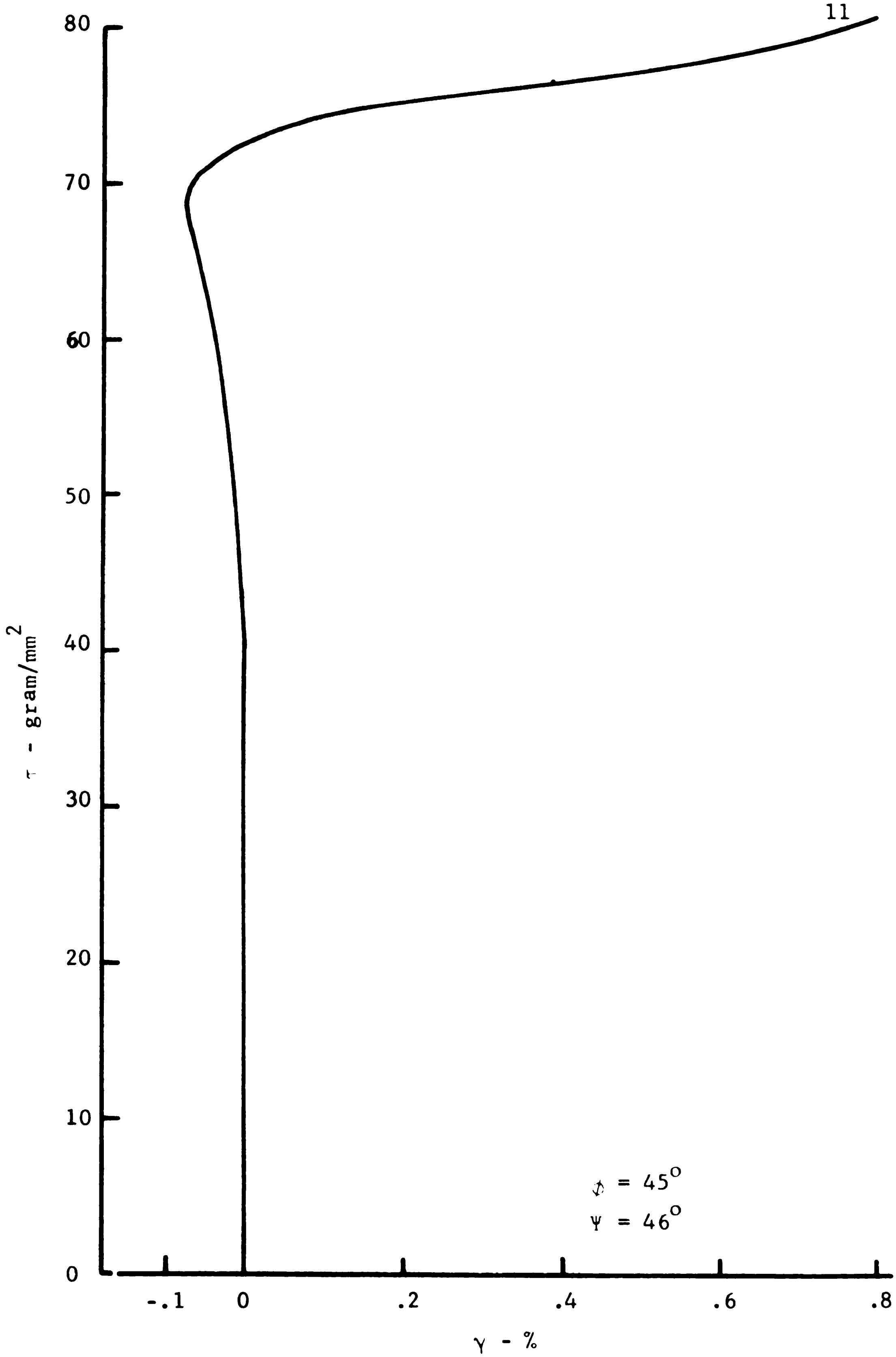

Figure 46. Resolved shear stress-strain curve Test No. 11

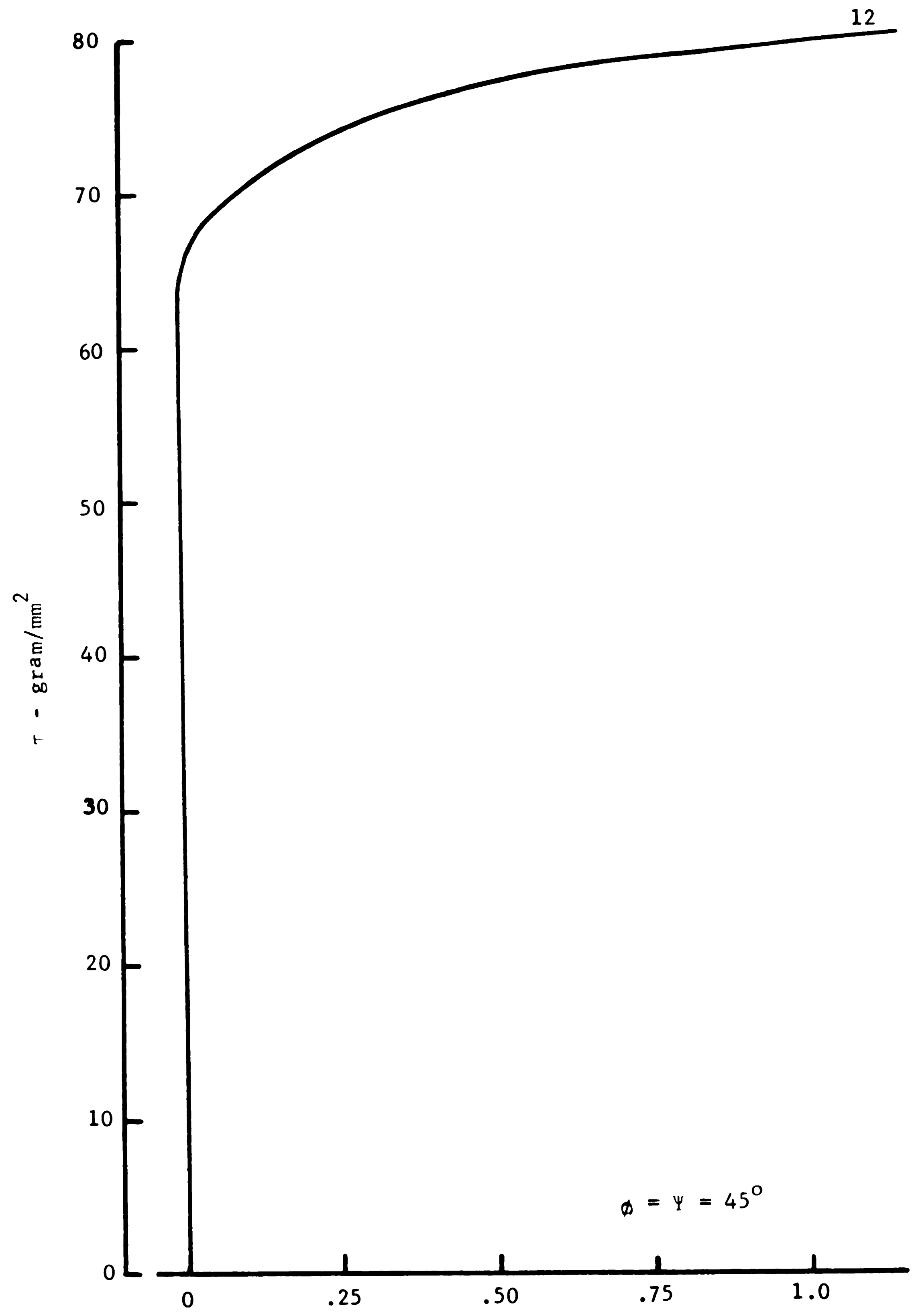

Figure 47. Resolved shear stress-strain curve Test No. 12

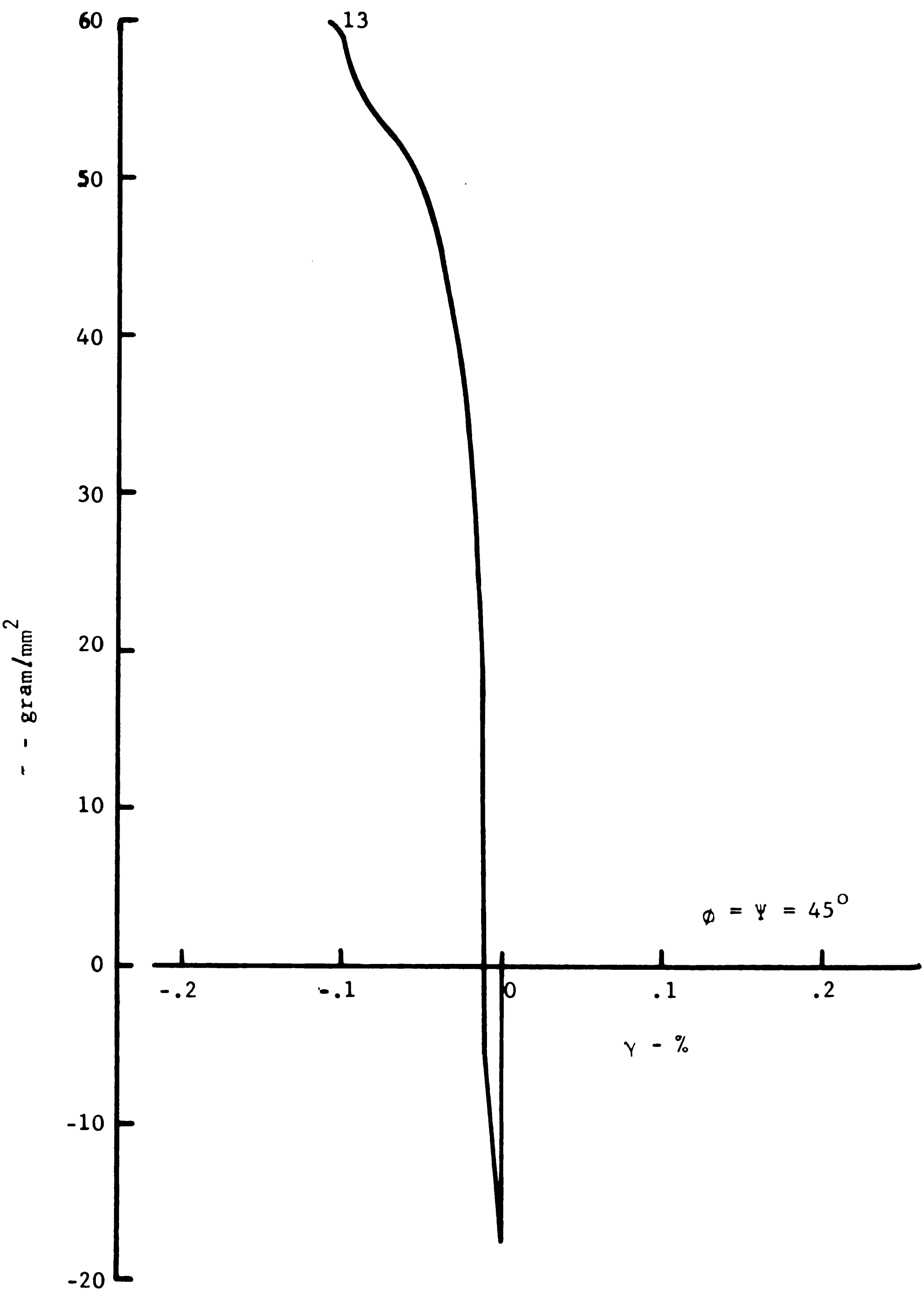

Figure 48. Resolved shear stress-strain curve Test No. 13

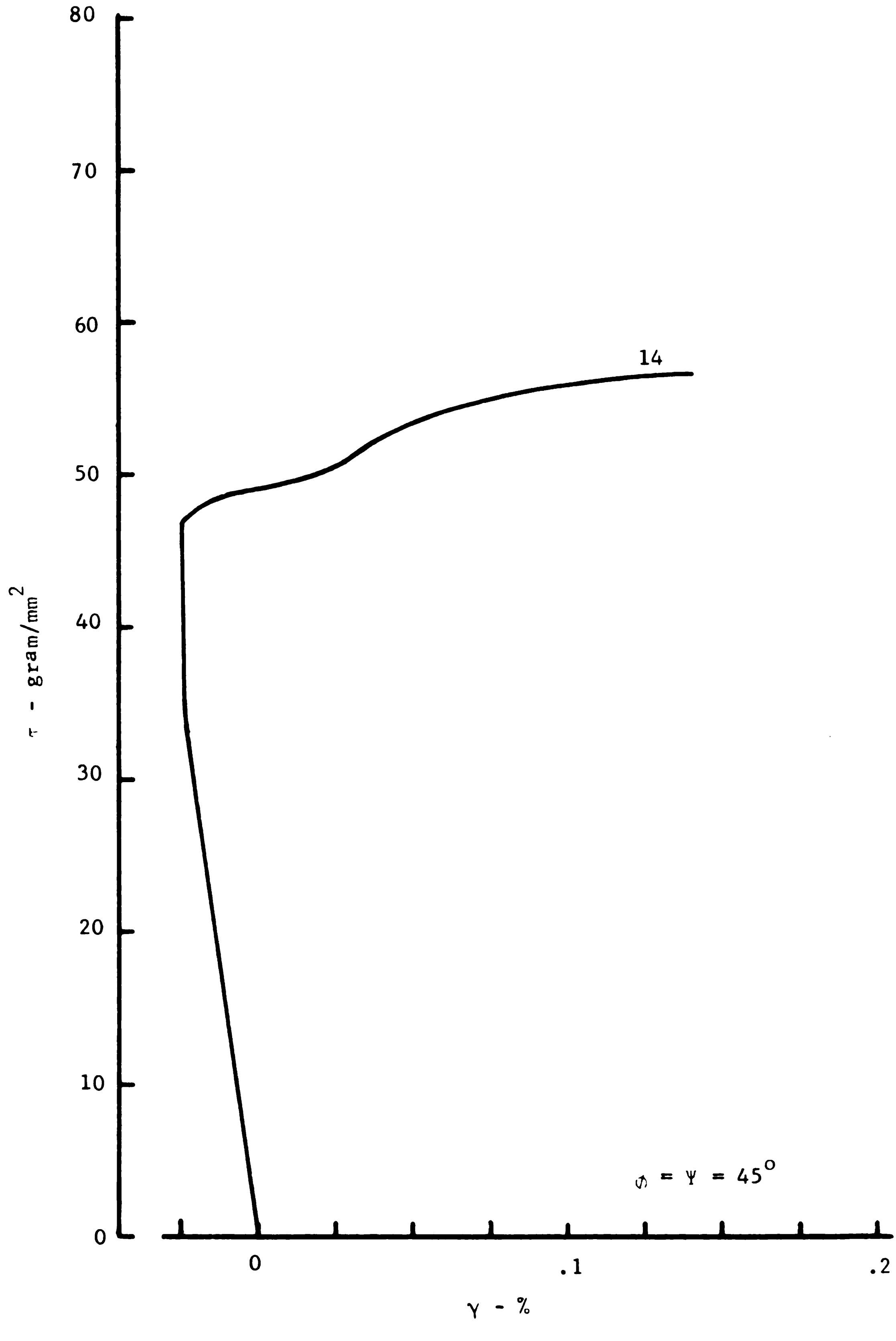

Figure 49. Resolved shear stress-strain Test No. 14

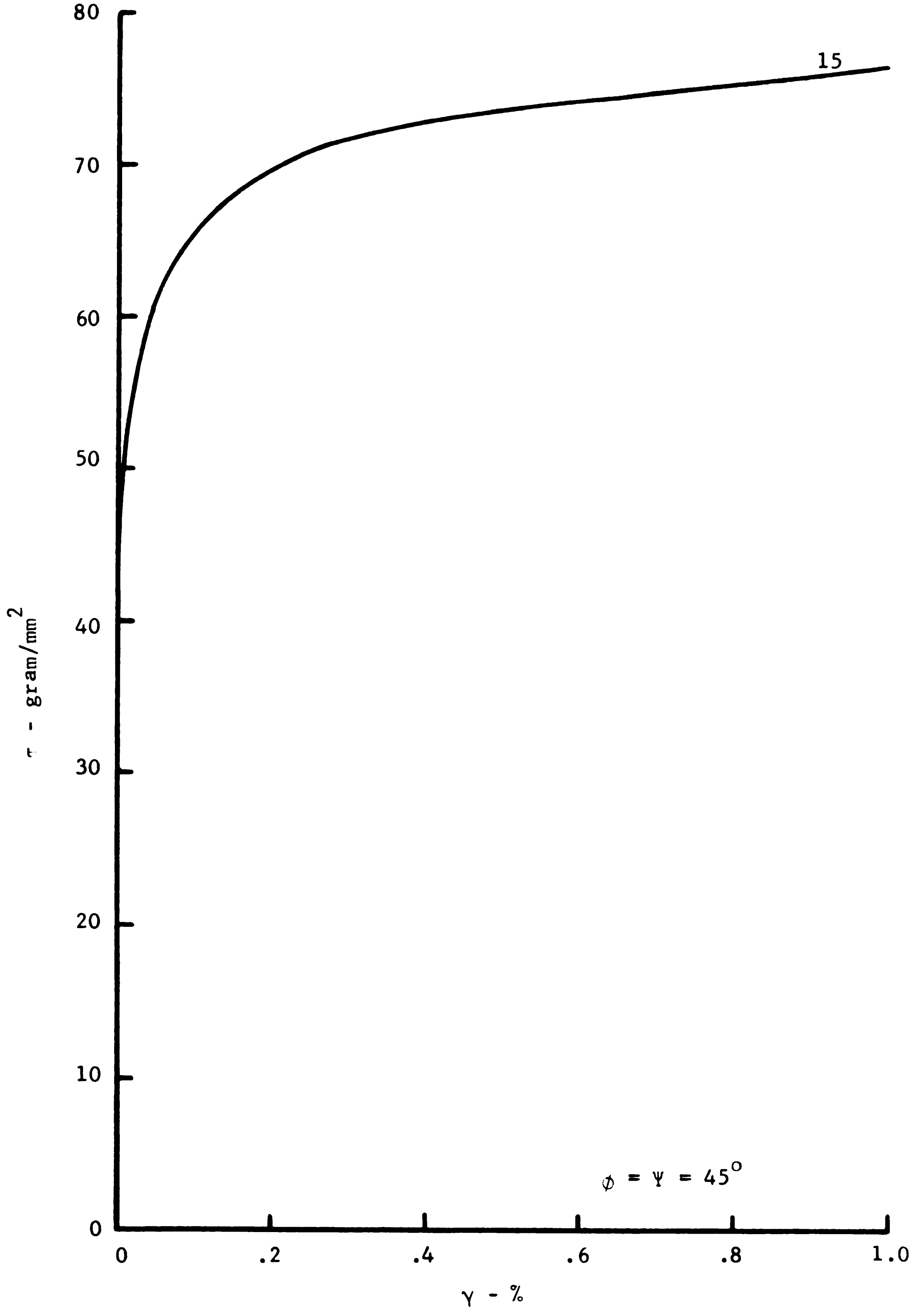

Figure 50. Resolved shear stress-strain curve Test No. 15

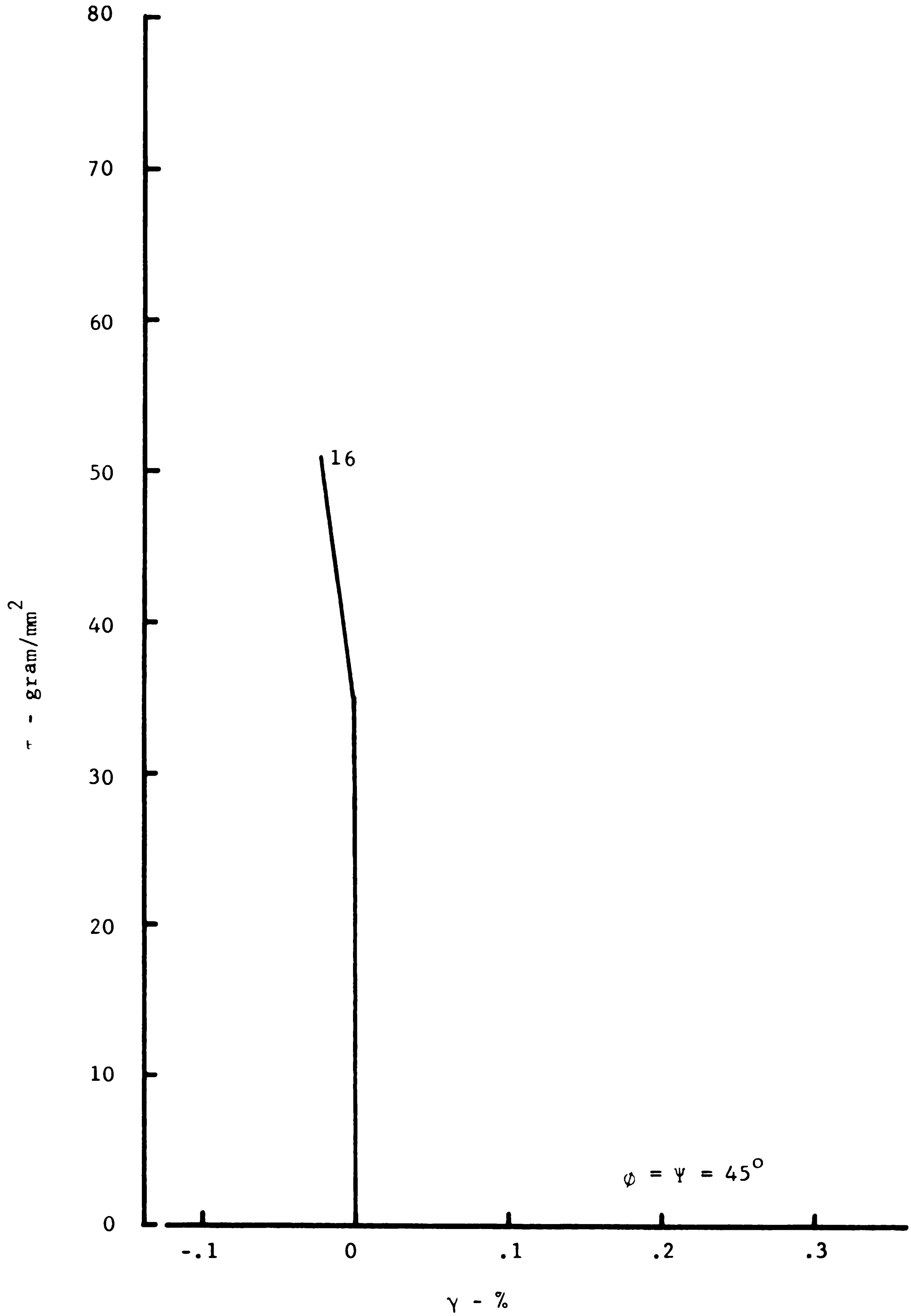

Figure 51. Resolved shear stress-strain curve Test No. 16

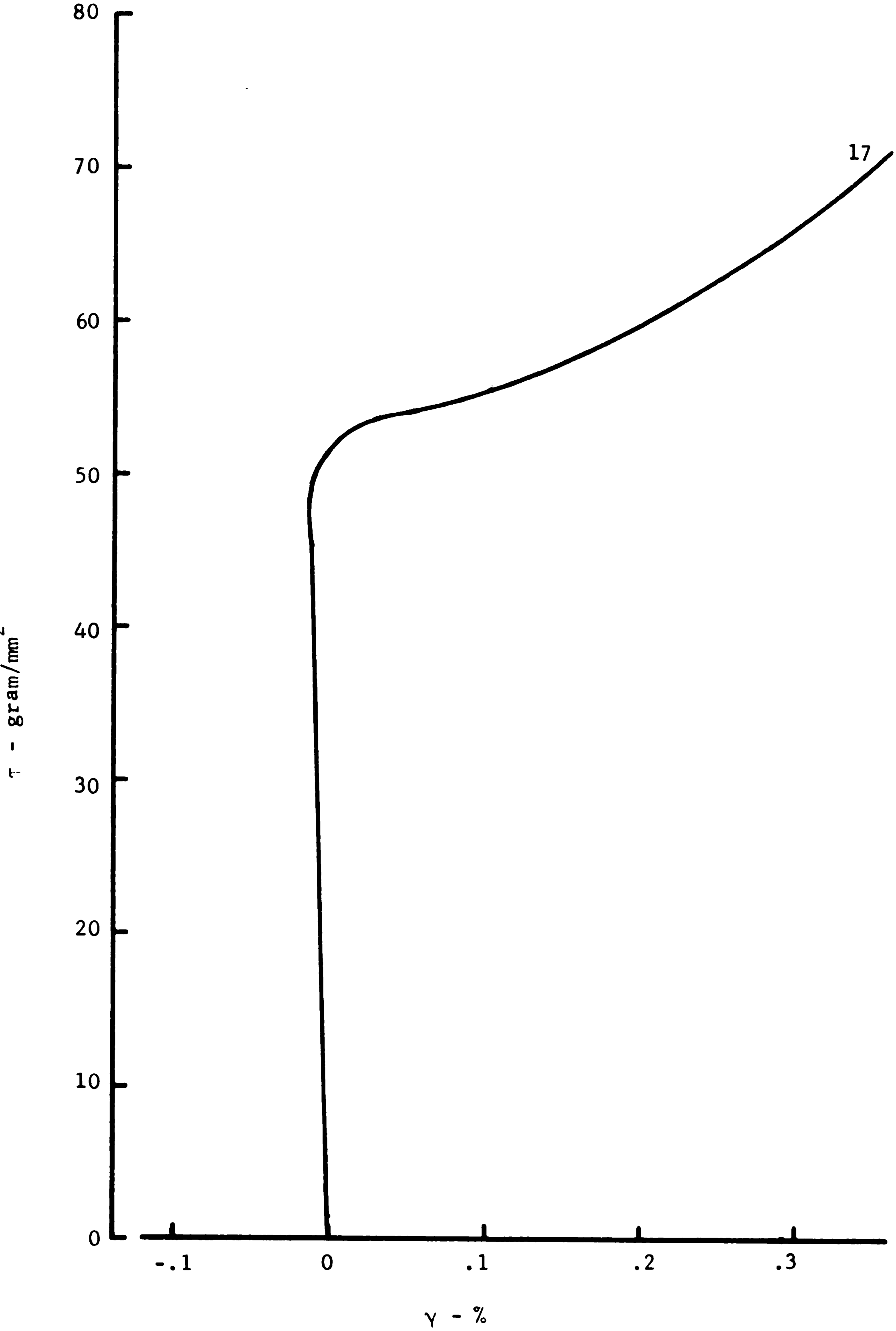

Figure 52. Resolved shear stress-strain curve Test No. 17

Table 5. Summary of

Test No.	Specimen No.	Orientation ϕ (deg.)	Orientation Ψ (deg.)	Type of Test	Area A_1 (mm^2)	Area A_2 (mm^2)	Gage Length (mm)	$\sigma_{11}\|_y$ (g/mm^2)
1	16	45	45	Uniaxial	80.5	39.6	20.32	0.0
4	6	45	45	"	79.4	39.2	20.32	0
5	3	45	45	"	-	36.3	20.32	0
9	2	45	45	Biaxial	81.2	39.6	20.29	29.7
10	11	45	45	"	80.0	40.0	20.11	53.6
11	12	45	46	"	79.9	38.4	20.33	36.2
12	14	45	45	"	80.4	39.4	20.31	66.7
13*	17	45	45	"	81.3	40.0	20.97	98.9
14	18	45	45	"	81.2	39.4	20.32	131.7
15	19	45	45	"	80.4	39.1	20.32	101.5
16*	20	45	45	"	81.3	40.0	20.32	160.5
17	15	45	45	"	81.2	40.0	20.32	138.1
18	8	45	46	Transverse	79.0	39.3	10.57	147.0

* Failure before yield

$\sigma|_y$ - Value of stress at yield (0.02% offset)

Shear Stress Experiment Data

$\sigma_{22}\|_y$ (g/mm^2)	$\dfrac{\sigma_{11}\|_y}{\sigma_{22}\|_y}$	$\sigma'_{11}\|_y$ (g/mm^2)	$\sigma'_{12}\|_y$ (g/mm^2)	$\dfrac{\sigma'_{11}\|_y}{\sigma'_{12}\|_y}$	$\dfrac{\sigma'_{11}\|_y}{\tau_0}$	$\dfrac{\sigma'_{12}\|_y}{\tau_0}$	$\dot{P}_1$ (kg/min.)	$\dot{P}_2$ (kg/min.)
145.5	0.0	70.5	70.5	1.00	1.01	1.01	-	50.0
-	0	68.0	68.0	1.00	0.97	0.97	-	21.5
-	0	70.0	70.0	1.00	1.00	1.00	-	21.0
169.0	0.18	99.0	70.0	1.41	1.41	1.00	16.8	24.5
198.2	0.27	125.6	72.0	1.75	1.79	1.03	15.4	21.5
181.2	0.20	108.6	72.5	1.50	1.55	1.035	21.8	25.9
202.7	0.33	134.7	68.0	1.98	1.92	0.97	20.5	26.5
218.8	0.45	158.8	59.9	2.64	2.26	0.86	30.7	22.4
229.7	0.57	180.7	49.0	3.69	2.58	0.70	31.3	22.0
223.5	0.45	162.5	61.0	2.66	2.32	0.87	30.0	27.0
262.5	0.62	211.5	51.0	4.14	3.02	0.73	25.4	28.5
243.0	0.57	190.6	52.0	3.67	2.72	0.74	27.8	21.5
-	-	72	72	1	1.03	1.03	31.7	-

the first deviation from linearity. The intermediate value of CRSS was determined by the 0.02 percent offset method and the maximum value by a 0.1 percent offset. The tabulated results listed in Table 5 for the biaxial tests are all based on the 0.02 percent offset method. These results show that the resolved normal stresses varied from 70 tó 212 gram/mm^2 by varying σ_{11}/σ_{22} at yield 0 to 0.62. This caused the resolved shear stress to drop from 70 to 49 gram/mm^2.

To better illustrate the effect of the resolved normal stress on the CRSS for {0001} <2$\bar{1}\bar{1}$0> type slip of zinc single crystals, the results of the uniaxial and biaxial tension tests were plotted as shown in Figure 53. The resolved shear stress at yield $(\sigma'_{12}|_y)$ and resolved normal stress at yield $(\sigma'_{11}|_y)$ were both normalized to τ_0, where τ_0 is the CRSS for the uniaxial tests. The maximum error bar indicates the maximum possible error in the interpretation of the data as described above. When $\sigma'_{11}|_y/\tau_0$ is increased above a value of approximately 2, the experimental results begin to fall below the theoretical curve. For $\sigma'_{11}|_y/\tau_0$ equal to 3, there is a 30 percent drop in $\sigma'_{12}|_y$.

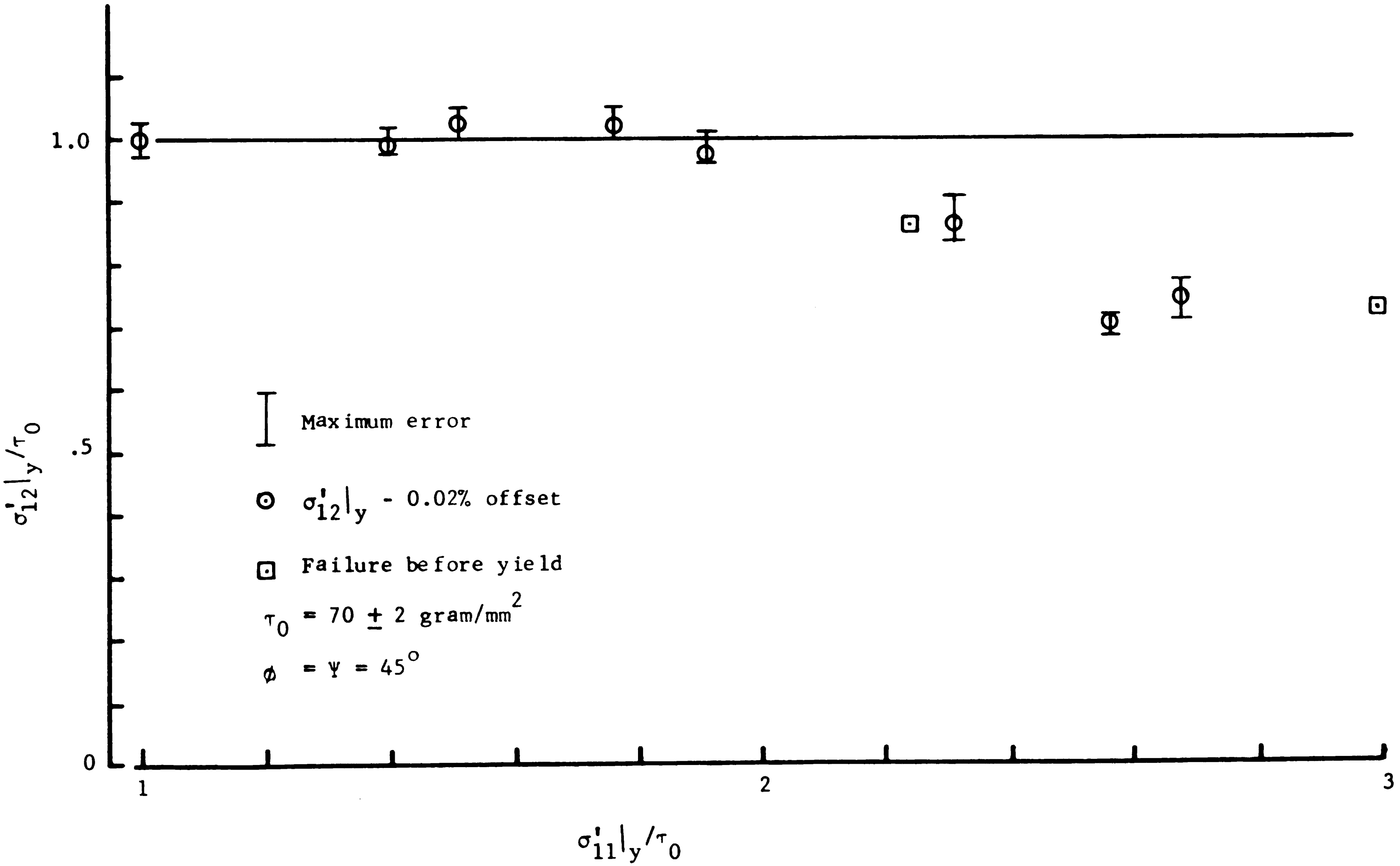

Figure 53. Resolved shear stress to τ_0-resolved normal stress to τ_0 at yield.

IV CONCLUSION

The mechanical behavior of polycrystalline materials has been tested extensively in a biaxial state of stress, but there has been little attention given to the effects of a complex state of stress on the mechanical behavior of metal single crystals. The effect of a complex stress field on a single crystal is important because aggregate theories use the value of the critical resolved shear stress determined by uniaxial testing to predict the stress-strain curve of aggregates, while the crystals within these aggregates are actually subjected to a complex stress field. In previous investigation, the orientation dependence of single crystals has been examined by subjecting single crystals to a uniaxial state of stress. When the crystal orientation was varied, the resolved normal stresses at yield on the active slip system were also varied. This coupling of the resolved normal stresses and the crystal orientation effects was separated by subjecting single crystals to a uniform biaxial state of stress. The main theme of this experimental investigation was to test the hypothesis that macroscopic yield in single crystals is determined only by the shear stress on the active slip system and is independent of the resolved normal stresses.

The following conclusions have been drawn from the present research program:

1. To obtain a uniform biaxial stress region in a flat tensile specimen over approximately 80 percent of the test section, the width to uniform transverse loading length ratio (H/C) should fall between 0.25 and 0.50. These limits were established by an extensive elasticity investigation.
2. Slitted rubber grips can be used to produce a uniform stress field at the surface of the sample. This is verified by the photoelasticity investigation for isotropic materials and by the uniform slip lines for anisotropic zinc crystals. The grips were made of a 1/8 inch thick neoprene rubber with slits at 1/8 inch intervals. These slits were cut to within 0.035 inch of the bonded interface. This was necessary in order to eliminate the shear stress at the bonded interface which arises as a result of the Poisson effect.
3. When tested biaxially, zinc single crystals show that the resolved shear stress for yield decreases with increasing resolved normal stress. The crystal orientation was held constant with $\phi = \Psi =$ 45 degrees and the resolved normal stress was varied from 70 to 212. This variation in the resolved normal stress resulted in a 30 percent drop in the resolved shear stress. Therefore, one could conclude that macroscopic yield of zinc single crystals is not only determined by the shear stress on the active basal slip system, but is also dependent on the normal stresses acting on that slip system when $\phi = \Psi = 45$ degrees for $\{0001\}$ $\langle 2\bar{1}\bar{1}0 \rangle$ type slip.

THE BIBLIOGRAPHY

THE BIBLIOGRAPHY

1. E. Schmid, Proc. Internat. Congr. of Appl. Mech. Delft, 342 (1924).

2. E. Schmid and W. Boas, Kristallplastizitat, Springer Verlag, Berlin, Original German edition (1935). English translation published by F.A. Hughes and Co., (1950).

3. P. Haasen, Phil. Mag., 3, 284 (1958).

4. W.N. Andrade, D.C. and D.A. Aboau, Proc. Roy. Soc., A240, 304 (1957).

5. J.Z.F. Diehl, Metallkunde, 47, 331 (1956).

6. K. Lücke and H. Lange, Z. Metallkunde, 43, 55 (1952).

7. R.W.K. Honeycombe, Progr. Mat. Sci., 9, 95 (1961).

8. F.D. Rosi and C.H. Mathewson, Trans. AIME J. of Metals, 188, 1159 (1950).

9. F.D. Rosi, Trans. AIME J. of Metals, 200, 1009 (1954).

10. R.W. Fenn, W.R. Hibbard, Jr. and H.A. Lepper, Jr., Trans. AIME, 188, 175 (1950).

11. R. Madin and N.K. Chen, Prog. Metal Phys., 5, 53 (1954).

12. C.S. Barrett, An International Conference held at Lake Placid by Fisher, Johnston, Thomson, Vreeland, 238 (1956).

13. C.S. Barrett, Structure of Metals, McGraw-Hill, 346 (1952).

14. D. Hull, J.F. Byron and F.W. Noble, Can. J. Phys., 45, 1091 (1967).

15. D.C. Jillson, Trans., AIME J. of Metals, 188, 1129 (1950).

16. E.C. Burke and W.R. Hibbard, Trans. AIME, 194, 295 (1952).

17. R.W.K. Honeycombe, The Plastic Deformation of Metals, St. Martin's Press, New York (1968).

18. G. Sachs, Z.D. Ver. deut. Ing., 72, 734 (1928).

19. G.I. Taylor, J. Inst. Metals, 62, 307 (1928).

20. F.F.W. Bishop and R. Hill, Phil. Mag., 42, 414, 1498 (1951).

21. C.K. Chyung, "On the Improvement of Lattice Perfection in High Purity Zinc Crystals Grown from the Melt," M.S. Thesis, Michigan State University, (1962).

22. Private communication - R.W. Little and notes for forthcoming book.

23. Private communication - J.L. Lubkin.

24. G.L. Cloud, "Improvement in Use of Photometric Methods for Measurement of Birefringence", Expr. Mech., 8, 138 (1968).

25. C.H. Peterson, "Special Adhesives for Rubber Bonding", Symposium on Adhesives for Structural Applications, 59 (1962).

26. W.M. DeCrease, Rubber Age, 87, 1013 (1960).

27. J.W. Gallagher, Adhesive Age, 29, Jan. (1968).

28. J.A. Svigelj - Supplied samples of Chemlok 305 adhesive - Hughson Chemical Company, Eire, Pennsylvania.

29. C.K. Chyung, "Nucleation of Deformation Twins in Zinc Bicrystals," Ph.D. Thesis, Michigan State University, (1965).

30. E.A. Anderson and D.C. Jillson, J. Met., 1191, Sept. (1953).

31. R.F. Miller, Trans. AIME, 122, 173 (1937).

GENERAL REFERENCE

1. R.W.K. Honeycombe, The Plastic Deformation of Metals, St. Martin's Press, New York, 1968.

2. E. Schmid and W. Boas, Kristallplastizitat, Springer Verlag, Berlin, Original German edition (1935). English translation published by F.A. Hughes and Co., 1950.

3. C.S. Barrett, Structure of Metals, McGraw-Hill Book Company, Inc., New York, Toronto, London, 1952.

4. R.C. Dove and P.H. Adams, Experimental Stress Analysis and Motion Measurement, Charles E. Merrill Books, Inc., Columbus, Ohio, 1964.

5. J.W. Dally and W.F. Riley, Experimental Stress Analysis, McGraw-Hill Book Company, New York, 1965.

6. R.F.S. Hearmon, An Introduction to Applied Anisotropic Elasticity. Oxford University Press, 1961.

APPENDIX

Computer Programs

1. Calculation of stress distribution in a finite rectangular beam.

```
      DIMENSION SXX(51,11), SYY(51,11),SXY(51,11),SDYX(51,11)
      SH(X)=(EXP(X)-FXP(-X))*.5
      CH(X)=(EXP(X)+EXP(-X))*.5
C  THIS PROGRAM SOLVES FOR THE STRESSES SXX, SYY, SXY AND SDYX= SYY-SXX USING
CTHE FOURIER METHOD FOR A RECTANGULAR BEAM.  H/XL IS ASSUMED TO BE APPROXIMATELY
C EQUAL TO 1.  H IS THE HALF WIDTH.  XL IS THE HALF LENGTH.  C IS THE HALF
CLENGTH OF THE TRACTION  AREA.  P IS THE APPLIED TRACTION AT THE SURFACE Y= H.
CNX= NO. OF EQUAL SIVESIONS ALONG THE X-AXIS.  NY = NO. OF EQUAL SIVISIONS ALONG
C THE Y-AXIS.  NMAX = N/. OF TERMA SUMMED IN THE SERIES.
      NPR=3
      NCR=2
    1 READ (NCR,2) C,H,XL,P,NX,NY,NMAX
    2 FORMAT(4F15.5,2I5,I10)
      IF (NX)99,99,3
    3 WRITE(NPR,4) C,XL,H,P
    4 FORMAT(1H2,5X'C ='F15.5,5X'XL ='F15.5,5X'H ='F15.5,5X'P ='F15.5//)
      HX=XL/NX
      HY=H/NY
      NXE=NX+1
      NYE=NY+1
      PL=3.14159265/XL
      PY=P*C/XL
      DO 50 J=1,NXE
      DO 50 K=1,NYE
      SYY(J,K)=PY
      SXX(J,K)=0.
      SXY(J,K)=0.
      SDYX(J,K) =0.
   50 CONTINUE
```

```
      DO 100 N=1,NMAX
      BNN=N*3.14159265
      BN=N*PL
      BNC=BN*C
      BNH=BN*H
      CHH=CH(BNH)
      SHH=SH(BNH)
      CA=BNH*CHH +SHH
      CB=SIN(BNC)
      CC=2.*P/BNN
      BC=CC*CB
      CD=BNH+SHH*CHH
      FR=BC/CD
      XN=BN*HX
      YN=BN*HY
      DO 100 K=1,NYE
      BNY=(K-1)*YN
      SHY=SH(BNY)
      CHY=CH(BNY)
      FAX=CA*CHY
      FBX= SHH*(BNY*SHY + 2.*CHY)
      FBXY=SHH*(BNY*CHY+SHY)
      FAY=SHH*BNY*SHY
      FXY=CA*SHY
      DO 100 J=1,NXE
      BNX=(J-1)*XN
      SSX=SIN(BNX)
      CSX=COS(BNX)
      SXX(J,K)=SXX(J,K) + FR*(FBX - FAX)*CSX
      SYY(J,K)=SYY(J,K) + FR*(FAX - FAY)*CSX
      SXY(J,K) =SXY(J,K) + FR*(FBXY-FXY)*SSX
      SDYX(J,K)=SYY(J,K) - SXX(J,K)
  100 CONTINUE
```

```
      BNY=NY
      Z=1.000
      DO 125 K=1,NYE
      Y=(K-1)/BNY
      WRITE (NPR,30) Y,NXE,Z,NMAX
   30 FORMAT(//    3X'STRESSES AT Y/C =' F7.4' FOR 'I4' VALUES OF X/L FR
     1OM 0 TO 'F7.4' USING 'I4' TERMS.'//)
      WRITE (NPR,31) (SYY (J,K),J=1,NXE)
   31 FORMAT (//5X'YY -  STRESS'/(/10F12.6))
      WRITE (NPR,32) (SXX (J,K),J=1,NXE)
   32 FORMAT (//5X'XX -  STRESS'/(/10F12.6))
      WRITE (NPR,33) (SXY (J,K),J=1,NXE)
   33 FORMAT (//5X'XY -  STRESS'/(/10F12.6))
      WRITE (NPR,34) (SDYX(J,K),J=1,NXE)
   34 FORMAT (//5X'YY-XX STRESS'/(/10F12.6))
      WRITE (NPR,35)
   35 FORMAT (1H2)
  125 CONTINUE
      GO TO 1
   99 CALL EXIT
      END
```

2. Calculation of principal stress difference distribution in photoelastic models.

```
      DIMENSION SNP(10,20),SNPF(10,20),PS12(10,20),PSD(10,20)
      M=3
      N=2
   99 READ(N,100) R,W,T
  100 FORMAT(4F10.4)
      READ(N,1) CALK,THETA
    1 FORMAT(2F10.4)
      IF(CALK) 91,91,92
   92 CONTINUE
C     R=RO-RF FOR LOAD INPUT    W= WIDTH    T=  THICKNESS
      PK=0.00310559
C PK= SLOPE OF THE CALIB. CURVE FOR THE LOAD TRANSDUCER.
      P= R*PK
      SO= P/(W*T)
      WRITE(M,101) SO,P,W,T
  101 FORMAT(1H2,//,5F10.4)
      DO 2 I=1,9
    2 READ(N,3) (SNP(I,J),J=1,15)
    3 FORMAT(8F10.2)
      DO 10 I=1,9
      DO 10 J=1,15
   10 SNPF(I,J)=SNP(I,J)/180.
      WRITE(M,11)
   11 FORMAT(1H2,'  ORIGINAL DATA')
      WRITE(M,15)
   16 FORMAT(//, '  NORMAL INCIDENCES')
```

```
      DO 12 I=1,9
   12 WRITE(M,15) (SMP(I,J),J=1,15)
   15 FORMAT(//,15F8.4)
      WRITE(M,82)
   82  FORMAT(1H2,//,5X,'  FRACTIONAL FRINGE ORDER')
      WRITE(M,16)
      DO 80 I=1,9
   80 WRITE(M,15) (SMPF(I,J),J=1,15)
      DO 30 I=1,9
      DO 30 J=1,15
      DS12(I,J)= CALK*SMPF(I,J)
   30 PSD(I,J) = DS12(I,J)/S(
      WRITE(M,31)
   31 FORMAT(1H2,5X,'  FINAL RESULTS FOR NORMAL INCIDENCE-UNIFORMITY')
      DO 32 I =1,9
   32 WRITE(M,15)  (PSD(I,J),J=1,15)
      GO TO 99
 91   CALL EXIT
      END
```

3. **Calculation of resolved shear stress and resolved shear strain.**

```
      DIMENSION PI(25),PII(25),TIMA(25),TIME(25),STRND(25),SI(25)
      DIMENSION SII(25),SIIP(25),SIIIP(25), STRN(25),D(25),TA(25),A(25)
      NR=2
      NP=3
100   READ(NR,1) N
      IF(N)102,102,103
  1   FORMAT(I10)
 103  READ(NR,2) WI,WII,T,TSTN,SPCN,PHI,PSI,PIR,GI,GF
  2   FORMAT(10F8.4)
      READ(NR,3) CRA,Z,BALW,FLC
  3   FORMAT(4F8.5)
      DO 11 I=1,N
      READ(NR,10) PI(I),PII(I),TIMA(I),STRND(I)
 11   PI(I)=PI(I)+BALW
10    FORMAT(4F15.5)
      DO 9 I=1,N
  9   TIME(I)=TIMA(I)*60.
      WRITE(NP,8)
  8   FORMAT(1H2,//,5X'INPUT DATA')
      WRITE(NP,12) TSTN,SPCN
 12   FORMAT(//50X'TEST NUMBER 'F4.0/50X'SPECIMEN NO.'F4.0)
      WRITE(NP,13)
 13   FORMAT(//,13X'TIME'13X'P(1)'13X'P(2)'12X'STRAIN'/12X'SEC. '13X'(KG
     1)'13X'(KG)'12X'(DIV.)')
      DO 30 I=1,N
      WRITE(NP,14) TIME(I),PI(I),PII(I),STRND(I)
 14   FORMAT(//,4F19.3)
30    CONTINUE
      WRITE(NP,15) GI,GF
 15   FORMAT(//,5X'GAGE LENGTH    ='F6.2,2X'(MM)'/,5X'FINAL G. LTH.   ='F6
     1.2,2X'(MM)')
```

```
      WRITE(NP,16) WI
16    FORMAT(//,5X'WIDTH-WI'6X'='F6.2,2X'(MM)')
      WRITE(NP,17) WII
17    FORMAT(//,5X'WIDTH-WII'5X'='F6.2,2X'(MM)')
      WRITE(NP,18) PHI
18    FORMAT(//,5X'PHI (NORMAL AND X2)'5X'='F6.0,2X'DEGREE')
      WRITE(NP,19) PSI
19    FORMAT(//,5X'PSI(DIRECTION AND X2) ='F6.0,2X'DEGREE ')
      WRITE(NP,20) PIR
20    FORMAT(//,5X'LOADING RATE-PI  ='F6.2'  KG/MIN. ')
      WRITE(NP,21) Z
21    FORMAT(//,5X'PERCENT STRAIN/DIV. ='F10.6)
      STRMM= (GF-GI)/GI*100.
      WRITE(NP,22) TSTN
22    FORMAT(1H2,//,5X'RESULTS FOR TEST NUMBER 'F6.0)
      WRITE(NP,23) STRMM
23    FORMAT(//,5X'MAXIMUM STRAIN MEASURED  = 'F10.2'  PERCENT')
      WRITE(NP,24)
24    FORMAT(//,9X'P(1)'8X'P(2)'7X'STRAIN'8X'SI'10X'SII'8X'SIIP'7X'SIIIP
     1'9X'TA'11X'A')
      WRITE(NP,25)
25    FORMAT(/,9X'(KG)'8X'(KG)'9X'(ALL STRESSES IN GR/SQ. MM)')
      AI=WI*T
      AII=WII*T
      PHIR = PHI*3.14159265/180.
      PSIR = PSI*3.14159265/180.
      CRAR = CRA*3.14159265/180.
      CPHI=COS(PHIR)
      SPHI= SIN(PHIR)
      CPSI=COS(PSIR)
      SPSI=SIN(PSIR)
      CLA= COS(CRAR)
```

```
      DO 70 I=1,N
      SI(I)=PI(I)/AI*CLA*1000.*ELC
      SII(I)=PII(I)/AII*CLA*1000.
      SIIP(I)=SI(I)*SPHI**2+ SII(I)*CPHI**2
      SIIIP(I)=(SII(I)-SI(I))*CPHI*CPSI
      STRN(I)=Z*STRND(I)
      D(I)=1. + STRN(I)/100.
      SQT=SQRT(D(I)**2-SPSI**2)
      TA(I)=(SII(I)-SI(I))*CPHI/D(I)**2 *SQT
      A(I)=1.0/CPHI*(SQT-CPSI)*100.
 80   WRITE(NP,81) PI(I),PII(I),STRN(I),SI(I),SII(I),SIIP(I),SIIIP(I),TA
     1(I),A(I)
 81   FORMAT(//5X,F10.3,4X,F10.3,F13.6,F10.2,F13.2,3F12.3,F15.6)
 70   CONTINUE
      GO TO 100
102   CALL EXIT
      END
```